Computational and Experimental Studies of Isolated Mixed-Charge Complexes: From Amino Acids to Ionic Liquids

Andrew James Alan Harvey

Doctor of Philosophy

University of York

Chemistry

August 2016

ABSTRACT

Counterion interactions are ubiquitous in the condensed phase, but isolated molecular systems containing counterion pairs have been poorly characterized in the gas-phase compared to isolated anionic and cationic systems. In this thesis, a new series of computational and experimental investigations of isolated mixed-charge ion clusters are presented. Alkali metal clusters are prototypical model systems for studying mixed ion-pair interactions.

In Chapters 3 and 4, ab initio computational studies of halide ions, bound to the amino acid arginine, are presented. Arginine can exist in either a zwitterionic or non-zwitterionic form. Chapter 3 presents a study exploring the influence of molecular conformation on the relative energies of the zwitterionic and non-zwitterionic halide-arginine complex. While Chapter 4 explores the applicability of a new series of density functionals (M06, M06-2X, M06-HF) for accurately predicting the energies of the halide ion-arginine clusters as a test of a system that contains hydrogen-bonding and dispersion interactions

In Chapter 5, a study of gas-phase ionic liquid clusters is presented. Mixed charge interactions dominate within condensed-phase ionic liquids. These compounds have been widely studied for applications across chemical and materials science. The first UV laser action spectra of mass-selected aggregates composed of the cationic and anionic constituents of two ionic liquids, *i.e.* $[BMIM^+]_n[Tf_2N^-]_m$ and $[EMIM^+]_n[Tf_2N^-]_m$ where $n \neq m$ and n, m = 1,2 are reported. These spectra compare well to other gas-phase spectra of ionic liquids, demonstrating the general utility of the method used here.

Finally, In Chapter 6, the first UV laser photodissociation spectra of gas-phase $I^-{\cdot}MI$ (M = Na, K, Cs) alkali halide anionic microclusters are presented. The photodepletion spectra of these clusters display strong absorption bands just below the calculated vertical detachment energies, indicative of the presence of dipole-bound excited states.

Contents

List of Figures

List of Tables

Acknowledgements

I would like to thank my supervisor, Dr. Caroline Dessent, for her continued support and guidance throughout my thesis. I would like to thank Dr Naruo Yoshikawa and Dr Ananya Sen for their support and training on using the different instrumentation in the Dessent group. I would like to thank Dr. John Slattery for his help as my IPM during my PhD. Finally, I would like to thank all members of the Dessent group and physical sciences office, past and present, who have helped make the darker days a little brighter.

Author's Declaration

I hereby certify that the research presented in this paper is my own and, to the best of my knowledge, original, except where due reference has been made to other workers. This thesis has not been submitted for any other award at this or any other institution.

The conformer sorting program, AUTODETECT, used in Chapters 3 and 4, was developed by Martin Walker, a former member of the group.

The work in Chapters 3 and 4 was carried on from the work started by Martin Walker before my arrival.

Chapter 3 has been published; *Walker. M, Sen. A, Harvey. AJA, Dessent. CEH, Chem. Phys. Lett., 588, 43 (2013)*

Chapter 4 has been published; *Harvey. AJA, Sen. A, Walker. M, Dessent. CEH, J. Phys. Chem. A, 117, 12590 (2013)*

Chapter 5 has been published; *Harvey. AJA, Sen. A, Yoshikawa. N, Dessent. CEH, Chem. Phys. Lett., 634, 216 (2015)*

Chapter 6 has been published; *Harvey. AJA, Yoshikawa. N, Wang. JG, Dessent. CEH, J. Chem. Phys., 143, 101103 (2015)*

Chapter 1

Introduction

1.1 Gas-phase studies of ionic, molecular clusters

"Clusters" in chemistry is a term used to refer to an aggregate of a number of atoms (from $2 \rightarrow 10^7$), while the phrase "molecular cluster" represents a cluster that contains at least one intact molecule. Molecular clusters can be studied in the gas phase, using various mass spectrometry or optical spectrometry techniques, and are often said to 'bridge the gap' between isolated molecular and bulk phases. One important result to come from this is a molecular-level description of solvation.[1-5]

Molecular clusters are of interest in modern chemistry for many reasons. Firstly, they are models for solvation phenomena, where the properties of a solute molecule of particular interest can be investigated as a function of individually added solvent molecules.[1-5] Secondly, molecular clusters are found in 'real' chemical environments, including atmospheric chemistry.[5b] Thirdly, molecular clusters provide many important benchmarks for testing computational chemistry.[1-5]

The interactions within molecular clusters can be considered to fall within one of two groups: firstly, the covalent bonds within a molecule, and secondly, the weaker intermolecular (or non-covalent) bonds. These weaker interactions include, van der Waals bonds, hydrogen-bonds, ion-dipole bonds, and induction effects. The clusters are held together by these weaker interactions. The reader is referred to a general chemistry textbook for more information on these different types of bonds.

This thesis will attempt to explore a number of different systems which overall are linked by all being gas-phase systems, and all containing mixed charge species. The individual experiments in each chapter will attempt to elucidate various physicochemical phenomena of each system in study and, in part, to evaluate the currently used methodology (be that experimental or computational). In this introduction, further discussion follows on a selection of different types of molecular clusters, all of which contain at least one charged species.

Studies of isolated ionic molecular systems in the gas phase are desirable, as they allow for the study of a system without interfering interactions from bulk-phase phenomena such as solvation effects. Investigation of mass selected molecular ions and ionic clusters allow for the detailed characterization of the geometric structures, energetics and reactivities of these systems.[1-7] These attributes of the ionic molecular system of interest can then be extrapolated to the bulk phase, through the study of the associated microsolvated clusters, to give a better understanding of a condensed-phase system's physicochemical properties. In addition, gas-phase studies of isolated ionic molecular clusters provide detailed information that can be

compared with the results of high-level computational chemistry.[2] The gas-phase experiments therefore provide high-quality data for "benchmarking" the computational results.

The first gas-phase studies of ionic clusters were carried out on emission spectra from electrical discharges of neutral diatomic radicals, such as OH, CN and NH.[8] The spectra obtained from these experiments were complex, as the temperatures involved meant that many different quantum levels of the ions were populated on formation. The bands that arise from these hot molecules lead to spectra which are difficult to deconvolute. More recently, more refined methods have been developed which allow high-density ionic species to be produced within such discharges, with a lower spread of energies. Perhaps most importantly, the ability to mass select particular clusters (which can also be formed within such discharges) for study is now readily available, and allows for much more definitive measurements.

Ion spectroscopy allows for the study of systems that are hard-to-reach in the bulk phase, for example photodetachment of anions leads to neutral free radicals. These often exist as transient intermediate species; so the opportunity to study them in the gas phase from anionic precursor clusters is extremely useful.[9] Another example of an elusive system being brought to the forefront of science is the discovery of C_{60} fullerenes, found during mass spectral studies of carbon in a molecular beam.[10] Ions are a huge part of modern chemistry, from production and processing of materials (e.g. semiconductor thin films) to the forefront of space exploration.[11]

Rather than just using gas phase studies as a way to extrapolate physicochemical phenomena of isolated clusters to the chemistry of the bulk phase, some studies choose to look at the ways in which gas phase spectra show properties that are unique from the condensed phase. These kinds of studies are equally useful, as exploiting unique phenomena is a key strategy in fields such as nanotechnology[12] where being able to manipulate individual atoms is a vital element.

Gas-phase studies of ionic hydrogen-bond containing clusters are a particularly important, current are of chemistry.[13] This type of bond is found in a large number of systems and are important for a wide array of chemistry, including ion-solvation, acid-base chemistry and the structures of molecular crystals.[14] Again, a key part of such studies is the comparison of the results obtained from experiments with high-level computational results. Over recent years, a growing number of ionic clusters containing biological molecules have been studied in the gas phase to characterise the non-covalent interactions that are present. These include nucleobase pairs such as those found in DNA,[15] peptide-ion interactions,[16] and adenosine-triphosphate ion interactions.[17]

1.2 Cationic and Anionic Clusters

While ionic clusters (i.e. a cluster containing an ionic species) can be neutral overall, there also exist clusters with an overall cationic or anionic charge. These types of clusters are of particular interest because they play important roles in diverse areas such as marine biology[18]

and material science, such as in ionic self-assembly.[19] Moreover, these systems, because of their excess charges, are able to be mass-selected and therefore isolated and fragmented using traditional mass spectrometry techniques, like those described in Chapter 2. Indeed, trapping charged species for further study has been prevalent in the physical chemistry scientific literature since the 90s.[20-22]

Another driving factor for the research of these systems is that they are challenging to model using current computational methods. Whilst smaller clusters are reasonably easy to model computationally, the difficulty increases exponentially as the clusters grow in size, due to the possible geometries of the clusters becoming greater.[23] Common subjects for computational study are solvated ionic clusters, where a shell of water molecules surround a molecular ion.[24]

The first mass-selected experiment on molecular ions was performed in 1962, by Dehmelt and Jeffers, where measurements of H_2^+ in a quadrupole ion trap (QIT) were taken,[25] and this approach was then extended to related ionic clusters. Much work has taken place since that first experiment, with important contributions from Oka, who explored H_3^+ molecular ions generated from discharges,[26] Saykally and co-workers engineered a method for measuring infra-red absorption spectroscopy of molecular ion beams, which they termed ‘direct laser absorbtion spectroscopy in fast ion beams (DLASFIB)[27]. Finally, the group of Lee generated infra-red photodissociation spectra of molecular ion beams,[28] to name just a few of the pioneers in this field.

As the field of ion spectroscopy has evolved, it has become clear that there are a few key areas to improve the quality of results gathered using it. Namely:

1. Ion preparation: Ions must be prepared in high densities, with few initial quantum states.
2. Mass Selection: The process of mass selection must preserve the initial ion density; this process must also move the ion to the detector.
3. Optical Detection

As mentioned previously, ion densities are already low in gas-phase compared to the solution phase, even before the mass-selection step (somewhere in the region of ~10^5 ions/cm^3 are produced by traditional sources), so the method of spectroscopy employed to study the ion cluster cannot be a traditional absorption-type spectroscopy.[5] One way of getting around this problem, is combining high intensity light sources (i.e. lasers) with photodissociation action spectroscopy. In such an approach, the laser interacts with the mass selected ionic clusters either at a focal point or in an ion trap. Following resonant absorption of a photon, the ionic cluster falls apart producing a "photofragment" of lower mass to the parent ionic cluster. The photofragment production can then be measured as a function of laser excitation wavelength to give the spectrum of the parent ionic cluster.[29]

The vaporisation source plays a large role in whether charged or neutral clusters are formed. Early studies used discharges,[8] electron impact or chemical ionisation.[3-32] The problem with these early methods is that the ions are hot. Over time, more desirable techniques were developed, using various expansion methods, which created cooler ions with less populated quantum states. Initially, this was achieved by coupling ion sources with supersonic

molecular expansions, and this advance led to the possibility of studying small ionic systems, such as $X^-.(H_2O)_n$ ion clusters.[33] It was found that often there was a 'magic number' of coordinated units to the ion, giving a particularly stable cluster conformation. This occurs even more noticeably with Ar and Xe ionic clusters.[34-36] With water clusters however, there does not appear to be such a magic number.[33] A more accurate method of searching for a 'magic' cluster is to monitor the temperature dependence of the cluster distribution. From this it is found that, disappointingly, there is no 'magic number' for a water shell, the binding energy simply drops off as the number of waters around the central ion increases; the solvent shell is therefore ultimately determined by the ionic strength of the central ion or ion cluster.[37]

More recently, the internal temperatures of gas-phase ions and clusters have been reduced by cryogenic cooling of ions and clusters after they have been initially produced as hot or ambient temperature gas-phase ions. (Electrospray is increasing being used as an excellent technique for introducing interesting ions from solution to the gas-phase for further study, but does suffer from the problem of producing ambient temperature ions). Another very interesting area that has grown significantly over the last decade is the use of helium droplets for trapping and hence cooling of ionic clusters, prior to further spectroscopic or reactivity studies. The original mechanism was developed by Scheidemann *et al* in 1993.[38] An electron hits a helium atom in the droplet, ionising it to a He^+ ion. This charge then moves around the cluster, beginning a cycle of resonant charge transferral to other neutral molecules that have been entrained in the cluster. This process terminates either by the formation of He_2^+, or by ionisation of the dopant species in the droplet. If the initial size of the helium droplet was

small relative to the size of the dopant, the energy transfer by ionisation causes sufficient heat to drive off the helium sheath, leaving the bare ion in the gas phase.[39, 40]

1.3 Solvated Neutral clusters $(X^-Y^+).(H_2O)_n$

Charge separation induced by solvents is one of the most facile, but also most fundamental processes in nature. Solvation effects in atoms,[41, 42] molecules[43] and ions[44-46b] have been studied for many years, allowing for step-by-step analysis of the changes in a potentially charge-separated system's physical and chemical properties as the number of solvent molecules associated with the system increases. In these molecular systems, the ions can be categorised as either being Contact Ion Pairs (CIPs) or Solvent Separated Ion Pairs (SSIPs), i.e. a neutral unit solvated ((Na^+Cl^-) --- $(H_2O)_n$) or as two individual, charged, solvated units ($Na^+.(H_2O)_x$ --- $Cl^-(H_2O)_y$). This process is important in the chemistry of aerosols[47, 48] and in the process of 'cloud seeding'; engineering clouds to produce rain, using silver salts.[49]

In order to study neutral clusters (i.e. clusters that contain ions but do not have an overall charge) using mass spectrometry, an ionisation step is necessary. There are several ways of achieving this ionisation; such as laser desorption/ionisation of a liquid beam,[50, 51] ionisation and charge separation via cluster impact on a surface[52] or multiphoton ionisation of neutral salt/solvent clusters.[53, 54]

In the first type of ionisation, a liquid beams enters a vacuum and is irradiated using an ultraviolet laser.[55, 56] Ions are ejected from the liquid surface and are then detected by a time-of-flight (ToF) mass spectrometer.[56] In the second type of ionisation, a beam of neutral clusters of polar molecules is produced. These clusters are collided with a surface, which creates fragments with either a positive charge, or both positive and negative fragments, depending on the molecules studied.[52, 57, 58] Finally, in the third type of ionisation, resonance enhanced multiphoton ionisation (REMPI) of neutral salt/solvent clusters analysed using ToF mass spectroscopy is used to probe the electronic states of the cluster and how they change as the size of the cluster evolves.

A standard REMPI study can be divided into three parts. Firstly, there is the initial generation of neutral clusters using a supersonic expansion. Next, these clusters are excited and ionised at a space-time focus using either one- or two-colour lasers with nano-, pico- or femtosecond resolution. Finally, the ions (parents and fragments) from the cluster are detected. Clusters of up to $n = 60$ can be created using this method.[53, 54, 59]

1.4 Mixed charge clusters with overall negative charge

Charged clusters of the form $[X_nY_m]^{m-n}$ (where $m > n$) yield negatively charged clusters. A prevalent source of such complexes are alkali metal halide clusters[60-63] where X = Li, Na, K etc. and Y = F, Cl, Br etc.. The potential surfaces for these systems are relatively simple, being dominated by coulombic interactions. By systematically studying clusters it is possible to trace how the delocalised charge from the additional halide ion affects the electronic and

geometrical structures of these species. Generally, these species have very high electron detachment energies[64, 65] in excess of those displayed by monoatomic halogen anions.[66] The reasons that the energies are so high are twofold. Firstly, the interaction between anion and cation in a neutral $[X^+Y^-]$ unit is strongly binding. Secondly, the excess charge in the overall anionic unit, i.e. $[X_nY_m]^{(n-m)}$ $n < m$ is delocalised effectively around the whole cluster. This behaviour has earned these families of molecules the nickname 'superhalogens'.[67]

'Superhalogens' are an exciting class of compounds with many possible applications. One of which is the possibility of using them as a way of storing hydrogen for fuel cells.[68] In this particular example, the group aimed to exploit the well documented hydrogen storing capabilities of a borohydride by creating large clusters of $Li[BH_4]$ where hydrogen atoms on the BH_4 are substituted for further BH_4^- units. Thus with one hydrogen substituted, the complex would be $Li[BH_3[BH_4]]$. These complexes were found to be more efficient at storing hydrogen than traditional borohydrides alone, which signifies a potential use for them in the field of hydrogen storage.[68]

There may also be a potential for 'superhalogens' to be used in nanoparticle chemistry, after the discovery that they can be used to form stable radical cation salts when combined correctly with C_{60} fullerenes.[69] Such systems could play important roles in areas as diverse as solar cells and cancer therapy[70, 71] fields which fullerenes are currently seeing interest in. In the aforementioned study, C_{60} fullerenes were being used as electron donor (reducing) agents, which is not their normal role. This is possible due to the strong oxidising power of superhalogens, and is one of the reasons why the radical cationic salts formed are fairly

stable. In all of the systems explored, superhalogens bound to the outside of the C_{60} cage, and stable salts were formed by any of the superhalogens studied with excess electron binding energies exceeding 5.9 eV were able to successfully ionise the C_{60} fullerene.

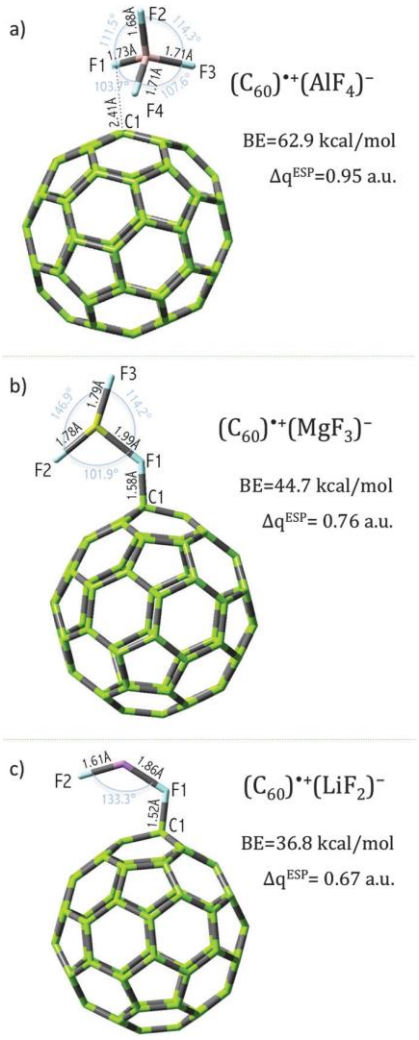

Figure 1.1; The equilibrium structures of the $C_{60}AlF_4$, $C_{60}MgF_3$, and $C_{60}LiF_2$ compounds obtained at the B3LYP-D3/6-31+G(d) level. The binding energy BE (i.e. interaction between the constituting fragments) and the amounts of the charge flow are also provided. Reproduced from reference [69].

A separate area where mixed charge systems with an overall negative charge have been studied includes systems such as $SO_4^{2-}\cdot Na^+\cdot(H_2O)_n$. As these clusters have an overall charge, they can be mass selected, allowing the details of the microsolvation to be investigated one water molecule at a time. A number of IR spectroscopy studies of such systems have been conducted over recent years, allowing the hydration structures of the ion-pairs to be characterized.[72]

1.5 Mixed charge clusters with overall positive charge

Charged clusters of the form $[X_nY_m]^{n-m}$ (where $n > m$) yield positively charged clusters. One recent study of interest involves creating small, cationic silver clusters,[73] which play important roles in partial oxidation and catalytic reactions.[74-76]

Uranium chemistry is an area of sustained interest, as research on uranium and uranium species has many wide-ranging areas of application, from nuclear fuel processing,[77] to mobility of the geological subsurface.[78] Solution chemistry of Uranium is dominated by the uranyl ion, UrO_2^{2+}, with studies[80] suggesting that the solvating species act like equatorial ligands with respect to the uranyl ion. One recent study explored uranyl ions complexed with monoanionic ligands to explore the effects these ligands had on the solvation of uranyl ions.[81] Using electrospray ionisation (ESI) and ion-trap mass spectrometry (IT-MS) the group found that the solvation rate of the uranyl ion was different, depending on the anion complexed to it. Acetate anions bound to the uranyl ion resulted in a solvation speed of 3 times longer, when compared to hydroxide anions complexed to the uranyl. This study would

prove useful when considering other anions such as phosphates, polycarboxylates and silicates, which are important for industrial and environmental processes. Another, recent, study analysed the clusters formed by electrospraying an aqueous solution of magnesium(II) nitrate.[82] This generated clusters of the form $[Mg(NO_3)(H_2O)_n]^+$ with n =7 as a maximum value. These clusters then underwent collision induced dissociation (CID) to remove individual water units. It is apparent from the results that there is an intrinsic stability to the cluster when n = 3 or less. Clusters where n = 4 were found to be more reactive (i.e. the waters were more loosely bound to the core). This indicates a second, weaker, solvation shell around the first.

1.6 Zwitterions

Zwitterions are hugely important in biological fields as they play crucial roles in both structure and function. In the aqueous phase at neutral pH, single amino acids and oligopeptides tend to be found in the zwitterionic form, whereby the N-terminus carries an additional proton and the C-terminus is deprotonated.[83, 84] These zwitterions exist due to stabilising interactions with solvent molecules in vivo. Gas phase studies on zwitterions have yielded a lot of information about relative energies, especially in systems such as amino acids, where an often small energy barrier marks the difference between a complex adopting a canonical conformation versus a zwitterionic conformation. Some recent studies have explored such energy barriers between these tautomers when they are influenced by nearby salt clusters[85] water molecules,[86] or anions.[87]

In the recent salt cluster-amino acid study of Wilenska *et al.*, computational calculations were performed to generate energies for a number of $MAlF_4$ salts (M = Li, Na, K) in proximity to proline or glycine amino acids in zwitterionic and canonical tautomers.[85] It was found that the zwitterionic tautomer was indeed stabilised by the addition of any of the $MAlF_4$ salts, to the point that they could compete energetically with the conventionally more stable canonical tautomer in the gas phase. In some cases, namely where M = Na or K interacted with glycine, the zwitterionic tautomer actually represented the global minimum of the complex.

In water molecules in clusters with amino acids,[86] both experimental and theoretical studies were carried out into whether water molecules could stabilise the zwitterionic forms of an array of amino acids, as well as several dipeptides (diglycine, dialanine, diproline). It was found that, water molecules generally clustered around the central zwitterion and lowered the energy gap between the canonical and zwitterionic tautomers by stabilising the zwitterionic form. For example, $\Delta E_{zwitt\text{-}canonical}$ for tryptophan (Trp) for $Trp(H_2O)_5$ was found to be 12.1 kJ mol^{-1}. Addition of another water molecule, i.e. forming $Trp(H_2O)_6$ reduces the $\Delta E_{zwitt\text{-}canonical}$ to ~4 kJ mol^{-1}. While addition of water molecules to a zwitterion therefore does seem to stabilise the zwitterionic tautomer, there is not such a great stabilisation as to make the zwitterion the preferential form.[85]

Milner *et al.*[87] have used simple anions to attempt to stabilise the zwitterionic form of arginine (Arg). This followed on from studies where excess electrons had been observed to stabilise zwitterion formation.[88] In the work of Milner *et al.*,[87] the first CID studies of X^-.Arg

were performed (X = F, Cl, Br, I, NO_3, ClO_3). Arg was selected for this study as it is the most basic amino acid, and thus the zwitterionic tautomer is more stabilised compared to other less basic amino acids. Because of this stabilisation, the energy gap between zwitterionic and canonical forms is fairly small[89]. With computational calculations to support the experimental results, it was found that of the anions used, Br^- could sufficiently stabilise the zwitterionic tautomer so as to make it lower in energy than the canonical form. Multiple dissociation pathways were observed for X^-.Arg when X = Br and NO_3, suggesting that there are multiple potential energy surfaces lying close together for these complexes.

1.7 Ionic Liquids in the Gas Phase

Ionic liquids are a class of compounds which, as their name implies, are comprised of two ionic components and exist as a liquid at room temperature or under 100°C, to differentiate them from molten salts.[90-92] They are highly desirable compounds, comprising of two separate ionic units, a cation and an anion, which can be 'mixed and matched' to tailor the ionic liquid to suit a specific application. The range of applications is truly staggering, from green solvents, to CO_2 extraction media and even rocket propellants.[93-96]

Ionic liquids have historically been rather difficult to transfer to the gas phase owing to their low volatility and high boiling points. In recent years, it has become apparent that by using high vacuum environments it was possible to transfer some ionic liquids to the gas phase.[97, 98] How ionic liquids behave in the bulk phase has been a subject of some debate, with some

recent literature attempting to clarify whether ionic liquids exist as neutral ion pairs.[99] The review of Kirchner *et al.* provided a detailed discussion of how ionic liquids behave as a bulk[100]. It concludes that whilst there is experimental evidence to support the theory of neutral ion pairs, there is just as much, if not more, evidence to disprove the theory. Overall, the current consensus seems to agree that ionic liquids behave as neutral ion pairs in the bulk, though it is clear that more work is necessary to provide a more suitable and generally applicable model.

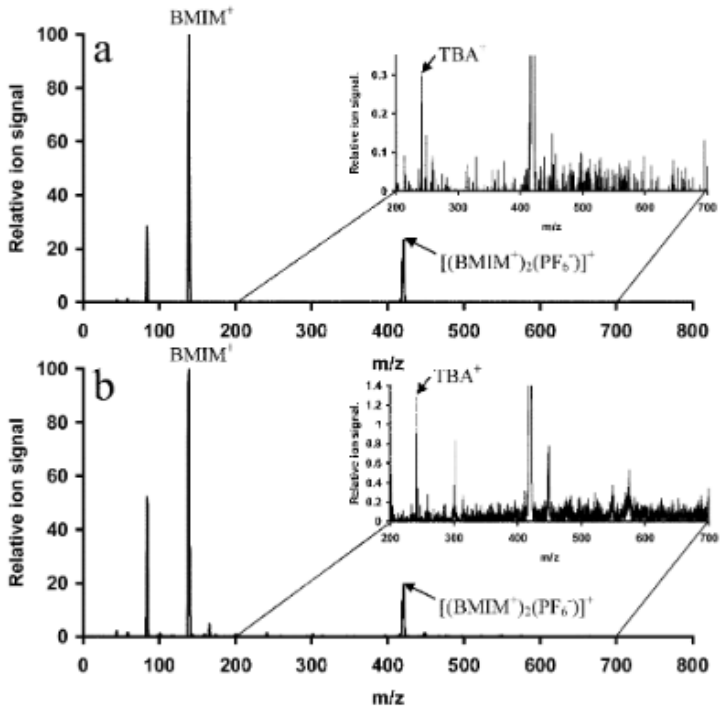

Figure 1.2; ES mass spectrum of BMIM-PF_6 containing 2 x 10^{-4} M TBAI, a) matrix electrosprayed without dissolution, b) RTIL matrix dissolved to 2 x 10^{-4} in methanolic solution. Reproduced from ref [102].

Transfer of ionic liquids to the gas phase was once a rather difficult process, as mentioned previously. However, recently there have been several works published on different methods of vaporisation of an ionic liquid, the first being a standard thermal liquid-to-gas transfer.[97] This transfer was only possible using a reduced pressure of 1 Pa (10^{-5} bar), as the boiling points of ionic liquids tend to be very high. Electrospray ionisation (ESI) is another possible method for obtaining gas phase ionic liquids.[101, 102] Electrospray is a very soft method of ionisation, and so much of the structure of the ionic liquid is preserved. It was found that under ESI, charged clusters were formed of the type $[(A_nC_m)_xA]^-$ // $[(A_nC_m)_xC]^+$ where A = anionic part of IL and C = cationic part of IL, $n \neq m$, $x > 1$[102,] .

1.8 Overview of thesis

In this thesis, a range of mixed charge ionic clusters are investigated using laser spectroscopic, mass spectroscopic and computational methods. Chapter 2 goes into detail on the methodology employed in the experimental and computational studies. Chapter 3 covers a computational study of a series of conformers of arginine tautomers complexed with Br^- and Cl^- halide anions, attempting to find if an anion can stabilise an otherwise unstable tautomer. Chapter 4 evaluates the suitability of the M06 suite of density functionals for use on non-covalent interaction dominated systems of comformationally flexible anionic clusters, drawing on findings from Chapter 3 that the M06 functionals performed well on the arginine halide tautomers. Chapter 5 explores the behaviour of mass selected, charged, cationic and anionic aggregates of imidazolium-based ionic liquids in the gas phase, using laser spectroscopy to fragment parent clusters and analyse the fragmentation pathways of

the isolated systems. This experiment used the modified mass spectrometer as described in Chapter 2. The success of this experimental methodology paved the way for the experiment conducted for Chapter 6, which looks at the interactions between mass selected, gas-phase, alkali halide cationic clusters, and the dissociation of the charged cluster units. These species had a similar structure to those studied in Chapter 5. The thesis concludes with Chapter 7, which summarises the main discoveries made during this work, and also plans for future work within each chapter.

Chapter 2

Experimental and Theoretical Techniques

2.1 Experimental methods

2.1.1 Mass Spectrometer Setup

Mass Spectrometry studies were carried out on a Bruker Esquire 6000 Quadrupole Ion Trap Mass Spectrometer[103] which has been modified in-house to allow a laser beam to pass through the ion trap, irradiating the trapped sample ions to cause photodepletion by UV radiation. The laser beam is produced by a frequency doubled Panther OPO producing light in the region of 220-310nm which is pumped by a Surelite pulsed laser. The spectrometer itself can form charged clusters using an ESI ionisation source, a charged capillary, creating a way to ionise samples without fragmentation, giving cool ions in low energy quantum states. From the source, ions pass through a series of ion optics before entering into the quadrupole ion trap. Here they can be fragmented using CID with a helium buffer gas or, as above, using lasers through the custom-made windows into the trap (Figure 2.1). The spectrometer itself can search for m/z ratios of 35-3000 in normal running mode, with a typical resolution of 0.35 (fwhm) and allows for tandem mass spectrometry up to MS_n where

n = the number of iterations of isolation of the target species, subsequent fragmentation and re-isolation of a new target fragment.[104]

The same studies were also performed on a Bruker amaZon mass spectrometer, with the same laser setup. This mass spectrometer also had a quadrupole ion trap, but was more sensitive, making it more suitable to high-resolution spectroscopy.[105] The normal running mode of the amaZon spectrometer was 50-2000 m/z units and it had a typical resolution of 0.35 (fwhm) and allowed tandem mass spectrometry up to MS_n. [105]

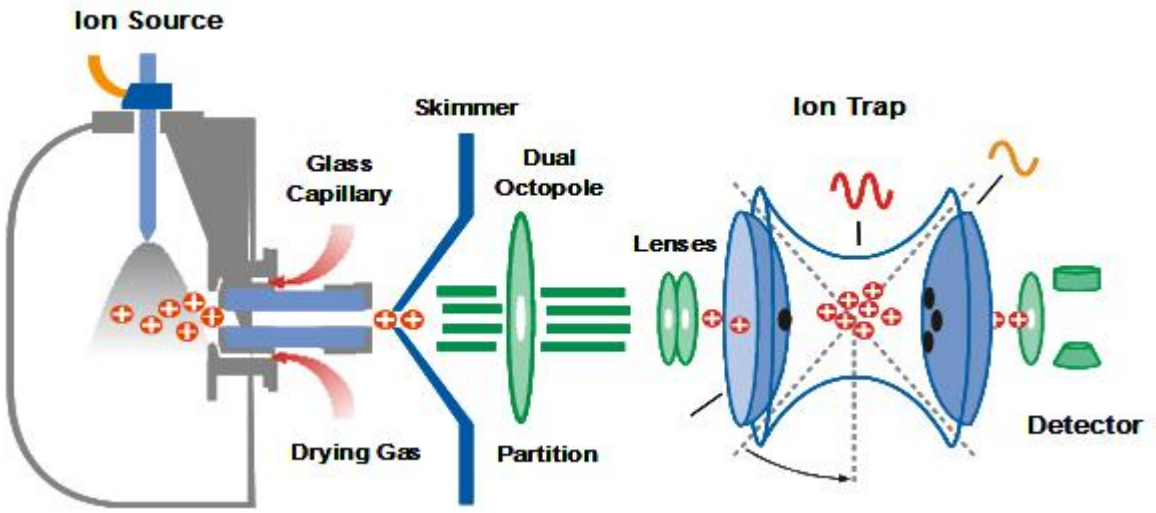

Figure 2.1; Schematic of the Bruker Esquire 6000 mass spectrometer[103]

2.1.2 Electrospray Ionisation

All experimental work on both spectrometers was done using an Electrospray Ionisation (ESI) source. The Agilent ESI source uses an orthogonal sprayer design, which is slightly different to the traditional design. The orthogonality increases the robustness, sensitivity and reproducibility of the spectrometer over a range of injection conditions[103]. Once ions have been electrosprayed, they move into a perpendicular electrostatic field, this directs them along a transport capillary, and a skimmer, and finally, into the optic region.

The ESI source (Figure 2.2), though orthogonal in set-up, will still perform as a standard design. [106, 107] A solution which contains a precursor of the species desired for study is injected via syringe through a fused-silica capillary using a computerised syringe driver at a constant rate (typically 2-5 μL min^{-1}). The capillary moves the solution to a charged needle, where ions accumulate at the tip, forming a Taylor cone[108]. With the aid of a nitrogen nebuliser gas, droplets of highly charged ions will break from the tip of the cone and start to evaporate. As the droplet evaporates, the repulsion of the ions in the droplets increases as they are forced closer together. Eventually the repulsion becomes large enough to overcome the surface tension of the droplet, and it undergoes a Coulombic explosion. This creates a number of smaller droplets which repeat the process of evaporation and fission[109].

There are two models for the eventual production of bare ions which enter the quadrupole ion trap (QIT). The cycle of solvent evaporation and Coulombic explosion can continue until a droplet only contains a single ion, at which point the solvent evaporation leaves only the bare ion[110, 111]. This is known as the charge residue model. In the second model, as the droplets get smaller, and the charge density of the droplet increases, the repulsion interactions become large enough to fully eject an ion from the droplet, into the gas phase.[112] Smaller ions, like those studied in this thesis, seem to mainly use the first mechanism.[113] The ions are then directed through a heated capillary with variable temperature (generally 100-300ºC). Along with a nitrogen drying gas, this removes any residual solvent from the ions. These pass through a skimmer and into the ion optics region of the mass spectrometer.

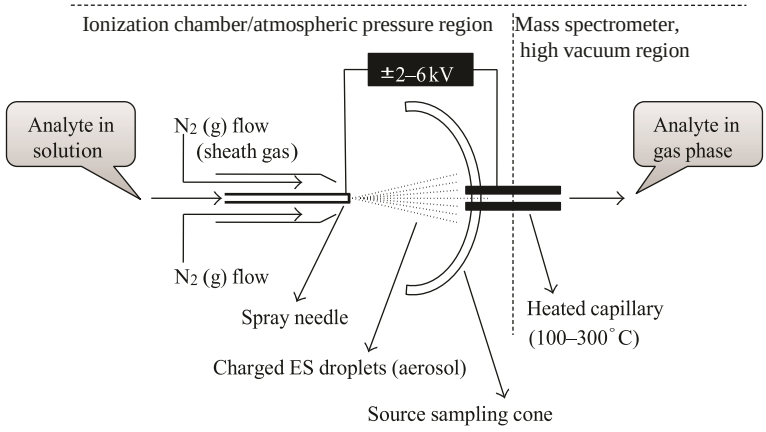

Figure 2.2; Schematic representation of the electrospray ionisation source. Reproduced from [114]

2.1.3 Ion Optics

For the ions to be detected, they must pass from the ionisation chamber (at atmospheric pressure) to the low-pressure ion-trap region of the instrument. A set of ion optics is used to achieve this. The ions enter an octupole, which directs them through a vacuum partition and into a second octupole. From here, the ions are directed through a pair of electrostatic lenses. These focus the ions into the QIT.

2.1.4 Quadrupole Ion Trap (QIT)

The QIT (Figure 2.3) contains the ions within an area of space by use of electrostatic forces generated by three electrodes; a ring electrode and two hyperbolic end-cap electrodes.[115, 116] Once in the trap, the ions move according to a Lissajous curve (similar in shape to a bow-tie), as described by the Mathieu equation. [117, 118] A damping gas, usually Helium at ~10^{-3} Torr, is used to expunge excess energy from the system, preventing uncontrolled ejection of ions from the trap, by collisions of the trapped ions with the helium gas. This is referred to as ion-cooling.[115] Ions can be ejected from the trap in a controlled fashion by using resonant excitation. This involves applying an oscillating potential to the end cap electrodes, which causes a given m/z of ion to be accelerated from the trap. Varying the oscillation varies the m/z of the ion that is ejected.[115]

In the spectrometers, ions enter the QIT via a hole in one of the end cap electrodes. They are held in the QIT for a short time window before being resonance excited out of the trap and into the detector. This generates a plot of ion intensity vs. RF voltage, which is calibrated to produce a mass spectrum. The mass spectra in this thesis are produced by averaging individual mass spectra, generated as previously described.

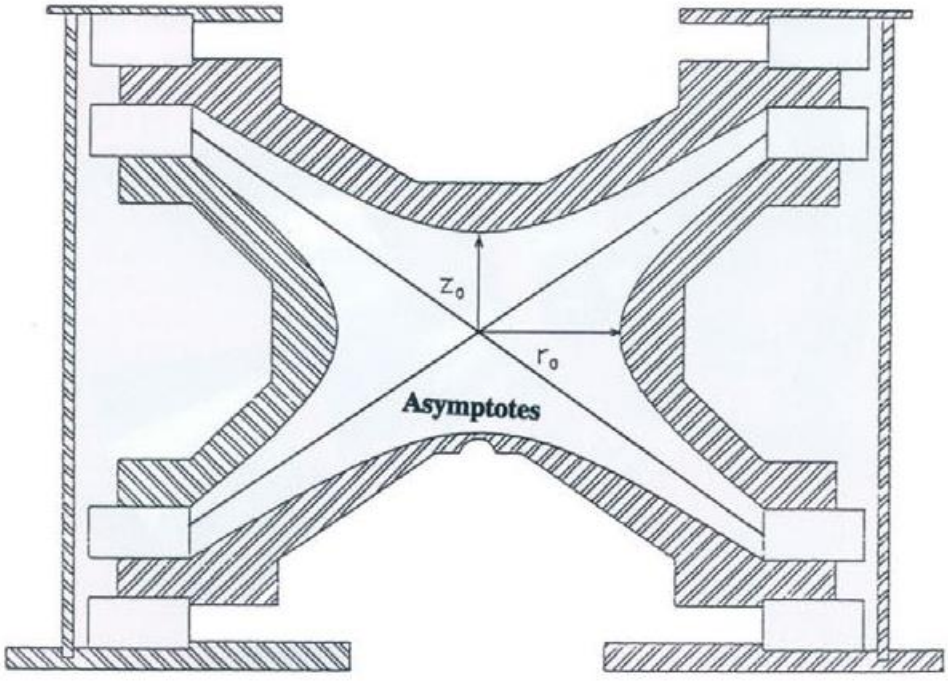

Figure 2.3; Schematic representation of the quadrupole ion trap. Reproduced from [115]

2.1.5 Laser Dissociation

As previously described, the spectrometers used in this thesis have been modified in-house to allow for an Nd:YAG laser pumping an OPO (Optical Parametric Oscillator) to generate a laser beam which then enters the QIT via a small (2mm) hole, drilled through the instrument (see Figure 2.4). The laser passes through the QIT and excites any ions in its cross-section, and exits the trap via another small hole. Reflective mirrors underneath the QIT then reflect the beam at right angles to an exit hole at the top of the machine. The exit hole allows for the alignment of the laser beam to ensure that it travels correctly through the trap. Before entering the instrument, the laser is reflected by a series of prisms (A, E) passes through a series of focusing lenses (D), irises (B) and a shutter (C). This shutter is synchronised with the mass spectrometer's ion accumulation time, such that the time that the ions spend in the trap overlays with a packet of laser photons entering the trap. The laser has tuneable power, and this is referred to explicitly in each chapter where the laser was used experimentally.

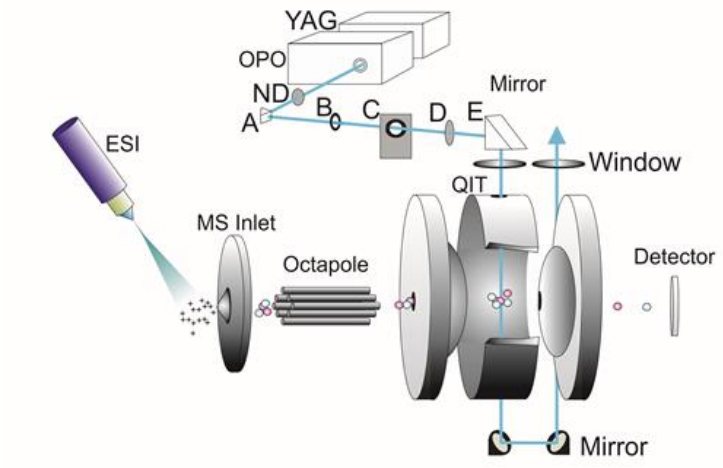

Figure 2.4; Schematic representation of the photodepletion spectroscopy set-up

2.1.6 Action Spectroscopy

The mass spectra obtained by laser photodissociation are essentially identical to the mass spectra that would be acquired by collision induced dissociation (CID). Each overall scan at an individual laser wavelength is made up of 20 averaged scans, and each overall scan was performed first with the laser blocking the trap, and then with the laser entering the trap. Each overall scan is repeated 3 times, and the data on the parent intensities and fragment intensities is averaged. The wavelength is then moved by 0.5-1.0 nm and the measurement taking process repeated until the full range of wavelengths for the study have been completed. The overall spectrum for a range of wavelengths is then built up from each individual averaged scan at a fixed wavelength, tracking the decay of parent peaks and formation of fragment peaks over the whole wavelength range. This type of spectroscopy is known as action spectroscopy.[119]

2.2 Computational methods

Computational studies were performed using Gaussian ’09 and a range of functionals and basis sets. ‘Functionals’ are mathematical functions of functions. In density functional theory (DFT) the functional is the electron density, which is a function of space and time. Basis sets are groups of functionals which can be combined linearly to create molecular orbitals. Early preliminary work was performed on systems of Arginine in zwitterionic and canonical forms complexed with Bromide and Chloride anions using the post Hartree-Fock M06 suite of

functionals, attempting to ascertain the accuracy of the M06 suite when compared to the more complex MP2 level of theory. After finding the M06 functionals to perform well on calculations of charged species, they were chosen for further studies on the geometries of charged clusters of ionic liquids.

2.2.1 Density Functional Theory

Quantum mechanical calculations are based on solving the Schrödinger equation (2.1),

$$H\Psi = E\Psi \qquad (2.1)$$

H is the Hamiltonian operator, E is the energy and Ψ is the wavefunction of the system under study. Solving the Schrödinger equation allows for the energy of a specific molecular arrangement to be determined, which in turn allows for a potential energy surface (PES) to be generated. This is the principle by which *ab initio* structure optimisations, such as those found in Chapters 3 and 4, are conducted.

The Born-Oppenheimer approximation treats the motion of the electrons and nuclei involved separately, this hugely simplifies the Schrödinger equation to only three terms; the kinetic energy of the electron, the electron-nucleus attraction and the electron-electron repulsion. [120] In density functional calculations, the energy of a system is determined using a functional of the electron density. [121, 122] Basis sets are sets of functionals used to generate molecular orbitals by linear combination of functionals. The basis sets used in the work presented in this thesis are talked about in more detail in the respective chapters.

2.2.2 Molecular Mechanics

Molecular mechanics is a fairly inexpensive computational method for calculating energies and geometries of molecular systems by using classical mechanics. Force fields, containing empirically derived information relating to the energy associated with various structural parameters, can be used to calculate energies for a given molecular arrangement[123, 124]. By using an energy minimisation algorithm, structure optimisation is achieved. The algorithm works by taking a molecular structure of known energy, slightly adjusting the structure and calculating the new energy. If the new energy is lower, the process is repeated. If the new energy is higher the original structure is modified in a different orientation and the energy is calculated. This process is repeated iteratively until a local minimum for a PES is obtained.[125]

2.2.3 Autodetect: Conformational Sorting Software

Conformer searches, as in Chapters 3 and 4, can be used to quickly generate a slew of low-energy structures. By taking a set number of these structures and using user-defined parameters, such as average bond lengths between two atoms across a series of structures, a number of conformational families can be generated. In this work, a program developed within the group, Autodetect, was used to fulfil this purpose. By setting up parameters for typical hydrogen bond lengths between specific atoms in a series of structures of arginine it was possible to sort 100 slightly different conformations into a smaller number of families

which shared similar bonding characteristics. From these smaller families, additional structure optimisation calculations could be run, in order to remove degenerate structures and get a local minimum-energy structure for each family.

Chapter 3

Complexation of anions to gas-phase amino acids

3.1 Introduction

In recent years, gas-phase studies of cation-amino acid clusters have been a popular topic for study in order to probe the mechanisms of ion-amino acid interactions.[126, 127, 128-135] These investigations are motivated by the fact that many critical biochemical processes involve peptides and amino acids interacting with ions.[136, 137] While there has been some computational work done on these systems,[138–140] it is surprising that isolated anion–amino acid interactions have only very recently been explored experimentally in two distinctive studies.[87, 141] In one set of experiments, Infrared Mutiphoton Dissociation (IRMPD) spectroscopy was carried out on a series of halide ion–amino acid clusters, revealing that the X^-Arg (X = Cl, Br, I, Arg = arginine) complexes tend to exist with Arg in the zwitterionic form. [141] Another, complementary, study applied low-energy collision induced dissociation (CID) to these clusters, and found that Arg adopted a zwitterionic conformation in the Br^-.Arg cluster, although the fragmentation potential energy surfaces were found to be distinctive for the Cl^- vs Br^- vs I^- clusters.[87]

Using arginine as the amino acid in these experiments is an important choice, since the difference in energies between zwitterionic and canonical forms of isolated arginine molecule is very small, with the zwitterion being slightly higher in energy than the canonical form. [89, 142, 143] This scenario arises because the gaunidinium side chain is strongly basic in the gas-phase (arginine is the most basic of the naturally occurring amino acids), which stabilizes the zwitterionic form relative to the canonical form compared to other amino acids. Despite the fact that both sets of experiments provided some evidence that anions can stabilize the zwitterionic form of Arg relative to the canonical form, neither experiment was able to unequivocally demonstrate this. This chapter aims to directly address this pivotal question in this work by applying computational methods to the Cl^-.Arg and Br^-.Arg complexes, with Arg in the canonical (Arg_{can}) and zwitterionic (Arg_{zwit}) forms, to allow for direct comparison with previous experiments on these complexes.

Considerable conformational flexibility is present in these X^-Arg clusters, making them a challenging system for ab initio computational study, in terms of both the ion– amino acid interactions, and also the intramolecular amino acid non-covalent bonds. In the calculations performed in this chapter, the clusters are conformationally surveyed then classified into conformeric families for the first time, using an automated procedure that had recently been developed in our group. By classifying the numerous possible conformers into family groups, it was possible to systematically select representative conformers for high-level geometric optimisation. This then allowed for reliable energies to be calculated, and a comparison made between the tautomeric forms of the clusters. For the anionic complexes studied in this chapter, this process is critical in allowing the key question of whether the

calculations predict that the zwitterionic or canonical form is the global minimum tautomer for this system to be answered.

3.2 Computational Methods

Initial conformational searches of the zwitterionic and (lowest energy) canonical forms of X^-Arg (X = Cl, Br) were performed using MMFF94 and a Monte Carlo algorithm as implemented in SPARTAN 08.[144] The MMFF94 force field was selected for this study as it has been assessed to provide the best performance among the traditional fixed charge fields (which included AMBER94, AMBER99, and OPLS) for a set of amino acids.[145] It should be noted that it is unlikely that the force field will identify all possible conformers. However, 20000 conformers were examined for each tautomeric cluster in this work, and from previous work, 'missing' conformers are generally the higher energy species, and thus can be considered irrelevant.[145] The 100 lowest energy structures for each tautomeric isomer were subdivided into families displaying similar non-covalent interactions (hydrogen-bonds) using a structure sorting algorithm (AUTODETECT) that has been developed within the group, automating a previous family sorting strategy.[146, 147]

Optimisations were performed using GAUSSIAN 09,[148] first at the HF/6-311+G** level (with counterpoise correction) and then at the MP2/6-311+G**level, thus providing a proper treatment of dispersive interactions for these systems for the first time. This should be particularly important for the Br system. Frequency calculations were performed for the

three lowest energy structures (conformers I–III) to confirm the conformers exist as minima, to provide some zero-point energy (ZPE) corrections, and to provide ΔG^{o}_{298} relative energies for comparison with the absolute relative energies. Frequencies were only calculated for a limited number of conformers due to the computational expense of performing MP2 frequency calculations for these large X^{-}Arg clusters. (However, the integrity of the conformers as minima was confirmed through performing B3LYP/6-31+G* frequency calculations, where no negative frequencies were found.) Basis set superposition errors were corrected in the binding energy calculations,[148, 149] which were performed with full structural flexibility. The uncertainties in the calculated relative energies within conformer sets, and between tautomers, are expected to be on the order of 2 kJ/mol.[150]

3.3 Results and Discussion

Figure 3.1 shows the six lowest-energy conformers (from a collection of 18) of the $Br^{-}.Arg_{can}$ cluster. Each structure displays a distinctive set of non-covalent interactions, thus distinguishing the different families, with each conformer displaying four or five key hydrogen-bonding type interactions. (Inter and intramolecular hydrogen bonds are indicated by dashed lines on the figures.) In these conformers, the Br^{-} ion forms either three or four ionic hydrogen bonds with the OH and NH groups of the neutral Arg moiety. Additional intramolecular bonds between the arginine NH_2 and carboxylate groups are also present. The corresponding conformers for the $Br^{-}.Arg_{zwit}$ cluster, are presented in Figure 3.2. It is notable that only five low-energy conformer families are identified for the zwitterionic cluster, in distinct contrast with $Br^{-}.Arg_{can}$ where a much larger number of low-energy conformer

families were identified. This is due to strong ion–dipole interactions that are present in the zwitterionic cluster, but not in the canonical clusters. This mirrors results obtained for other anion–amino acid clusters where fewer zwitterionic than canonical conformers have been observed.[140, 151] (Indeed, neutral Arg also appears to have a lower number of low-energy conformers in its zwitterionic form relative to its canonical form.)[143] Inspection of the $Br^-.Arg_{zwit}$ structures reveals that numerous hydrogen-bonding interactions are also present. However, in contrast to the canonical structures, the Br^- forms just two (or in the case of conformer V, just one) ionic hydrogen-bonds with the protonated guanidinium N–Hs, due to the deprotonated Arg carboxylate group forming intramolecular ionic hydrogen-bonds.

Figures 3.3 and 3.4 present the conformer structures for the corresponding Cl^- complexes. As in the Br^-.Arg system, there are considerably more conformers for $Cl^-.Arg_{can}$ than $Cl^-.Arg_{zwit}$ (Figure 3.3 presents 6 out of the 17 conformers we identified for $Cl^-.Arg_{can}$). The general pattern of structural motifs follows a similar trend to Br^-.Arg, i.e. three-four ionic hydrogen bonds for the $Cl^-.Arg_{can}$ complex, and one-two Cl ionic hydrogen bonds for $Cl^-.Arg_{zwit}$. The three key ionic hydrogen-bonding interactions are identical for the lowest energy conformers of $Cl^-.Arg_{can}$ and $Br^-.Arg_{can}$ (Figures 3.1 and 3.3), although the intramolecular hydrogen bonds present in these clusters are different. (The $Cl^-.Arg_{can}$ conformer I is more like conformer VI of $Br^-.Arg_{can}$). This indicates that it is not good practice to simply ‘exchange’ a larger halide ion into a structure obtained for a smaller, computationally more tractable anion and compute single point energies for assessing relative stability. Table 3.1 presents further calculations to illustrate this.

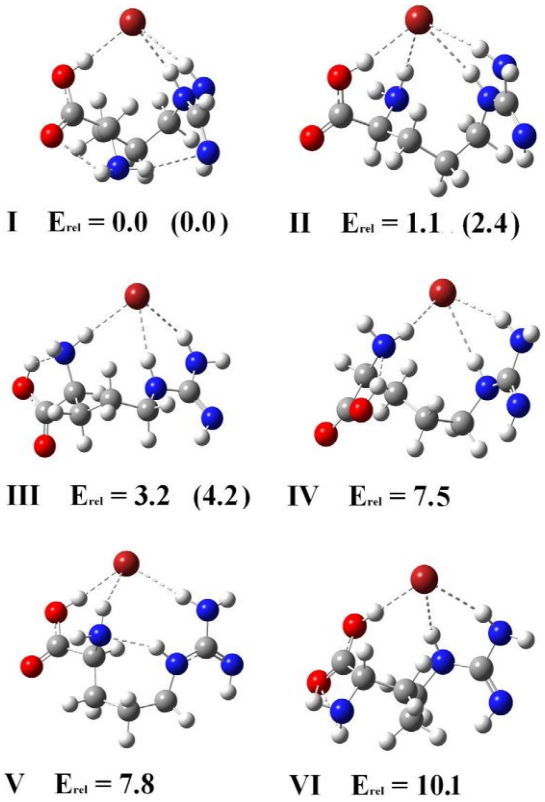

Figure 3.1; Structures of the six lowest-energy (MP2/6-311+G**) conformers of $Br^{-}.Arg_{can}$, labelled from I to VI. Relative energies (kJ/mol) are displayed, with ZPE corrected values in parentheses.

Table 3.1; Absolute (in Hartrees) and relative (in kJ/mol) energies for conformers of $Br^{-}\cdot Arg$ produced by substituting Br- into the optimized conformers for $Cl^{-}\cdot Arg$.All calculations are single point energies at the MP2/6-311+G** level.

Conformer	canonical		zwitterionic	
	Energy	Relative Energy	Energy	Relative Energy
I	-3177.69313	0.0	-3177.69033	0.0
II	-3177.68854	12.0	-3177.6881	5.9
III	-3177.68854	12.0	-3177.68707	8.5
IV	-3177.69119	5.1	-3177.68558	12.5
V	-3177.68636	17.8		
VI	-3177.68623	18.1		

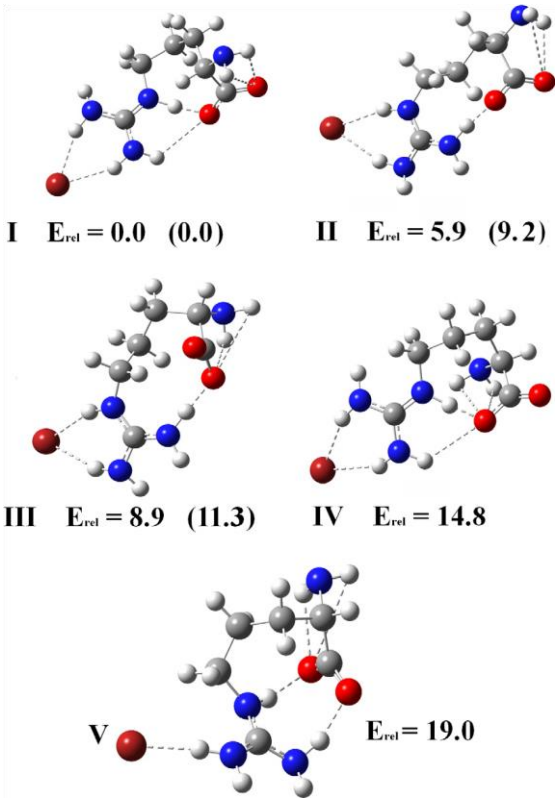

Figure 3.2; Structures of the five (MP2/6-311+G**) conformers of $Br^-.Arg_{zwit}$, labelled from I to V (increasing energy). Relative energies (kJ/mol) are displayed, with ZPE corrected values in parentheses.

For the $Cl^-.Arg_{zwit}$ and $Br^-.Arg_{zwit}$ complexes (Figures 3.2 and 3.4), the two lowest energy conformers (I and II) have very similar structures, but the energetic ordering is reversed. That is, conformer I of $Cl^-.Arg_{zwit}$ resembles conformer II of $Br^-.Arg_{zwit}$, while conformer II of $Cl^-.Arg_{zwit}$ resembles conformer I of $Br^-.Arg_{zwit}$. Hydrogen-bond lengths for the conformers displayed in Figures 3.1–3.4 are included here in Tables 3.2.1-3.2.4. The closeness of energies of the conformers is notable, particularly for the $Br^-.Arg_{can}$ cluster (Figure 3.1), where conformer III is only 3.23 kJ/mol above conformer I. Table 3.3 displays the ΔG^o_{298} relative energies for isomers I–III for comparison. For the $Br^-.Arg_{can}$ tautomer

where the relative energies are very close, the ΔG^{o}_{298} relative mirror this, with isomer III now predicted to lie lowest in energy. Overall, these close relative energies reveal that multiple conformers are expected to be populated under ambient equilibrium conditions, particularly for $Br^{-}.Arg_{can}$.

Table 3.2.1; Hydrogen-bond distance data for $Br^{-}\cdot Arg_{can}$, defining the distinctive conformational families. All distances are in Angstroms, x refers to no hydrogen bond (i.e. interatomic distance > 3.5Å).

Family	Br-H1	Br-H2	Br-H3	Br-H4	Br-H5	Br-H6	Br-H7	O2-H2	O2-H3	N1-H1	N3-H2	N3-H3	N1-H4
I	2.21	x	x	2.37	x	2.64	x	2.21	x	x	x	2.50	x
II	2.28	2.47	x	2.55	x	2.61	x	x	x	x	x	x	x
III	x	2.43	x	2.33	x	2.68	x	x	x	1.76	x	x	x
IV	x	x	2.50	2.48	x	2.50	x	x	x	1.81	x	x	x
V	2.19	x	2.47	x	x	2.53	x	3.26	x	x	x	x	2.11
VI	2.16	x	x	2.76	x	2.56	x	2.58	2.71	x	x	x	x

Table 3.2.2; Hydrogen-bond distance data for $Br^{-}\cdot Arg_{zwit}$, defining the distinctive conformational families. All distances are in Angstroms, x refers to no hydrogen bond (i.e. interatomic distance > 3.5Å).

Family	Br-H3	Br-H4	Br-H5	Br-H6	Br-H7	O1-H1	O1-H2	O1-H4	O1-H5	O2-H1	O2-H2	O2-H3	O2-H4	O2-H5
I	x	x	2.39	2.27	x	2.31	3.05	x	x	x	x	1.42	2.77	x
II	2.26	x	x	x	2.32	2.38	3.09	3.45	x	x	x	x	1.58	x
III	2.28	x	x	x	2.32	x	x	2.89	x	2.24	3.08	x	1.55	3.2
IV	x	x	2.38	2.27	x	x	x	x	x	3.07	2.62	1.42	2.69	x
V	x	x	x	2.14	x	x	x	1.73	3.32	2.32	3.15	1.82	2.81	x

Table 3.2.3; Hydrogen-bond distance data for $Cl^{-}\cdot Arg_{can}$, defining the distinctive conformational families. All distances are in Angstroms, x refers to no hydrogen bond (i.e. interatomic distance > 3.5Å).

Family	Cl-H1	Cl-H2	Cl-H3	Cl-H4	Cl-H5	Cl-H6	Cl-H7	O2-H2	O2-H3	N1-H1	N3-H2	N3-H3	N1-H4
I	1.97	x	x	2.23	x	2.47	x	2.96	2.43	x	x	x	x
II	1.98	2.30	x	x	x	2.34	x	x	3.28	x	x	x	2.09
III	2.11	x	2.36	2.43	x	2.39	x	3.45	x	x	x	x	x
IV	x	2.22	x	2.14	x	2.51	x	x	x	1.75	x	x	x
V	1.96	x	x	2.19	2.94	x	x	2.96	2.43	x	x	x	x
VI	1.97	x	x	2.17	3.24	x	x	3.26	2.26	x	3.02	x	x

Table 3.2.4; H-bond distance data for $Cl^{-}\cdot Arg_{zwit}$, defining the distinctive conformational families. All distances are in Angstroms, x refers to no hydrogen bond (i.e. interatomic distance > 3.5Å).

Family	Cl-H3	Cl-H4	Cl-H5	Cl-H6	Cl-H7	O1-H1	O1-H2	O1-H4	O1-H5	O2-H1	O2-H2	O2-H3	O2-H4	O2-H5	N2-H1	N2-H2
I	2.07	x	x	2.13	x	2.38	3.08	3.48	x	x	x	x	1.59	3.15	x	x
II	x	x	2.20	2.06	x	3.01	2.27	x	x	x	x	1.51	2.67	x	x	x
III	x	x	2.18	2.07	x	x	x	x	x	2.62	3.05	1.44	2.72	x	2.20	x
IV	x	x	x	1.90	3.49	2.39	2.99	1.75	3.34	x	x	1.81	2.84	x	x	x

Table 3.3; MP2/6-311+G**DG^{o}_{298} relative energies for (kJ/mol) the three lowest-energy conformers (I–III) of the canonical and zwitterionic forms of Br^{-}.Arg and Cl^{-}.Arg.

Br^{-}.Arg	Canonical	Zwitterionic	Cl^{-}.Arg	Canonical	Zwitterionic
I	0	0	I	0	0
II	0.3	10.2	II	13.9	3.7
III	-1.1	12.9	III	12.5	5.5

Table 3.4 displays the absolute energies for the lowest energy conformers of the canonical and zwitterionic forms of Cl^{-}.Arg and Br^{-}.Arg. For Br^{-}.Arg, the zwitterionic complex is predicted to lie very slightly lower in energy (0.5 kJ/mol) than the canonical form, indicating

that a Br^- ion can indeed stabilize the gas-phase Arg zwitterion relative to the canonical form. The very small energy difference between the $Br^-.Arg_{zwit}$ and $Br^-.Arg_{can}$ reflects the extremely delicate energetic balance that exists for these tautomers. It is clear that the Arg conformeric structure within the cluster is key in determining the overall energetics, i.e. the conformer relative energies of both Cl^-.Arg and Br^-.Arg presented here cover an energy range greater than the zwitterionic–canonical energy difference, thus confirming the importance of properly surveying the conformational isomers as part of such calculations. Surprisingly, the key result is reversed for the Cl^-.Arg cluster, where $Cl^-.Arg_{can}$ is predicted to lie considerably below $Cl^-.Arg_{zwit}$ (16.8 kJ/mol). This result is valuable, as it reveals that the presence of an adjacent excess negative charge (i.e a halide ion) is not a sufficient criterion to stabilize the zwitterionic form of the amino acid in the gas-phase, as discussed for amino acid dipole-bound excess electron systems. [88, 152–154]

In order to further explore the differences between the Cl^-.Arg and Br^-.Arg systems, counterpoise corrected binding energies were calculated for the lowest energy conformers (Table 3.5). These are in line with values that would be expected for Cl^- and Br^- ions forming three-four ionic hydrogen bonds.[155]

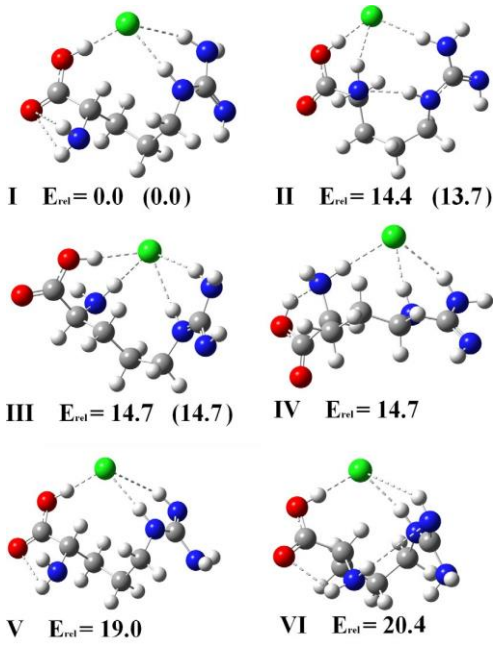

Figure 3.3; Structures of the six lowest-energy (MP2/6-311+G**) conformers of $Cl^-.Arg_{can}$, labelled from I to VI. Relative energies (kJ/mol) are displayed, with ZPE corrected values in parentheses.

It is worth noting that for $Br^-.Arg$, where $Br^-.Arg_{zwit}$ lies below $Br^-.Arg_{can}$, the halide ion is more strongly bound to the Arg moiety in the canonical form. $Cl^-.Arg$ shows a similar correlation, i.e. $Cl^-.Arg_{can}$ is now lower in energy, while the $Cl^-.Arg_{zwit}$ is bound more strongly. Similar trends were observed for the binding energies of the BH_4-glycine complex.[140] These results illustrate that the factors affecting the relative stabilities of the zwitterionic and canonical forms of the amino acid are much more complex than simply by how strongly the halide ion binds to the Arg, but that the overall balance of non-covalent interactions within the binary complex must be considered.[156]

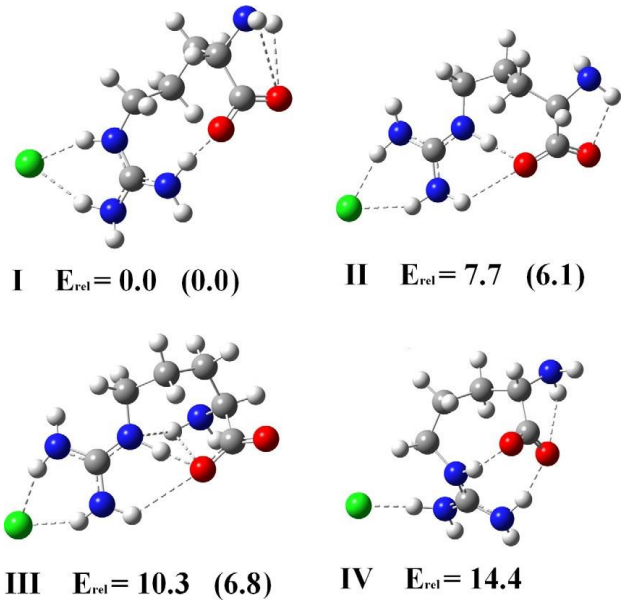

Figure 3.4; Structures of the four (MP2/6-311+G**) conformers $Cl^-.Arg_{zwit}$, labelled from I to IV. Relative energies (kJ/mol) are displayed, with ZPE corrected values in parentheses.

Table 3.4; MP2/6-311+G** absolute, ZPE corrected values (in parentheses) and ΔG^o_{298} (in parentheses in bold) of the lowest-energy conformers of the canonical and zwitterionic forms of Br^-Arg and Cl^-Arg

	Canonical (Hartrees)	Zwitterionic (Hartrees)	$\Delta E_{can\text{-}zwit}$ (Hartrees)	$\Delta E_{can\text{-}zwit}$ (kJ/mol)
Br^-.Arg	-3177.6954	-3177.6956	0.0002	0.5
	(-3177.4695)	(-3177.4713)	(0.0018)	(4.7)
	(**-3177.5129**)*	(**-3177.5160**)	(**0.0031**)	(**8.1**)
Cl^-.Arg	-1064.8428	-1064.8364	-0.0064	-16.8
	(-1064.6162)	(-1064.6106)	(-0.0056)	(-14.7)
	(**-1064.6586**)	(**-1064.6536**)	(**-0.0050**)	(**-13.1**)

* This value is for isomer III for $^{Br\text{-}.Arg}_{can}$ since this is the lowest energy ΔG^o_{298} isomer.

Table 3.5; MP2/6-311+G** counterpoise corrected binding energies of the lowest-energy conformers (**I**) of the canonical and zwitterionic forms of Br^-.Arg and Cl^-.Arg.

	Canonical (eV)	Zwitterionic (eV)	Canonical (kJ/mol)	Zwitterionic (kJ/mol)
Br^-.Arg (**I**)	-1.638	-1.610	-158.1	-155.3
Cl^-.Arg (**I**)	-1.890	-1.905	-182.4	-183.8

3.4 Conclusions

Comparing the computational and experimental results, the calculations predict that the zwitterionic cluster is likely to be more prevalent for Br^-.Arg, while the canonical tautomer will dominate for Cl^-.Arg.[87] Taking the non-zero-point energy corrected energies, the population ratio of zwitterionic/canonical for Br^-.Arg is predicted to be 55:45 while for Cl^-.Arg the zwitterion is expected to be present at only 0.1%. The results of the CID study, are in line with these results, since the CID signature of a zwitterionic system is much more prevalent for Br^-.Arg, with the CID pattern for Cl^-.Arg being consistent with a canonical cluster. Furthermore, the CID experiments are consistent with a mixture of tautomers being present in the experimental ensemble for Br^-.Arg.

The IRMPD spectrum of Cl^-.Arg was interpreted by O'Brien *et al*. as being dominated by spectral features associated with Arg being in the zwitterionic form.[141] This result seems at odds with the predictions from the calculations presented in this chapter for the Cl^-.Arg cluster. One explanation of this apparent discrepancy could be that kinetic bottlenecks exist on the photofragmentation potential energy surface for the canonical clusters: such effects have been observed in previous IRMPD experiments.[157] Indeed, a very recent study by

Schmidt and Kass on the related proline-chloride anion system has found that although both zwitterionic and canonical clusters are expected to be populated under the experimental conditions, only the canonical clusters can be observed using IRMPD.[151] This observation was determined to be due to the presence of a fragmentation bottleneck, leading the authors to conclude that both spectral and kinetic data are required to determine the structure of the proline-chloride anion cluster. An alternative, and highly desirable approach for future work would be to study these systems using cryogenic messenger tagged-ion methods.[158] In this technique, cold ions are produced in complexes with weakly-bound inert species (e.g. H_2) that are transparent in the IR region. These 'messenger' complexes can be readily dissociated upon absorption of a single IR photon resonant with one of the vibrational transitions associated with the cold ion, so that action spectra equivalent to a linear absorption spectrum can be recorded.[159]

The calculations presented in this chapter are the first optimized MP2 level calculations of an amino acid–anion cluster that directly link to an experimentally observed system, and provide lessons for future calculations on such systems. Of vital importance, these results illustrate the exigency of determining reliable energies for a large number of conformer families in order to achieve a proper representation of canonical and zwitterionic relative energies, i.e. the relative energies of canonical and zwitterionic forms are within the range of the relative energies of different conformers. In previous work on such systems, the importance of conformeric structure has often been underestimated, presumably due to the assumption that the tautomeric energy differences would dominate the overall energetics. The calculations also show that it is not good practice to simply exchange the anion in order

to obtain reliable relative energies for the larger, more computationally expensive halides. Both of these points can be directly attributed to the subtle balance of non-covalent interactions that determines the relative isomer energies of these structurally rich cluster systems that are now prototypes for understanding isolated anion–amino acid interactions.[141, 160]

Chapter 4

Evaluating the performance of the M06 suite of functionals for Conformationally Flexible Anionic Clusters

4.1 Introduction

The investigation of isolated biological molecules has developed into a rapidly growing research field over recent years.[88, 126, 158, 161-174] Understanding the factors that contribute to the geometric structure of systems where there is a high degree of flexibility is exceedingly challenging, and one of the key motivations of this research. In the gas-phase environment, interactions with counterions or solvent molecules can be disregarded.[163] Pertubations from solvent or counterions can be investigated through the study of molecular clusters.[161] This general approach follows the tradition of gas-phase cluster studies of smaller molecular systems, where considerable progress has been made in understanding the details of microsolvation.[1, 3, 4, 175] These gas-phase studies can provide crucial benchmarking data, allowing a critical assessment of the reliability of computational approaches to molecular structure determination. A particularly strong link exists between computational chemistry and gas-phase laser spectroscopic studies, since accurate calculations are essential for interpreting the spectra obtained.[156]

Despite the considerable size of some of the gaseous biological molecules and molecular clusters that are now amenable to study with high-resolution spectroscopic techniques, calculations generating geometric structures and vibrational frequencies using suitably accurate ab-initio computational methods (*i.e.* MP2 level calculations with a triple-zeta quality basis set) can still be extremely challenging. Time-tested density functionals, such as the ubiquitous B3LYP functional for instance, can provide a good alternative for systems where the energetics are dominated by hydrogen-bonding interactions.[167, 169, 171] However, many of the gas-phase biological systems now being explored with spectroscopic methods contain significant dispersion interactions. For these systems, it is often preferable to use contemporary density functions, specifically developed for describing the long-range correlation phenomena that constitute dispersion interactions.[176] A general problem with the application of density functional theory, however, is that it does not dictate a straightforward approach to determining reliable results, and it is therefore essential to test how accurate a specific density functional is for a particular type of molecular system. This can be particularly important for charged species, since ionic molecules are not often used in benchmarking studies.[176]

In this chapter, a study is presented to assess the suitability of the M06 suite of density functionals for calculating the relative conformer energies and geometric structures of anionic systems which potentially contain dispersion interactions as a key type of interaction.[176-178] While these functionals have already been widely tested for uncharged molecular systems,[179-181] little work has been done until very recently to assess their performance for negatively charged molecules.[150, 182] Herein is reported a computational study of two halide ion amino-acid complexes, Cl^-·arginine and Br^-·arginine (hereafter

abbreviated as $X^{-}\cdot$Arg, X = Cl, Br). These complexes are suitable to be used as prototypical complexes for exploring the phenomenon of zwitterion formation in a gas-phase amino acid induced by an anion, which has very recently been identified in some experimental studies.[87, 141, 151, 160] Conformational structure and non-covalent interactions have been shown to be very important for the relative energies of tautomers of these clusters[183], and they therefore represent an excellent anionic computational test system. Whilst other functionals have been shown to perform better for structures where dispersion interactions are prevalent, [150, 179-182] M06 was selected for this study as the complexes studied here contain both electrostatic and dispersion interactions. Additionally, the bio-anion complexes studied here are an important experimental target,[87, 141] and typical of the type of anionic biomolecular system that is now amenable to study with laser spectroscopy.

Dispersion interactions have always been difficult to explore using the most widely used density functionals due to the difficulty in expressing the long-range correlation coefficients which also account for the balance between correlation and exchange in a functional.[184, 185] Recently, progress has been made by using semi-local or hybrid functionals. These contain a significant number of free parameters in the functional form which can then be semi-empirically fit using broad experimental data sets inclusive of non-covalent interactions. This general approach has been used in the M06 suite of functionals, which scale in the amount of the exact Hartee-Fock exchange included with M06 including 27% of the HF exchange, M06-2X including 54% and M06-HF including 100%.[176-178] The suite has been proven highly successful at describing dispersion interactions for neutral molecular systems, particularly M06-2X which has an s6 scaling factor of Grimme's long range dispersion correction of only 0.06.[176, 186] In this chapter, MP2 results for the multiple conformers of

both Cl^{-}·Arg and Br^{-}·Arg are presented, to allow comparison against the M06 functionals, as well as the popular B3LYP (a hybrid generalised gradient approximation functional) functional for comparison.[187, 188] MP2 calculations were used as the standards in this experiment as they generally represent a level of computational expense that gives good accuracy at the cost of time taken to perform the calculation. A general hierarchy of computational chemistry methods might look something like:

$$HF < DFT < MP(2,3,4 \text{ etc.}) << CCSD < CCSD(T).$$

As we proceed through the hierarchy we experience, generally, higher accuracy, but also more computational expense for a given system. By choosing MP2 as the standards, we have the chance to compare the accuracy versus computational expense argument for 'neighbouring' computational methodology.

X^{-}·Arg is conformationally flexibile in both of its tautomeric forms, thus calculating the geometries of the lowest-energy structures is somewhat difficult. (Fig. 4.1). The conformational space of the X^{-}·Arg ion-molecule cluster was explored to generate initial conformeric structures and then an automated process was used to sort the obtained conformers into conformational families. This procedure both retains a good sized sample of structures for higher-level analysis and also reduces the number of conformationally similar structures, thus reducing the number of unnecessary calculations, and automates the strategy previously used in studies of deprotonated Adenosine 5'-triphosphate and its sodiated analogue.[146, 147]

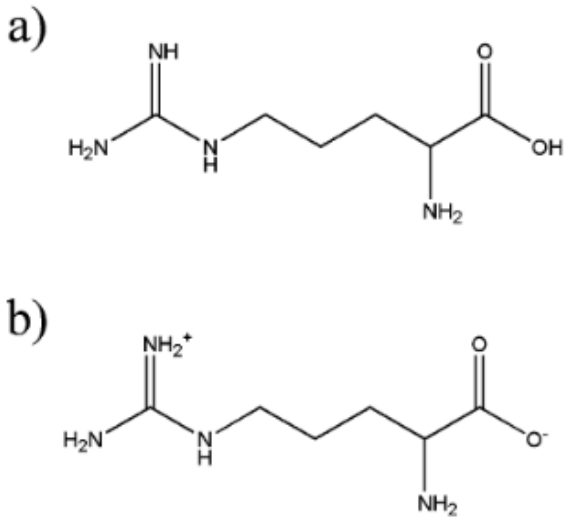

Figure 4.1; Lowest energy a) canonical structure and
b) zwitterionic structure of arginine

4.2 Computational Methods

Initial conformational searches of the zwitterionic and canonical (lowest energy) forms of Arg, illustrated in Fig. 4.1, complexed to a halide ion in the X^-·Arg (X = Cl, Br) complex were performed using the MMFF94 force fields and a Monte Carlo algorithm as implemented in the Spartan '08 package,[144] generating 100,000 initial structures. The 100 lowest energy structures, corresponding to 0.1% of the total number of generated conformers, for each of the two tautomeric isomers were subdivided into families based on the similarities between their intermolecular interactions using an automated procedure described below. Gaussian '09[148] was used to optimise single conformers from each of the conformer families identified, first at the HF/6-311+G* level (with counterpoise correction) and then at the MP2/6-311+G** level. (Geometry optimizations were also performed with

all functionals.) The basis set choice was made so as to be of reasonable quality, whilst still providing facile MP2 calculations for this relatively large system. Additional calculations were performed using the M06, M06-2X, M06-HF, and B3LYP density functionals,[176-178, 187] taking the MP2 optimized conformers as starting structures. Frequency calculations (MP2/6-311+G**) were performed just for the three lowest energy conformers of each tautomer, to allow the calculation of MP2 zero-point energy corrections. MP2 frequency calculations for all of the conformers presented here would have been prohibitive, and were therefore omitted. Frequency calculations were performed with the B3LYP functional for all of the conformers studied to test the integrity of the geometric structures and confirm that a true minima had been found. No negative frequencies were obtained, indicating that these were indeed true minima. Standard convergence criteria were initially employed in all calculations, but for the DFT calculated structures where the associated relative energy diverged significantly from the MP2 value, the structures were re-optimized with a finer grid to confirm the integrity of the result. Vertical detachment energies (VDEs) for the $X^{-}\cdot$Arg anionic clusters were calculated as the energy difference between the anion and the corresponding neutral, frozen at the optimized anion geometry. This would give the energy difference at the exact moment of electron detachment. The uncertainties in the calculated MP2 relative energies within conformer sets are expected to be on the order of 2 kJ/mol.[150]

In the group's previous studies of conformationally flexible molecular ions, conformational families were identified by inspection.[146, 147] For this work, a home-developed computer program, AUTODETECT, was used. This program automates and more formally defines the process of familial identification and the sorting of structures into families, by consideration of a number of user-defined characteristics. For the $X^{-}\cdot$Arg complexes, the

dominant intermolecular interactions are hydrogen bonds, however, the process of familial classification used here can be applied to structures displaying any columbic type interaction (H-bonding, dipole-dipole or anion-cation). All potential hydrogen-bonding centres in the X^-·Arg complexes were identified as either an electropositive centre (H atoms) or an electronegative centre (O, N, or Cl/Br atoms). Figure 4.2 illustrates these assignments. A matrix of distances for all possible hydrogen-bonding interactions was then calculated including both the electropositive centre and electronegative centre interactions. Where the distance was less than a selected critical value (3.5 Å in this study) the two centres were considered as interacting groups.

4.3 Results and Discussion

4.3.1 X^-·Arg

4.3.1.1 Description of the Conformer Families for Br-·Arg and Overview of Structures

Figure 4.3 shows eighteen distinct conformer families of the Br^-·Arg cluster, with Arg in its canonical form. Each of these structures displays an individual set of non-covalent interactions, listed in Table 4.1. The MP2/6-311+G** structures are displayed with structure I having the lowest energy and XVIII as the highest. Upon inspection it is revealed that most structures contain 4 or 5 hydrogen bonds. In the lowest-energy conformers, the Br^- additionally forms either three or four ionic hydrogen bonds with neutral Arg, through

combinations of electrostatic interactions with the carboxylic acid -OH, the guanidine –NHs, and the amine -NHs.

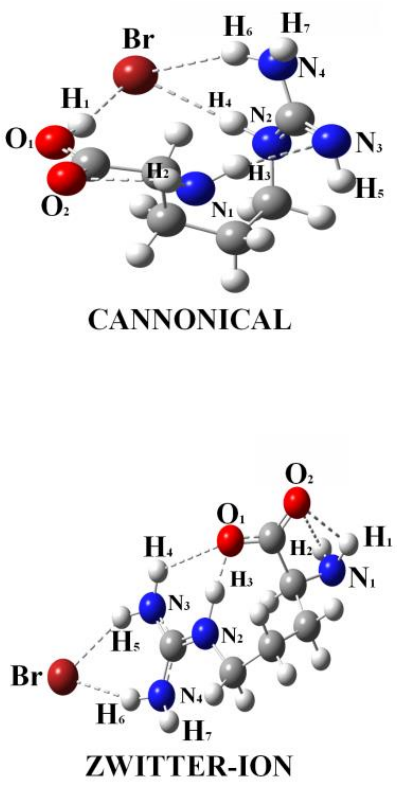

Figure 4.2; Diagram showing atom labels used to describe the canonical and zwitterionic forms of Br^{-}·Arg.

For example, in the lowest energy conformer I, the Br^{-} forms three ionic hydrogen-bonds, to the carboxylate -OH, and the -N4H7 and -N2H4 guanidine groups, with two additional Arg intramolecular hydrogen bonds being present (O2-H2 and N3-H2,3), while in conformer II, the Br- sits in a pocket of four ionic hydrogen bonding interactions (to the carboxylate -OH, the amine -NH, and the -N4H7 and -N2H4 guanidine groups). The involvement of the -N4H7 and -N2H4 guanidine groups is a common feature of many of the lowest energy

conformers (i.e. I, II, III, IV, VI), and can therefore be considered a key structural motif for the Br^{-}·Arg complex. The higher-energy conformers display fewer Br^{-} ionic hydrogen-bonds, although this is sometimes compensated for by a greater number of Arg intramolecular hydrogen-bonds. It is notable that in the structures where the Br- forms a single, near-linear, ionic hydrogen bond, i.e. conformers XIV (178.7^{o}), XVI (179.3^{o}) and XVII (178.4^{o}), there are three or four Arg intramolecular bonds present (O2-H2 and O2-H3 are H-bonded in all three conformers).

The corresponding low-energy conformer families for the Br-·Arg cluster, with Arg in the zwitterionic form, are illustrated in Figure 4.4. The MP2/6-311+G** structures displayed are labelled I-VI in order of increasing energy. Each of the structures interactions are defined in Table 4.2. There are only 6 conformational families for the zwitterionic structure, compared to the 18 families for the canonical structure. Whilst rather striking, this can be attributed to the greater number of strong ion-dipole interactions that are present compared to the canonical cluster, these stronger interactions cause many of the favoured conformations to fall within a smaller number of families.

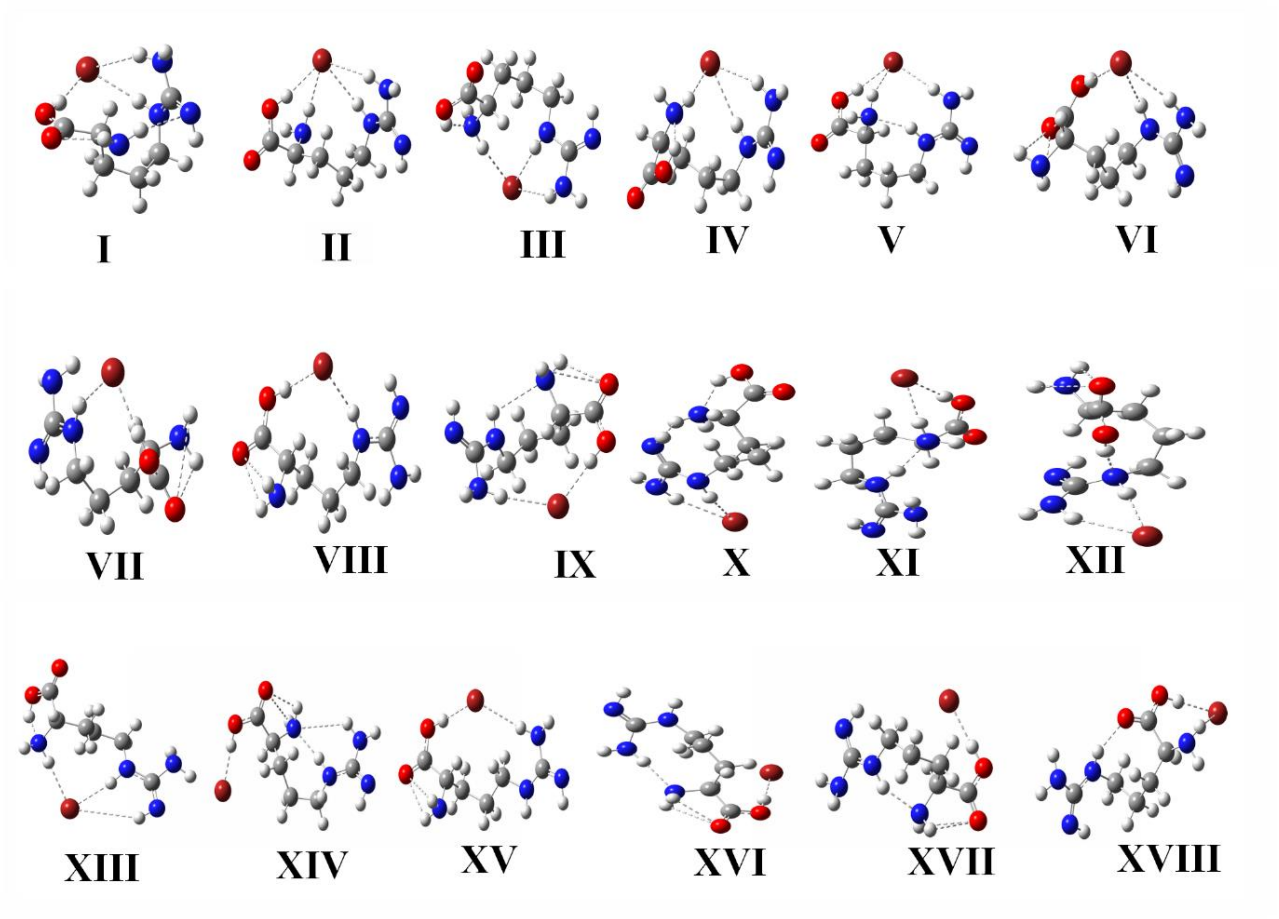

Figure 4.3; The 18 Families of the canonical form of Br^{-}·Arg

Inspection of the structures reveals that each of the conformers is characterised by either five or six hydrogen bonds, slightly more than in the canonical structures. In the four lowest-energy conformer structures (I-IV), the Br^{-} ion forms two ionic hydrogen-bonds with the -N4H6 and -N3H5 guanidium groups, with further intramolecular hydrogen bonds being present, whereas in the two highest-energy conformer families (V and VI), the Br^{-} forms a single, near linear, hydrogen-bond to the –N4H6 guanidinium group (174.2^{o} and 170.7^{o}, respectively), with four additional intramolecular hydrogen bonds being present.

Table 4.1: Relative Energies (kJ/mol) of the low-energy conformers of the canonical form of Br^{-}·Arg at the MP2, M06, M06-2X, M06-HF, and B3LYP levels.[a,b]

Family	MP2	M06	M06-2X	M06-HF	B3LYP	B3LYP-ZPE corrected[c]
I	0.00	0.00	0.00	0.00	0.00	0.00
II	1.11	0.29	3.05	4.33	-1.32	1.26
III	3.23	6.13	9.63	7.97	-5.32	-2.78
IV	7.49	7.25	12.81	13.08	2.76	6.65
V	7.81	6.06	7.61	8.23	0.53	1.63
VI	10.09	9.28	9.37	9.67	10.90	12.05
VII	13.79	16.65	18.37	16.58	12.15	13.14
VIII	15.90	16.12	19.01	19.82	8.68	9.33
IX	16.20	15.15	15.57	15.12	12.85	13.81
X	20.44	18.00	21.33	19.76	16.97	21.04
XI	20.72	23.32	24.00	21.06	11.30	12.91
XII	23.30	33.68	31.33	30.34	21.74	25.71
XIII	25.85	26.33	28.98	27.13	16.69	18.57
XIV	27.15	24.97	26.55	23.48	12.25	13.00
XV	28.11	25.73	27.11	28.02	16.56	16.54
XVI	28.49	27.77	25.22	23.82	19.33	21.42
XVII	28.97	32.65	31.50	29.16	21.82	23.30
XVIII	34.83	34.96	33.72	36.27	23.19	24.01
Mean Unsigned Error		2.10	2.75	2.44	6.71	-

[a] All calculations were conducted with the 6-311+G** basis set.

[b] The absolute energies of conformer I are −3177.69537730, -3180.4997678, -3180.7945232, -3181.0973308 and -3181.02070180 at the MP2 and M06, M06-2X, M06-HF and B3LYP levels, respectively.

[c] The mean unsigned error in the relative energies for the zero point energy corrected values compared to the uncorrected values is 1.60 kJ/mol, giving an estimate of the expected error when zero point corrections are omitted.

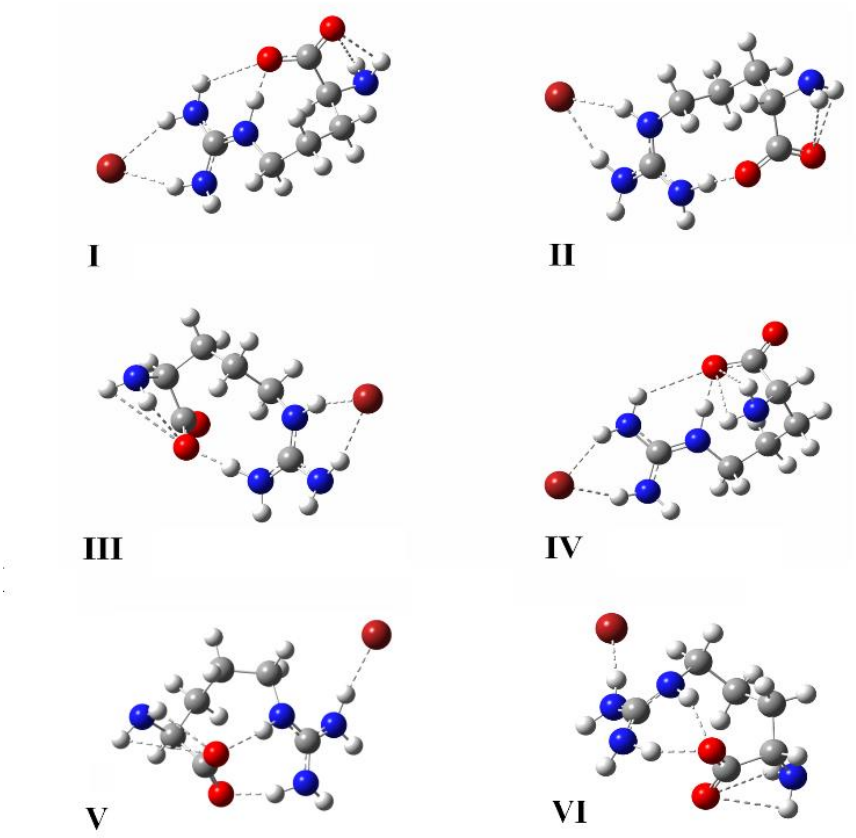

Figure 4.4; The 6 families of the zwitterionic tautomer of Br^{-}·Arg clusters

4.3.1.2 Energies of the conformers of Cl-·Arg: Comparing MP2 and DFT Energies

Dispersion interactions play a lesser role in Cl-·Arg cluster structure energetics, and so the relative energies should not be as great a challenge for the density functionals as in the Br-·Arg system. The M06, M06-2X and M06-HF relative energies for the canonical conformers of Cl-·Arg (Table 4.3) are in good, general agreement with the MP2 values. The conformer I - conformer II energy gap is well replicated by all three functionals, and all predict the correct energy ordering for conformers I – IV, for example.

Table 4.2: Relative Energies (kJ/mol) of the low-energy conformers of the zwitterionic form of Br^-·Arg at the MP2, M06, M06-2X, M06-HF, and B3LYP levels.[a,b]

Family	**MP2**	**M06**	**M06-2X**	**M06-HF**	**B3LYP**	**B3LYP-ZPE corrected[c]**
I	0.00	0.00	0.00	0.00	0.00	0.00
II	5.88	4.76	4.40	5.14	6.17	8.97
III	8.86	8.55	8.38	8.45	11.80	14.24
IV	14.79	9.30	13.92	11.98	15.89	15.82
V	19.05	17.18	19.39	24.13	26.25	29.53
VI	21.19	15.40	20.09	28.45	26.66	29.69
Mean Unsigned Error		2.92	0.85	3.26	3.40	-

[a] All calculations were conducted with the 6-311+G** basis set.
[b] The absolute energies (in Hartrees) of conformer I are -3177.6956156, -3180.501852, -3180.7952854, -3181.1035279 and -3180.0310293 at the MP2 and M06, M06-2X, M06-HF and B3LYP levels, respectively.
[c] The mean unsigned error in the relative energies for the zero point energy corrected values compared to the uncorrected values is 2.3 kJ/mol, giving an estimate of the expected error when zero point corrections are omitted.

The M06 results lie closest to the MP2 results (with the exception of the conformer IX energy). As for the Br-·Arg results, the match between the M06 suite of functional results and MP2 was considerably better than for B3LYP. (it should be noted that both B3LYP and M06-HF give energy orderings that disagree with the MP2 predictions.) The mean unsigned errors from the MP2 values are 2.36, 2.87, 3.19 and 5.27 kJ/mol, respectively for M06, M06-2X, M06-HF and B3LYP, respectively. Looking at both Cl and Br systems, the M06 functional performs best at reproducing the conformer relative energies compared to MP2. Conformer VII, a structure where the alkyl section of the amino acid is in relatively close proximity to the halide ion, appears to prove challenging for all of the density functionals, with the discrepancy increasing on going from M06 to M06-2X to M06-HF. Figure 4.5a displays the MP2, M06, M06-2X and B3LYP relative energies graphically, to emphasize

how close the M06 calculated energies are to the MP2 benchmarks, as well as the lacklustre performance by B3LYP compared to both the M06 functionals and MP2.

Table 4.4 displays the relative energies for the zwitterionic conformers of Cl-·Arg, with Figure 4.5b displaying the results graphically. The MP2 benchmark relative energies predict that the lowest energy conformer family I of Cl-·Arg is at a considerably lower energy than the other three conformers (II-IV). These are then fairly evenly spaced energetically at 7.71, 10.33 and 14.41 kJ/mol. The Cl^{-}·Arg cluster energy ordering have been correctly predicted by all functionals, even B3LYP, thus as a test of the suitability of the different functionals in comparison to MP2 energies, the zwitterions are not as reliable. The mean unsigned errors from the MP2 conformer relative energies are 3.55, 1.23, 2.77 and 3.15 kJ/mol, for M06, M06-2X, M06-HF and B3LYP, respectively. Therefore, as for the zwitterionic Br-·Arg cluster, M06-2X gives the best density functional results for the zwitterionic Cl-·Arg conformers, with its relative energies most closely mirroring the MP2 energy ordering. It is notable that B3LYP performs better than M06 for this set of calculations.

Table 4.3: Relative Energies (kJ/mol) of the low-energy conformers of the canonical form of Cl^{-}·Arg at the MP2, M06, M06-2X, M06-HF, and B3LYP levels.[a,b]

Family	**MP2**	**M06**	**M06-2X**	**M06-HF**	**B3LYP**
I	0.00	0.00	0.00	0.00	0.00
II	14.38	12.66	12.07	11.62	9.37
III	14.68	13.33	13.46	13.85	9.21
IV	14.72	15.72	18.54	17.95	6.84
V	19.05	21.24	21.09	20.23	18.11
VI	20.38	21.07	20.01	18.66	21.70
VII	21.02	15.11	13.94	7.96	12.80
VIII	29.62	30.74	26.38	22.99	27.18
IX	29.83	21.41	33.08	28.92	27.52
X	33.30	33.76	35.93	33.31	25.11
XI	33.92	36.30	38.26	34.47	35.78
XII	38.95	38.70	38.59	40.25	40.18
XIII	38.98	37.87	39.72	37.23	38.40
XIV	40.29	41.40	38.36	39.20	38.74
XV	46.54	43.41	43.45	42.14	38.54
XVI	53.60	52.42	49.65	47.86	38.37
XVII	59.18	53.39	53.58	53.27	45.19
Mean Unsigned Error		2.36	2.87	3.19	5.27

[a] All calculations were conducted with the 6-311+G** basis set.
[b] Conformer I absolute energies are -1064.842816, -1066.675672, -1066.816540, -1066.901110, and -1067.098388 Hartrees with MP2, M06, M06-2X, M06-HF, and B3LYP, respectively.

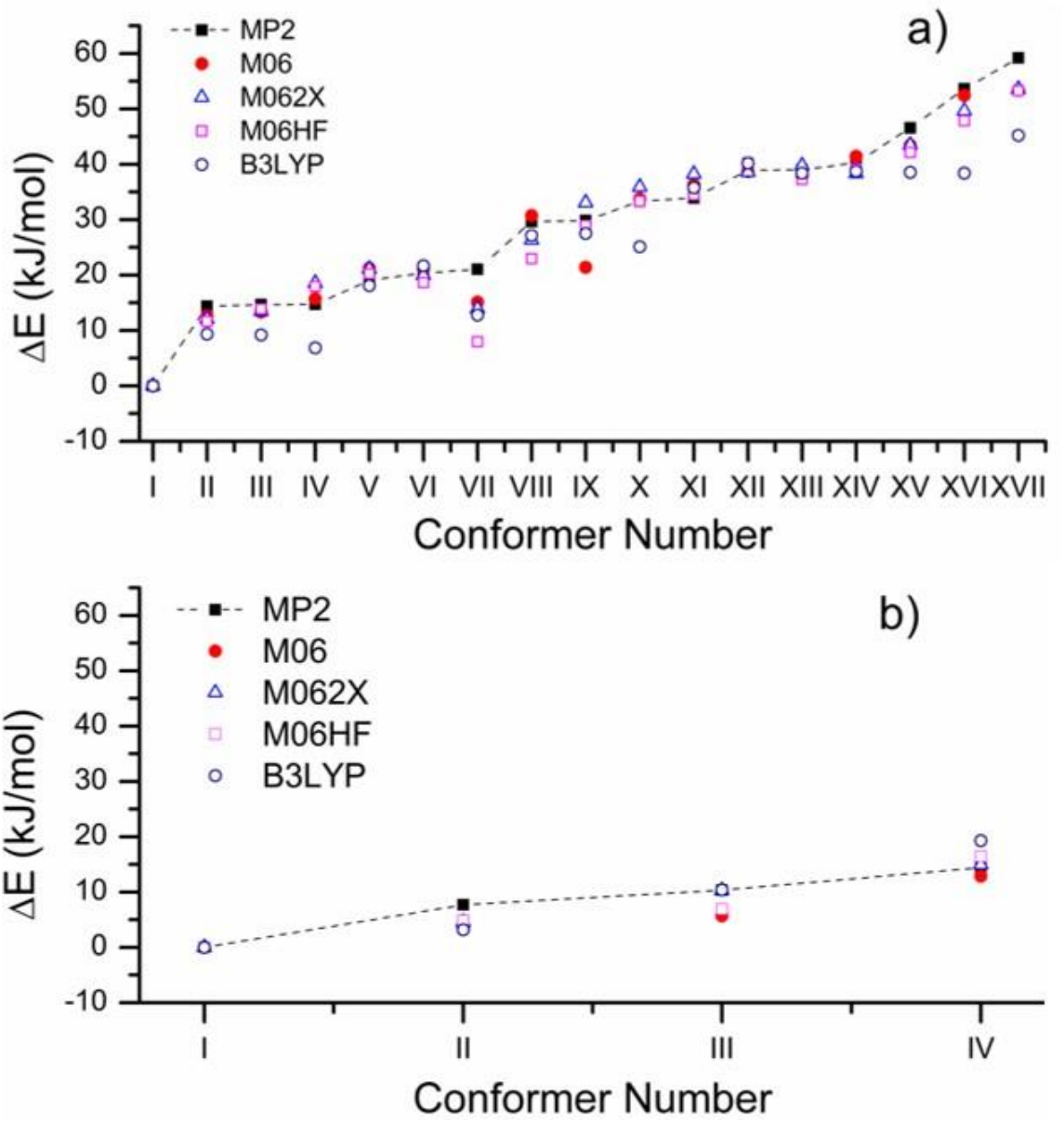

Figure 4.5; a) Canonical and b) Zwitterionic tautomer energy comparisons between different functionals

Table 4.4: Relative Energies (kJ/mol) of the low-energy conformers of the zwitterionic form of Cl^-·Arg at the MP2, M06, M06-2X, M06-HF, and B3LYP levels.[a,b]

Family	**MP2**	**M06**	**M06-2X**	**M06-HF**	**B3LYP**
I	0.00	0.00	0.00	0.00	0.00
II	7.71	3.23	4.57	4.85	3.18
III	10.33	5.72	10.31	6.92	10.37
IV	14.41	12.86	14.95	16.45	19.29
Mean Unsigned Error		3.55	1.23	2.77	3.15

a All calculations were conducted with the 6-311+G** basis set.
[b] The absolute energies (in Hartrees) of conformer I are -1064.8363579, -1066.6721231, -1066.8124088, -1066.9017785, -1067.1017602 at the MP2 and M06, M06-2X, M06-HF, and B3LYP levels, respectively.

4.3.1.3 Structural parameters of the Cl-·Arg conformers: Comparing MP2 and DFT results

Predictions with all halide-arginine clusters show good agreement between M06 and M062-X functional values and MP2 values. Tables 4.5 and 4.6 present the hydrogen bond lengths for conformers **I** – **IV** of canonical and zwitterionic Cl^-·Arg, respectively at the MP2, M06, M06-2X, M06-HF and B3LYP levels of theory. Overall, the performance of M06-2X is slightly better than M06 in terms of agreement with the MP2 values. The B3LYP functional reproduces the general conformer structures reliably, but there is a greater discrepancy in the calculated hydrogen bond lengths compared to the M06 functionals.

4.3.2 Vertical detachment energies of X-·Arg (X = Cl, Br) clusters

One of the motivating factors for this study of halide-amino acid complexes, was the possibility to experimentally identify zwitterionic or canonical structures through measurement of their vertical detachment energies (VDEs) using photodetachment photoelectron spectroscopy. Specific measured energies could highlight the presence of a canonical or zwitterionic form in a given cluster under study. To investigate this possibility, VDEs were calculated for all of the studied conformers of Br^-·Arg and Cl^-·Arg. In brief, the eighteen canonical conformers of Br^-·Arg are associated with VDEs that range from 5.50 – 6.46 eV, while the zwitterionic conformers have VDEs from 5.35 – 7.02 eV. (For Cl^-·Arg, the corresponding ranges are 4.71 – 5.84 eV and 5.14 – 5.69 eV, respectively.) Although the average VDE is higher for the zwitterionic complexes than the canonical clusters for both systems, there is not a simple relationship between VDE and tautomer structure. This is partly due to the ionization site not being localised on the halide ion, but also due to the different relative orientations of the –COOH and –NH-C(NH_2)NH groups in the canonical forms in particular, as pointed out by Skurski *et al.* in their study of isolated Arg.[142]

Tables 4.7 and 4.8 also present the calculated neutral dipole moments (*i.e.* the electric dipole moment for the neutral species at the optimised anionic conformer geometry) for both tautomers of the clusters. These values are again of interest for experimental measurements of the dipole-bound excited states of these systems.[127, 189] For Cl^-·Arg, there is a reasonable separation of the neutral dipole moments for the canonical and zwitterionic clusters indicating that the measurement of dipole-bound excited states could provide a means of distinguishing the tautomers. (The spread of values is more mixed for the two tautomers of Br^-·Arg, suggesting that a definitive measurement would be more challenging here.) It would

be useful to explore the potential for such experiments in the I^-·Arg cluster, where the VDE of I^- is lower (and hence the ionization site more localized) than for the halide ions studied here.[190]

Table 4.5: Comparison of calculated hydrogen-bond distances (Å) for canonical Br^-·Arg.[a]

	Family	Br-H1	Br-H2	Br-H3	Br-H4	Br-H5	Br-H6	Br-H7	O2-H2	O2-H3	N1-H1	N3-H2	N3-H3	N2-H1	N1-H4	O2-H4	N1-H6	N1-H7
I	**MP2**	2.21	x	x	2.37	x	2.64	x	2.21	x	x	x	2.50	x	x	x	x	x
	M06	2.25	x	x	2.42	x	2.65	x	2.22	x	x	x	2.55	x	x	x	x	x
	M062X	2.26	x	x	2.43	x	2.67	x	2.21	x	x	x	2.47	x	x	x	x	x
	M06HF	2.21	x	x	2.38	x	2.69	x	2.20	x	x	x	2.44	x	x	x	x	x
	B3LYP	2.21	x	x	2.47	x	2.71	x	2.35	3.22	x	x	x	x	x	x	x	x
II	**MP2**	2.28	2.47	x	2.55	x	2.61	x	x	3.50	2.67	x	x	x	3.08	x	x	x
	M06	2.30	2.50	x	2.56	x	2.63	x	x	3.52	2.67	x	x	x	3.13	x	x	x
	M062X	2.32	2.51	x	2.63	x	2.62	x	x	3.50	2.67	x	x	x	3.04	x	x	x
	M06HF	2.27	2.47	x	2.53	x	2.66	x	x	3.53	2.66	x	x	x	3.12	x	x	x
	B3LYP	2.32	2.55	x	2.62	x	2.76	x	x	3.49	2.71	x	x	x	3.14	x	x	x
III	**MP2**	x	2.43	3.70	2.33	x	2.68	x	x	x	1.76	x	x	x	3.19	x	x	x
	M06	x	2.44	3.73	2.38	x	2.63	x	x	x	1.81	x	x	x	3.20	x	x	x
	M062X	x	2.66	3.36	2.37	x	2.69	x	x	x	1.81	x	x	x	2.99	x	x	x
	M06HF	x	2.86	2.99	2.31	x	2.71	x	x	x	1.73	x	x	x	2.81	x	x	x
	B3LYP	x	2.48	3.80	2.43	x	2.70	x	x	x	1.79	x	x	x	3.28	x	x	x
IV	**MP2**	x	2.51	x	2.58	x	2.50	x	x	x	1.81	x	x	x	x	x	x	x
	M06	x	2.53	x	2.60	x	2.52	x	x	x	1.85	x	x	x	x	x	x	x
	M062X	x	2.56	x	2.66	x	2.53	x	x	x	1.86	x	x	x	x	x	x	x
	M06HF	x	2.57	x	2.62	x	2.51	x	x	x	1.80	x	x	x	x	x	x	x
	B3LYP	x	2.56	x	2.68	x	2.57	x	x	x	1.84	x	x	x	x	x	x	x

[a] x refers to no hydrogen bond (i.e. r > 3.5Å).

Table 4.6: Comparison of calculated hydrogen-bond distances (Å) for zwitterionic Br^{-}·Arg.[a]

	Family	O1-H1	O1-H2	O2-H1	O2-H2	O2-H3	O2-H4,5	O1-H4,5	Br-H4,5	Br-H6,7	Br-H3
I	**MP2**	2.31	3.05	x	x	1.42	2.77	x	2.39	2.27	x
	M06	2.26	3.07	x	x	1.58	2.58	x	2.39	2.29	x
	M062X	2.30	3.01	x	x	1.39	2.76	x	2.43	2.31	x
	M06HF	2.31	3.04	x	x	1.36	2.74	x	2.43	2.28	x
	B3LYP	2.28	3.08	x	x	1.51	2.84	x	2.44	2.31	x
II	**MP2**	2.38	3.09	x	x	x	1.58	x	x	2.32	2.26
	M06	2.31	3.04	x	x	x	1.62	x	x	2.31	2.34
	M062X	2.34	3.03	x	x	x	1.54	x	x	2.33	2.36
	M06HF	2.40	3.09	x	x	x	1.40	x	x	2.30	2.34
	B3LYP	2.32	3.07	x	x	x	1.60	x	x	2.34	2.36
III	**MP2**	x	x	2.24	3.08	x	1.55	2.90	x	2.33	2.28
	M06	x	x	2.19	3.11	x	1.64	2.97	x	2.31	2.35
	M062X	x	x	2.27	3.04	x	1.52	2.97	x	2.32	2.38
	M06HF	x	x	2.29	3.07	x	1.40	2.89	x	2.30	2.36
	B3LYP	x	x	2.25	3.14	x	1.59	3.08	x	2.33	2.38
IV	**MP2**	x	x	3.07	2.61	1.41	2.69	x	2.37	2.27	x
	M06	x	x	3.07	2.62	1.42	2.70	x	2.43	2.29	x
	M062X	x	x	3.11	2.60	1.40	2.71	x	2.44	2.30	x
	M06HF	x	x	3.07	2.67	1.35	2.69	x	2.44	2.26	x
	B3LYP	x	x	3.16	2.59	1.51	2.77	x	2.43	2.31	x

[a] x refers to no hydrogen bond (i.e. r> 3.5Å).

4.4 Conclusions

The X-·Arg (X = Cl, Br) results presented in this chapter indicate that the M06 suite of density functionals perform well compared to MP2 for predicting the structures and relative energies of the conformeric isomers of both the canonical and tautomeric forms of the amino

acid clusters. Importantly, M06, M06-2X and M06-HF accurately predict the identity of the global minimum conformer for each system, and also correctly predict the energy ordering of lowest energy conformers. Conversely, B3LYP was found to struggle with predicting even the trends in relative energies for the canonical tautomers of Br-·Arg. For the canonical tautomers of both Cl-·Arg and Br-·Arg, the M06 functional gave the lowest mean unsigned errors for the conformer relative energies compared to the MP2 results, while for the corresponding zwitterionic tautomers, the M06-2X functional performed best. These results emphasise the importance of evaluating the performance of density functional for specific types of molecular systems, since even within the limited test set considered in this work, different functionals have been found to work better for different tautomers. The X-·Arg complex studied here is challenging, since each conformeric structure contains many inter- and intramolecular hydrogen bonds as well as dispersion interactions. With this taken into consideration, discrepancies between relative energies calculated by functionals and MP2 are unsurprising, and the strong overall agreement between the tested functionals and MP2 values is impressive in this context.

With regards to comparative studies, at the time of writing, our group was aware of only two other recent studies that have investigated the applicability of the M06 functionals to anionic systems. Mardissian *et al.* studied the performance of 24 density functionals, including M06 and M06-2X, for predicting the energies of 49 sulphate water clusters, while Jones *et al.* assessed the suitability M06-2X for describing halide ion-π interactions.[150, 182] For the sulphate water clusters, M06-2X performed very well (root mean square deviation = 1.46

kJ/mol) compared to MP2 with a triple-zeta quality basis set for prediction of the relative energies, with M06 performing less well but still respectably (root mean square deviation = 2.59 kJ/mol).[150]

Table 4.7: MP2/6-311+G** vertical detachment energies,[a] and neutral dipole moments (Neudip),[b] calculated for the $Br^{-}\cdot Arg$ complex.

	Canonical			Zwitterionic	
Family	VDE (eV)	Neudip	Family	VDE (eV)	Neudip
I	5.72	12.46	**I**	6.83	8.35
II	5.64	13.17	**II**	5.35	16.44
III	5.74	10.41	**III**	7.02	5.73
IV	5.61	8.84	**IV**	6.22	16.94
V	5.70	15.25	**V**	6.85	5.82
VI	5.67	10.90	**VI**	5.53	16.58
VII	5.81	11.83			
VIII	5.63	13.44			
IX	5.66	14.34			
X	5.70	9.90			
XI	6.32	20.21			
XII	6.03	10.60			
XIII	5.50	10.42			
XIV	6.27	20.76			
XV	5.75	18.10			
XVI	6.04	21.30			
XVII	6.03	17.50			
XVIII	6.46	21.77			

[a]Energy difference of the anion and the corresponding neutral, at the geometry of the anion.

[b] Electric dipole moment of the neutral, at the geometry of the optimised anion.

Table 4.8: MP2/6-311+G**.vertical detachment energies,[a] and neutral dipole moments (Neudip),[b] calculated for the Cl^{-}·Arg complex.

	Canonical			**Zwitterionic**	
Family	VDE (eV)	Neudip	Family	VDE (eV)	Neudip
I	5.80	3.93	**I**	5.69	16.22
II	5.66	3.22	**II**	5.55	16.12
III	5.84	4.78	**III**	5.54	15.15
IV	5.41	9.07	**IV**	5.15	11.56
V	5.53	5.06			
VI	5.57	4.88			
VII	5.04	9.01			
VIII	5.47	4.16			
IX	5.06	7.92			
X	5.47	6.84			
XI	5.58	6.53			
XII	4.97	6.39			
XIII	5.44	3.45			
XIV	5.49	10.54			
XV	4.95	6.76			
XVI	5.25	7.25			
XVII	4.71	9.84			

[a] Energy difference of the anion and the corresponding neutral, at the geometry of the anion.

[b] Electric dipole moment of the neutral, at the geometry of the optimised anion.

It is notable that this trend of the better performance of M06-2X compared to M06 mirrors this study's results for the zwitterionic clusters, where the energetics of both systems should be dominated by electrostatics. Mardissian *et al.* also assessed the performance of the functional for predicting binding energies, finding that both M06 and M06-2X performed poorly on this criterion. Jones *et al.* found that the interaction energies of the fluoride ion-

aromatic complexes (where electrostatic forces are more important) were overestimated by M06-2X while the energies of the chloride ion-aromatic complexes were extremely well reproduced by M06-2X.[182] (M06 and M06-HF were not evaluated in the study of Jones *et al.*)

The strong performance of the M06 functionals for the anionic biomolecular clusters explored in this study indicate that these functionals should prove highly useful for computational work that supports laser spectroscopy of such systems. The accurate identification of the lowest minimum energy structure is of key importance, along with the identification of other low-lying minima that could perturb the spectrum of the lowest energy structure. While there has been a tendency within the laser spectroscopy and broader gas-phase ions community to use the B3LYP functional for calculations of biological ions,[87, 127, 141, 190, 191] the results presented here strongly suggest that the M06 functionals offer a considerably more reliable choice when balancing computational speed and accuracy for anionic systems. The results presented here should also serve to motivate further testing of the newer density functionals for a greater range of ionic biomolecules.

Chapter 5

UV Laser Spectroscopy of Mass-Selected Ionic Liquid Building Blocks in the Gas-Phase

5.1 Introduction

Ionic liquids have attracted considerable attention in both the fundamental and industrial chemical community over the last decade as a result of their unique physiochemical properties such as low vapour pressure, high viscosity and good conductivity. Proposed applications range from green industrial solvents, CO_2 extraction media, through to rocket propellants.[93-96] A very considerable number of spectroscopic studies have been conducted on condensed phase ionic liquids (ILs) with the aim of developing analytical methods for characterising ILs as well as to investigate their fundamental structure.[192, 193] Such work has been complemented by gas-phase studies of IL vapours over recent years, following the discovery that certain ILs were sufficiently volatile to allow transfer into the vapour phase within a high vacuum environment.[97, 98] These studies indicate that the IL vapours typically consist of ion-pairs for aprotic ILs,[99, 194, 195] and spectroscopic characterisation of such

systems therefore provides an excellent opportunity for testing the large number of theoretical calculations that have been conducted on IL ion pairs.[196-198]

This chapter describes UV laser photodissociation spectra of mass selected aggregate clusters of the $[BMIM^+][Tf_2N^-]$ and $[EMIM^+][Tf_2N^-]$ ILs, i.e. $[BMIM^+]_n[Tf_2N^-]_m$ and $[EMIM^+]_n[Tf_2N^-]_m$ where $n \neq m$ and n, m = 1, 2. Schematic structures of these ILs are displayed in Scheme 5.1.

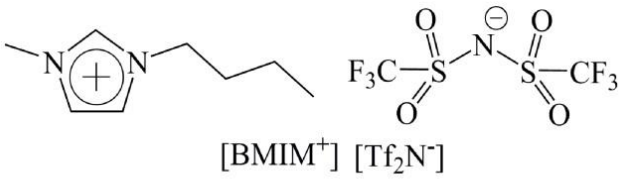

$[BMIM^+]$ $[Tf_2N^-]$

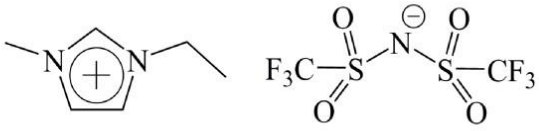

$[EMIM^+]$ $[Tf_2N^-]$

Scheme 5.1; Schematic structures of the two studied ionic liquids

The spectra presented in this chapter are the first such gas-phase UV spectra where the identity of the IL aggregate cluster can be definitively identified via mass selection prior to spectroscopic characterisation. The general strategy in this chapter mirrors that recently employed by Johnson and co-workers in their IR laser spectroscopy study of $[EMIM^+]_n[BF4^-]_m$ $n \neq m$ aggregate ions.[199] $[BMIM^+][Tf_2N^-]$ and $[EMIM_+][Tf_2N^-]$ were chosen as study

systems for this chapter as both have recently been the subject of vapour-phase UV spectroscopy studies,[200, 201] allowing the key point of how closely the spectra of these mass-selected aggregates resemble those of the vapour-phase ILs to be addressed. Wang *et al*. presented the first UV spectroscopic measurements of IL vapours (including the BMIM and EMIM systems) using high-temperature vaporization of ILs into quartz cuvettes,[200] while Ogura *et al*. subsequently acquired a UV absorption spectrum of vapour phase $[EMIM^+][Tf_2N^-]$ using cavity ring down spectroscopy.[201] Cooper *et al*. have introduced $[EMIM^+][Tf_2N^-]$ into the gas-phase in a supersonic expansion and applied UV photofragmentation to the resulting (non-mass selected) jet-cooled neutral clusters.[202] In this study, electrospray ionisation is used to transfer the ILs from the condensed phase into the gas-phase, prior to mass selection in a laser-interfaced mass spectrometer. Electronic spectra of the anionic and cationic aggregates for both ILs for comparison with the previous gas-phase studies are presented.

5.2 Experimental Details

Experiments were conducted in Bruker Esquire 6000 and Bruker amaZon Quadrupole Ion Trap mass spectrometers that have been custom-modified for performing laser spectroscopy.[203, 204] The ILs were purchased from Aldrich and used without any further purification. IL clusters were generated using positive and negative mode electrospray (100°C dry gas temperature) and 10^{-6} mol dm^{-3} (amaZon) solutions of the respective IL in acetonitrile, and specific mass-selected IL aggregates were isolated in the instrumental ion-trap and subjected to laser irradiation. UV photons were produced by an Nd:YAG

(Continuum Surelite) pumped OPO (Panther), producing ~1.5mJ per pulse across 220-300 nm. 220 nm is the high-energy limit of this laser. Action spectra were recorded by monitoring the production of photofragments as a function of laser wavelength.[208] All spectra are corrected for laser power. UV spectra of 0.1 mM $[BMIM^+][Tf_2N^-]$ and $[EMIM^+][Tf_2N^-]$ in acetonitrile were acquired with a Shimadzu UV-1800 spectrophotometer.

5.3 Results and Discussion

Figure 5.1a displays the positive ion mode electrospray ionisation mass spectrum (ESI-MS) obtained by electrospraying the $[BMIM^+][Tf_2N^-]$ IL in acetonitrile. The mass spectrum is dominated by the $[BMIM^+]_2[Tf_2N^-]$ aggregate cluster peak, with the $[BMIM^+]$ cation also clearly visible. Negatively charged aggregate clusters were observed when the instrument was operated in negative ion mode (Figure 5.1b), as illustrated by the strong appearance of $[BMIM^+][Tf_2N^-]_2$. Similar spectra were obtained in positive and negative ion mode when $[EMIM^+][Tf_2N^-]$ was electrosprayed in acetonitrile. The mass spectra obtained in this work resemble those observed in previous electrospray mass spectrometry studies of ILs.[206-209] In this chapter, spectra for the simplest aggregate clusters, i.e. the aggregates containing either two cations with an anion, $[C^+]_2[A^-]$, or two anions with a cation, $[C^+][A^-]_2$ are presented. Higher aggregate clusters are present in the ESI-MS, but with considerably lower intensities.

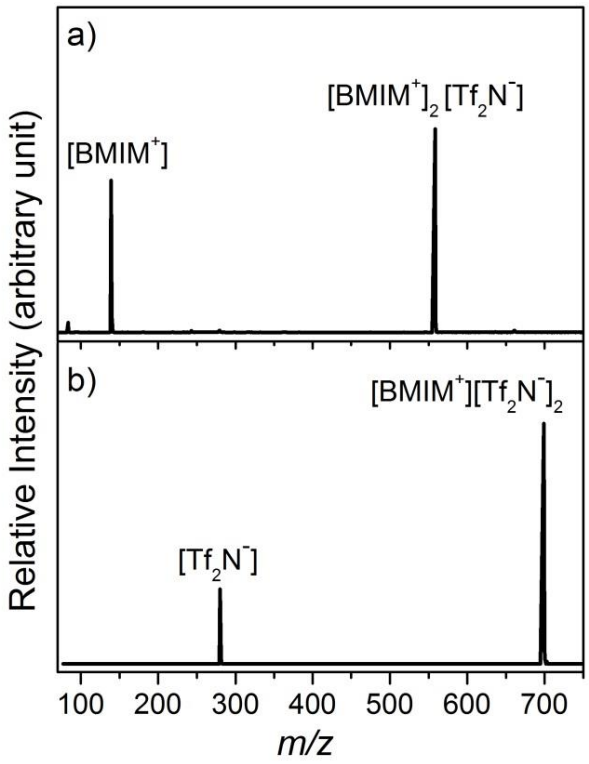

Figure 5.1; a) Positive ion mode ESI-MS of the $[BMIM^+][Tf_2N^-]$ ionic liquid in acetonitrile, and b) corresponding negative ion mode spectrum. The m/z values for the observed species are m/z $[BMIM^+]$ = 139, m/z $[BMIM^+]_2[Tf_2N^-]$ = 558, m/z $[Tf_2N^-]$ = 280, and m/z $[BMIM^+][Tf_2N^-]_2$ = 699.

5.3.1 Determination of fragment identity

All of the spectra presented in this chapter are action spectra, and it is therefore necessary to identify the photofragment ions prior to conducting spectral scans. Figures 5.2a and 5.2b present the photofragmentation mass spectra obtained upon 220 nm excitation of the mass-selected $[EMIM^+]_2[Tf_2N^-]$ and $[EMIM^+][Tf_2N^-]_2$ from the $[EMIM^+][Tf_2N^-]$ IL. Figure 5.2a illustrates that the cationic $[EMIM^+]_2[Tf_2N^-]$ cluster photofragments with production of $[EMIM^+]$ as the sole ionic photofragment, presumably accompanied by loss of a neutral ion pair which is undetected in the mass spectrometer, i.e.

$$[EMIM^+]_2[Tf_2N^-] \rightarrow [EMIM^+] + [EMIM^+][Tf_2N^-] \quad [1a]$$

The anionic cluster $[EMIM^+][Tf_2N^-]_2$ similarly produces $[Tf_2N^-]$ as the sole ionic photofragment (Figure 5.2b), again presumably along with an accompanying neutral ion pair:

$$[EMIM^+][Tf_2N^-]_2 \rightarrow [Tf_2N^-] + [EMIM^+][Tf_2N^-] \quad [1b]$$

The cationic and anionic aggregates from $[BMIM^+][Tf_2N^-]$ (Figures 5.2c and 5.2d) were observed to photofragment in the same way as for $[EMIM^+][Tf_2N^-]$. It is noted that the photofragmentation pathways mirror the cluster fragmentation patterns observed upon collision induced dissociation of ground state IL aggregates, which fragment by loss of a neutral ion-pair unit.[209]

5.3.2 Analysis of photofragments from action spectra

Figure 5.3a displays the photofragment action spectrum for the $[EMIM^+]$ fragment from $[EMIM^+]_2[Tf_2N^-]$ across the spectral range from 220-245 nm. The maximum photofragment production over this range occurs at 220 nm, the high-energy limit for the laser system, with the photofragment intensity falling away very rapidly to longer wavelengths (effectively zero

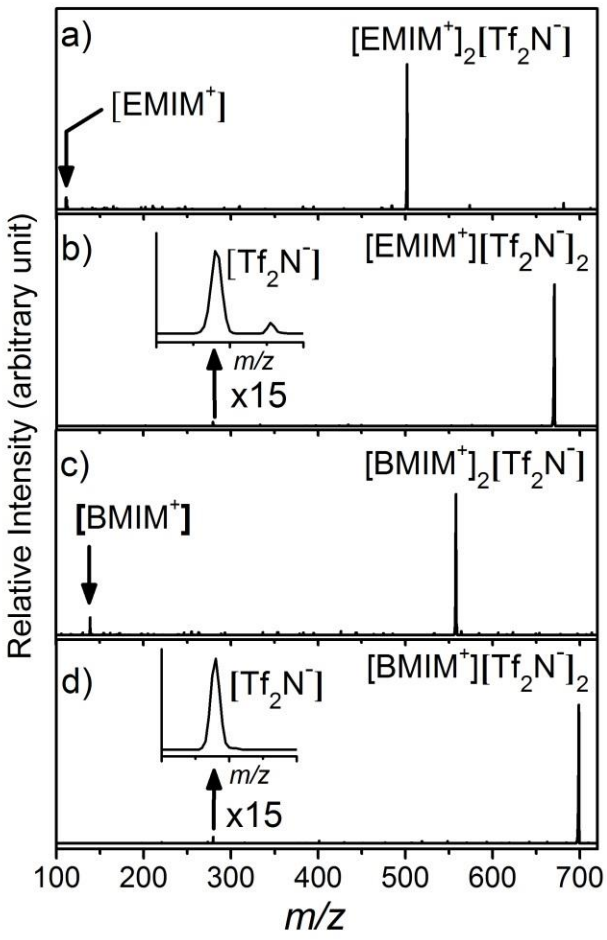

Figure 5.2; Photofragmentation mass spectra of a) $[EMIM^+]_2[Tf_2N^-]$, b) $[EMIM^+][Tf_2N^-]_2$, c) $[BMIM^+]_2[Tf_2N^-]$ and d) $[BMIM^+][Tf_2N^-]_2$ recorded at 220 nm. The m/z values for the observed species are m/z $[EMIM^+]$ = 111, m/z $[EMIM^+]_2[Tf_2N^-]$ = 502, m/z $[Tf_2N^-]$ = 280, m/z $[EMIM^+][Tf_2N^-]_2$ = 671, m/z $[BMIM^+]$ = 139, m/z $[BMIM^+]_2[Tf_2N^-]$ = 558, m/z $[Tf_2N^-]$ = 280, and m/z $[BMIM^+][Tf_2N^-]_2$ = 699.

above 230 nm). Figure 5.3b shows the action spectrum for production of $[Tf_2N^-]$ from $[EMIM^+][Tf_2N^-]_2$, again displaying a maximum value at 220 nm, but with a slightly less sharp fall-off in intensity towards longer wavelength. The intensity of the anionic photofragment from excitation of the anionic aggregate was much smaller than that of the cationic fragment from photoexcitation of the cationic aggregate, with anion photofragment signals typically being on the order of 100 times smaller than the cation photofragment.

The corresponding action spectra obtained for the $[BMIM^+][Tf_2N^-]$ IL aggregates (Figures 5.4a and 5.4b) are similar to those of $[EMIM^+][Tf_2N^-]$. The $[BMIM^+]$ fragment spectrum (Figure 5.4a), is very similar to the corresponding $[EMIM^+]$ fragment spectrum (Figure 5.3a), with the intensity falling away rapidly at wavelengths longer than 220 nm, while the decrease in the $[Tf_2N^-]$ fragment (Figure 5.4b) from excitation of the $[BMIM^+][Tf_2N^-]_2$ anionic aggregate is more gradual. The intensity of the anionic photofragment was again significantly smaller than the cationic photofragment, as in the $[BMIM^+]_n[Tf_2N^-]_m$ aggregates.

Solution-phase UV spectra (Figure 5.5) were recorded for both $[EMIM^+][Tf_2N^-]$ and $[BMIM^+][Tf_2N^-]$ for comparison with the gas-phase action spectra. Each IL displays a strong UV band with an onset around 235 nm and absorption bands peaked around 220 nm (λmax = 211 nm for $[EMIM^+][Tf_2N^-]$ and λmax = 210 nm for $[BMIM^+][Tf_2N^-]$). This band is associated with excitation of the π-π^* chromophore which exists in imidazole-type molecules in this region.[211] Gas-phase spectroscopic studies of the isolated imidazole molecule have revealed the presence of a bright optical excited state that is coupled to a dark dissociative state, resulting in a broad absorption band.[211, 212]

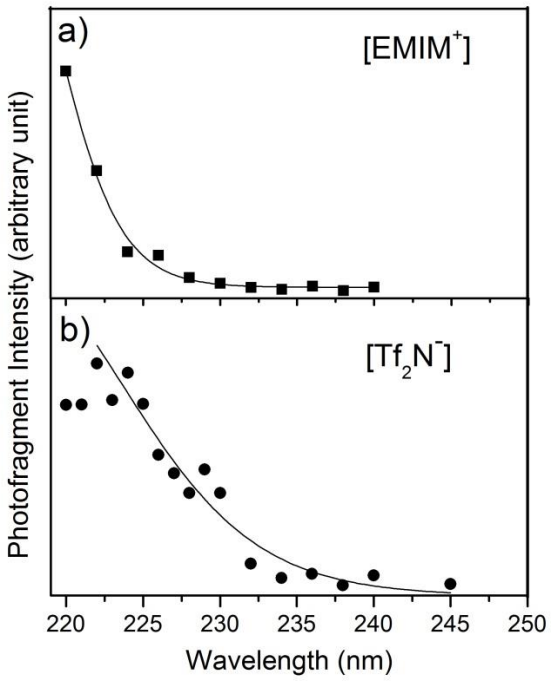

Figure 5.3; Cluster photofragment action spectra of a) $[EMIM^+]$ from the $[EMIM^+]_2[Tf_2N^-]$ cationic aggregate and b) $[Tf_2N^-]$ from the $[EMIM^+][Tf_2N^-]_2$ anionic aggregate.

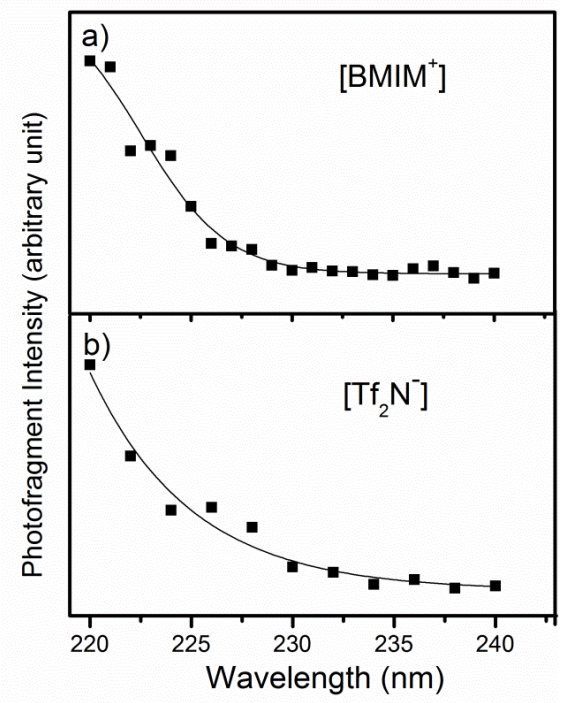

Figure 5.4; Cluster photofragment action spectra of a) $[BMIM^+]$ from the $[BMIM^+]_2[Tf_2N^-]$ cationic aggregate and b) $[Tf_2N^-]$ from the $[BMIM^+][Tf_2N^-]_2$ anionic aggregate.

Although the photofragment spectra display maximum values at 220 nm, currently λmax values for the gas-phase aggregate clusters are unable to be assigned due to the limitations of the laser system. (Figure 5.6 presents a second set of photofragmentation action spectra for the $[EMIM^+][Tf_2N^-]$ aggregates, which have been recorded up to 215 nm with an additional laser system that provided photons deeper into the UV. The photofragment intensity is still increasing at 215nm, indicating that λmax occurs at shorter wavelengths still.)

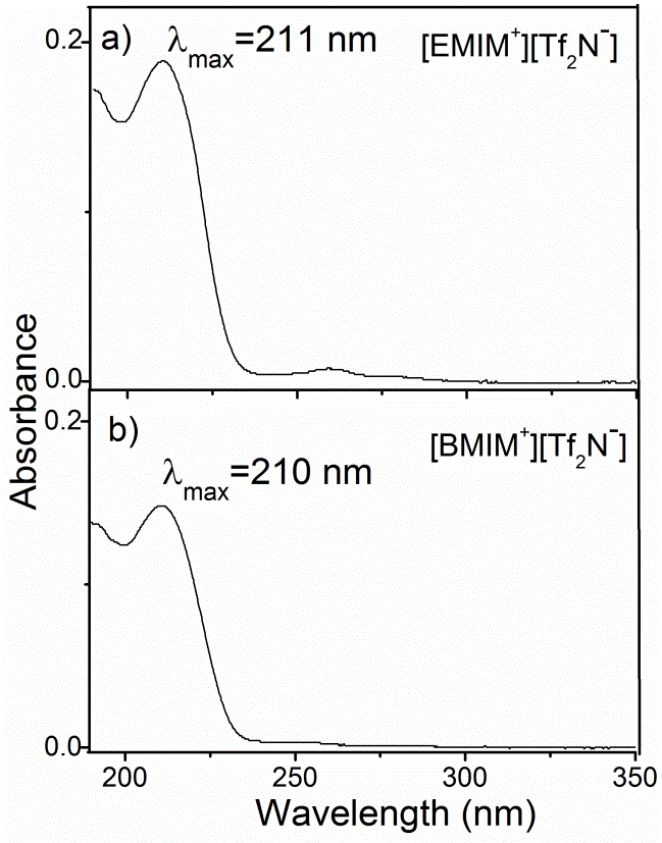

Figure 5.5; Liquid phase UV absorption (arb. Units) spectra of a) $[EMIM^+]$ $[Tf_2N^-]$ and b) $[BMIM^+]$ $[Tf_2N^-]$

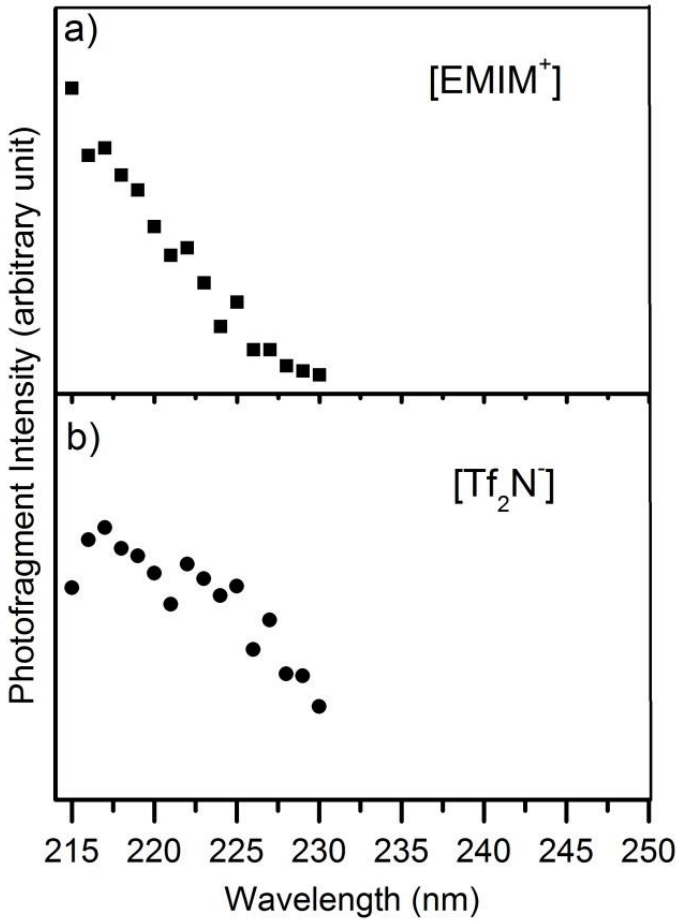

Figure 5.6; Cluster photofragment action spectra of a) $[EMIM^+]$ from the $[EMIM^+]_2[Tf_2N^-]$ cationic aggregate and b) $[Tf_2N^-]$ from the $[EMIM^+][Tf_2N^-]_2$ anionic aggregate. These spectra were recorded with an Nd:YAG pumped OPO system that provided photons to 215 nm at the high energy limit. The spectra display similar profiles to the spectra presented in Figure 5.3, with an additional scanned range from 220-215 nm.

5.3.3 Comparison with previous studies

The photofragment action spectrum for the IL aggregates displayed in Figures 5.3 and 5.4 display similar absorption profiles to the UV absorption spectra of these ILs recorded by Wang *et al.* for the IL vapour (557 K) contained in a quartz cuvette, i.e. broad onset above

240 nm with rising absorbance towards 200 nm.[200] Wang *et al.* recorded spectra at temperatures from 533-573 K, showing that the absorption onset is displaced to longer wavelength at higher temperature. The redder onset absorptions seen in the high-temperature vapour spectra are likely due to higher-energy conformations (of IL ion-pairs), as well as rotational and vibrational excitation. The ESI aggregates studied in this experiment are thought to have temperatures of ~373K,[203] hence explaining the comparatively blue-shifted absorbance onsets. The $[BMIM^+][Tf_2N^-]$ photofragment action spectra are also very similar to those obtained for this IL by Ogura *et al.* using single-path absorption and cavity ring-down absorption spectroscopy.[201] The spectra of Ogura *et al*. were obtained at temperatures (406-429 K) much closer to the temperature of the aggregates in this study, and hence display absorption onsets (~233 nm at 418 K) closer to the value found here (230 nm). Finally, it is of interest to compare this set of $[EMIM^+]_n[Tf_2N^-]_m$ aggregate data to the spectra recorded by Cooper *et al*. in their photodissociation study of the IL $[EMIM^+][Tf_2N^-]$ in a supersonic expansion.[175] (Figure 5.7 displays the $[EMIM^+][Tf_2N^-]$ data gathered here in the same form as the Cooper *et al*. data allowing a direct comparison.) Again, the data from this study are very similar to the Cooper *et al.* results. The overall picture to emerge from these spectroscopic comparisons is that the mass-selected aggregates studied in this work appear to behave as simple ion-pairs, with the excess charged unit (i.e. $[EMIM^+]$ in the cationic cluster and $[Tf_2N^-]$ in the anionic cluster of the $[EMIM^+]_n[Tf_2N^-]_m$ aggregates) only weakly perturbing the photoexcitation and photodissociation dynamics.

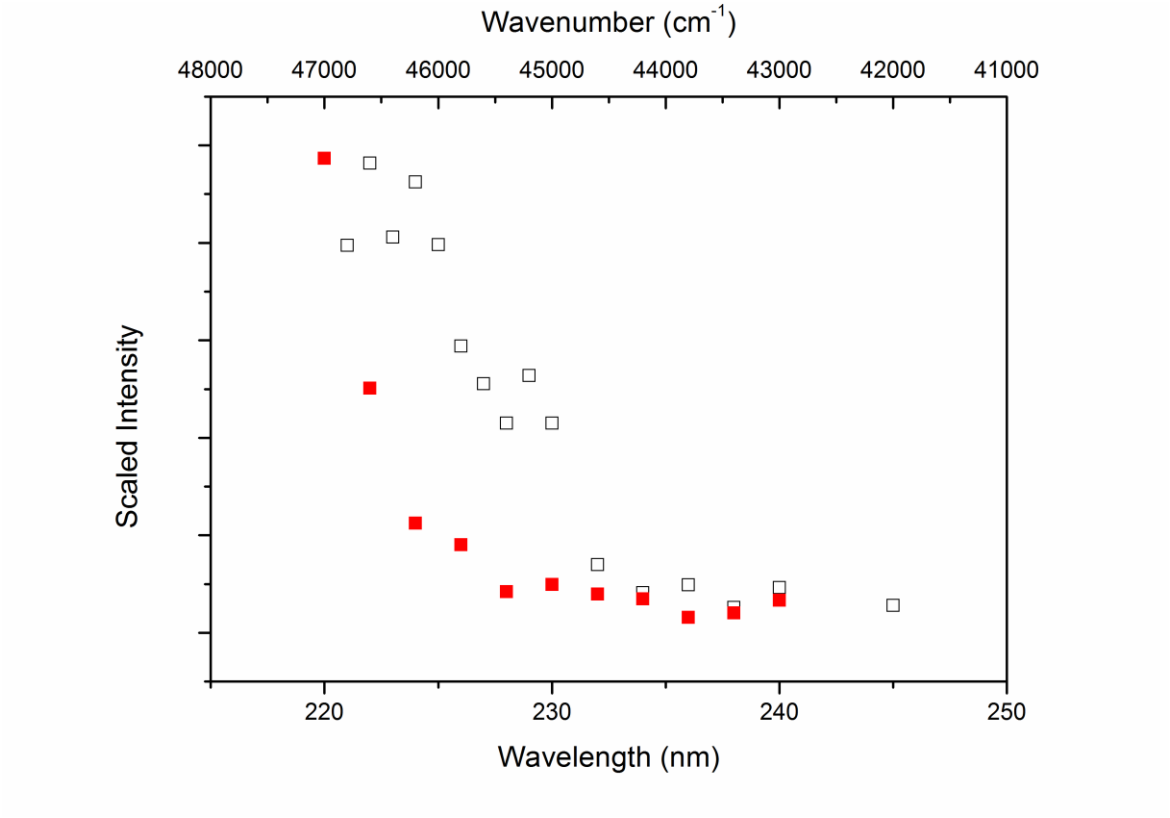

Figure 5.7; Overlay of the cation (closed squares) and anion (open squares) photofragment action spectra from the cationic and anionic aggregates of $[EMIM^+][Tf_2N^-]$. The anion and cation signals are scaled to be shown with the same intensity (arb. Units) for the maximum points.

5.3.4 Further Discussion

The similarity between the $[EMIM^+]_n[Tf_2N^-]_m$ aggregate photofragment spectra observed in this work, and the $[EMIM^+][Tf_2N^-]$ supersonic jet spectra measured by Cooper *et al.* suggest that similar photophysics may be present in photoexcitation of the aggregates as in the isolated ion-pairs that are thought to be present in the jet experiment. Cooper *et al.* have proposed a mechanism that involves initial photoexcitation to an electronic excited state of the $[EMIM^+][Tf_2N^-]$ ion-pair.[202] They postulate that the major pathway for decay of the

excited state is predissociation by a charge-transfer state as seen by Leone and co-workers,[213] resulting in production of the [EMIM·][Tf_2N·] radical pair, where the reduced cation moiety can then be ionized by a second photon to produce [$EMIM^+$]. Thus, the dominant ionic photofragment is [$EMIM^+$], produced in a two-photon process. In addition, they suggest that a much more minor pathway exists corresponding to direct decay of the excited state back to the ground electronic state, from where ergodic dissociation occurs producing [$EMIM^+$] and [Tf_2N^-] as minor ionic photofragment products.

The strong production of the cationic photofragments and comparatively weak production of the anionic photofragments observed following excitation of the IL aggregates in this work mirrors the observations of Cooper *et al.* and suggests that a similar mechanism may be operating. For the cationic aggregates, $[C^+]_2[A^-]$, the following mechanism of Cooper *et al.* would be modified as follows:

$$[C^+]_2[A^-] + h\nu \rightarrow ([C^+][C^+][A^-])^* \rightarrow [C^+] + [C\cdot] + [A\cdot] + h\nu \rightarrow [C^+] + [C^+] + [A\cdot] + e^- \quad [2a]$$

$$\rightarrow ([C^+][C^+][A^-])\dagger \rightarrow [C^+] + ([C^+][A^-]) \quad [2b]$$

where [2a] corresponds to the dominant pre-dissociation pathway followed by C· ionization (IEC· is thought to be ~3.9 eV for [EMIM·][202]) while [2b] is the minor excited-state to ground-state decay route. (The thermally excited ground-state cluster, $([C^+][C^+][A^-])\dagger$, will decay with loss of a neutral ion-pair unit as observed for collision induced dissociation of

the ground state clusters.)[209] Overall, the combined [2a]+[2b] pathways would lead to strong production of the [C^+] ion, consistent with the experimental observation. It is of note that no anionic photofragment is produced in either step [2a] or [2b], but due to the limitations of the experimental set-up only cationic photofragments can be detected after isolating a cationic precursor. The analogous pathways for the anionic aggregates would be:

$$[C^+][A^-]_2 + h\nu \rightarrow ([A^-][C^+][A^-])^* \rightarrow [A^-] + [C\cdot] + [A\cdot] + h\nu \rightarrow [A^-] + [C^+] + [A\cdot] + e^- \quad [3a]$$

$$\rightarrow \quad [A^-] + [C\cdot] + [A\cdot] + h\nu \rightarrow [A\cdot] + [C\cdot] + [A\cdot] + e^- \quad [3b]$$

$$\rightarrow \ ([A^-][C^+]\,[A^-])\dagger \ \rightarrow [A^-] + ([C^+][A^-]) \quad [3c]$$

where [3a] and [3b] correspond to the dominant pre-dissociation followed by either C· ionization or [A^-] photodetachment (the detachment energy of [Tf_2N^-] is calculated to be around 5.6 eV at the M06/6-311++G** level),[202] whereas [3c] is a minor pathway that results in [A^-] as the sole ionic photofragment. This photofragment would again be susceptible to photodetachment through interaction with a third photon during the time the ions are stored in the ion trap. It is clear that [A^-] is only likely to be observed as a weak photoproduct from the combined series of [3a]-[3c] pathways. Cooper *et al.* have performed power dependent measurements to support their proposed mechanism, but such definitive measurements that unambiguously determine the number of photons involved in production of each photofragment have not been performed in the ion trap instrument used in this study, since

precursor ions and photofragment ions may undergo multiple interactions with different photons over the timescale that ions are stored in the trap. Nonetheless, preliminary measurements of photofragment intensity versus laser power for the $[BMIM^+]_n[Tf_2N^-]_m$ aggregates clearly revealed that the power dependence for production of the cationic photofragments is different from the anionic photofragments, consistent with distinctive fragmentation pathways.

5.4 Conclusions

Since the chemical and physical properties of ILs can be controlled by the combination of cationic and anionic components, ILs can be used for an increasingly wide range of technical applications.[93-96] Given the wealth of possible cation-anion combinations, it is highly desirable to be able to rationally predict the properties of an IL based on the constituents.[214] Ab initio computational studies of ILs make a considerable contribution to this general effort, but such calculations are typically performed on isolated "gas-phase" systems.[196-198] It is therefore important to be able to study IL building blocks (i.e. ion-pairs or aggregates) in the gas-phase. While IR vibrational spectroscopy of gas-phase ILs focus on characterising geometric structures, studies of the electronic spectroscopy of gaseous ILs are also of crucial importance for determining the intrinsic absorption and fluorescence behaviour of ILs both to clarify liquid-phase anomalies (e.g. additional charge transfer bands, contributions from clusters, and charge transfer to solvent bands in mixed media),[201, 215, 216] and also to provide benchmark data for TD-DFT and other excited state calculations.[214]

The experiments performed in this chapter demonstrate the feasibility of exploring the excited state photophysics of ILs via the study of mass-selected charged aggregates produced via electrospray ionisation. The UV gas-phase absorption profiles measured in this way show that this technique provides a facile route to obtaining gas-phase UV spectra of ILs. One considerable advantage of this technique over other methods is that there is no contamination of spectra from impurities due to the mass-selection employed prior to laser excitation. Indeed, the presence of impurities in IL samples can be substantial,[217] and considerable effort needs to be expended to ensure that samples are pure prior to routine spectroscopic analysis.

Numerous further experiments are possible from these initial spectroscopic measurements, and it will be valuable to move to cationic units that lack the dissociative excited state, and also to explore anionic units that possess a chromophore. Further theoretical work is also certainly desirable to more accurately characterise the rich photophysics evident in these mixed charge gas-phase clusters, both as a basis for understanding the fundamental photophysics of other novel mixed charge systems but also to inform our understanding of UV processes in bulk ILs.[215, 216]

Chapter 6

Evidence for Dipole-Bound Excited States in Gas-Phase $I^{-}\cdot MI$ (M = Na, K, Cs) Anionic Salt Microclusters

6.1 Introduction

Dipole-bound excited states are fairly common observations in anionic molecular systems, often dominating near-threshold spectroscopy and dynamics in such systems.[218-228] Dipole-bound excited states (DBES) were first identified by Brauman and co-workers in 1979,[228] and they are still very much relevant today, being of key fundamental importance and centric to interpreting physicochemical phenomena such as detachment dynamics of molecules and electron scattering in nucleobases.

A lot of recent work on DBES has focused on their role in reactive processes,[222, 223] however it is important to note that previously they have been found to be useful for structural studies and can even be used to probe the spatial geometries of polar solvent molecules in the vicinity of halide ions.[206, 229] Quite recently, in fact, there has been a resurgence of interest concerning the use of DBES as structural probes.[229-232]

The vision of using DBES as structural probes is yet to be fully realised, as the limitations implemented on most gas-phase anion spectroscopy instruments are too great, due to the molecular sources used. For this chapter a laser-interfaced electrospray quadrupole ion-trap mass spectrometer was developed,[204, 205] allowing production of an array of halide ion-polar molecule clusters using electrospray ionisation (ESI). Such systems were photoexcited across their detachment thresholds, reavealing structural information on the cluster by characterization of DBES that were present. Data generated in this study can be extrapolated to provide evidence for charge separation in systems such as amino acids.[87, 88, 233, 234]

This chapter describes the first UV laser photodissociation spectra of gas-phase $I^-\cdot MI$ (M = Na, K, Cs) alkali halide anionic microclusters. Photodepletion spectra taken exhibit strong absorption bands sitting just below the calculated vertical detachment energies, which indicates of the presence of dipole-bound excited states. Excitation at the peak of the transition to the dipole-bound excited state results in formation of a primary $[MI]^-$ photofragment, coupled with an I^- ion of lower intensity. Alkali halides possess substantial dipole moments,[235] which allows them to support dipole-bound electrons which are reasonably stable. This chapter is also of interest with relation to the nature of excess electron binding on alkali halide thin films and electron-induced salt nanocrystal self-assembly,[236, 237] as well as the understanding of electronic excitation of nanotube confined alkali halides.[238]

6.2 Experimental

6.2.1 Experimental Methods

Experiments were conducted in a Bruker amaZon Quadrupole Ion Trap mass spectrometer, custom-modified for performing laser spectroscopy.[204, 205] Anionic salt clusters were generated using negative mode electrospray ionization of 10^{-3} mol dm^{-3} aqueous solutions of the respective salt (purchased from Sigma Aldrich), and specific mass-selected salt clusters were isolated in the instrumental ion-trap and irradiated. UV photons were produced by an Nd:YAG (Continuum Surelite) pumped OPO (Panther), providing ~0.8 mJ per pulse across 220-340 nm. The spectral resolution is determined by the laser step size (1 nm or ~0.018 eV in the mid-spectral region). All spectra have been corrected for laser power by normalisation.

6.2.2 Computational Methods

Ab initio calculations (M06-2X/LANL2DZ) of the $I^{-}{\cdot}MI$ (M = Na, K, Cs) clusters were performed to provide approximate vertical detachment energies (VDEs), since any DBES would be expected to appear close to the VDE.[206] For each cluster, the global minimum energy structure corresponded to a $D_{\infty h}$ 'rod' structure with the metal cation located equidistant from the two iodide ions, in line with the known structure of $Cl^{-}{\cdot}NaCl$.[63] Table 6.1 presents the results of the calculations. (The calculated VDEs are expected to be accurate

to ~0.2 eV.[241] Calculations were conducted using Gaussian 09,[148] and harmonic frequencies were calculated to confirm that structures are true minima.)

Table 6.1; Ab initio results (M06-2X/LANL2DZ) for the I^-·MI (M = Na, K, Cs) clusters.

	VDE (eV)[a]	**Dipole Moment of MI (D)**	**M-I bond length (Å)**	**M-I vib. freq. (cm^{-1})[b]**
I^-·NaI	4.75	10.4	2.968	234 (175)
I^-·KI	4.61	13.1	3.348	180 (140)
I^-·CsI	4.41	15.4	3.751	109

[a] Not zero point energy corrected.

[b] In neutral MI (uncorrected). Experimental values from Ref [32] are shown in parentheses.

6.3 Results and Discussion

6.3.1 I^- NaI clusters

Figure 6.1a displays the negative ion mode electrospray ionisation mass spectrum (ESI-MS) obtained via ESI of an aqueous solution of NaI. The mass spectrum is dominated by the I^-·NaI salt cluster peak, with higher anionic salt clusters (e.g. $I^-·(NaI)_2$) also clearly visible. Similar spectra were obtained when aqueous solutions of KI and CsI were electrosprayed under analogous conditions.

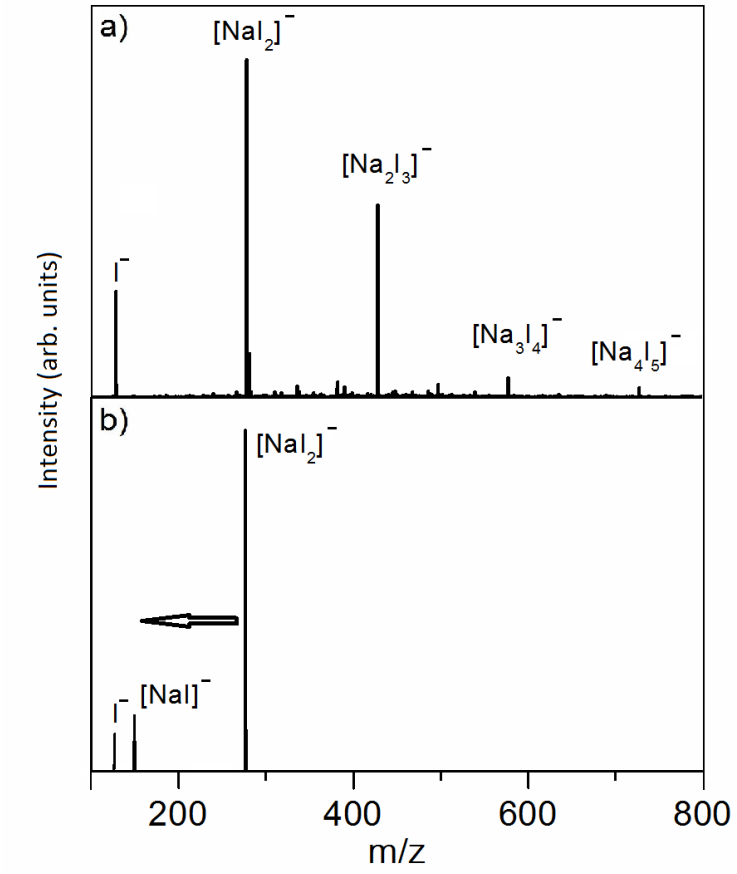

Figure 6.1; a) Negative ion mode ESI-MS of NaI illustrating production of $[Na_nI_{n+1}]^-$ n = 0-4 clusters, and b) photofragmentation mass spectrum of $[NaI_2]^-$ obtained at 4.7 eV showing production of I^- and $[NaI]^-$ photofragments.

The photodepletion (absorption) spectrum for the I^-·NaI cluster was obtained across a region (~4.2 - 5.6 eV) scanning the calculated VDE (4.75 eV) with the result shown in Figure 6.2a. The spectrum has an onset below the calculated VDE (marked by an arrow on the figure) indicating that an excited state of the cluster exists in the region below the VDE, as would be expected for a DBES.[191, 206] The absorption spectrum displays a significant intensity enhancement in the region immediately below the VDE, followed by a region of increasing absorption intensity towards the high-energy limit of the scans. This increase in absorption towards the high scan region arises due to the onset of a second DBES associated with the

upper ($^2P_{1/2}$) spin-orbit state of iodine which lies ~0.94 eV above the lower ($^2P_{3/2}$) spin-orbit state.[239, 240] There is a discernible shoulder on the low-energy side of the λ_{max}~4.63 eV band, which may be associated with excitation of the vibrational envelope in the DBES cluster. It is notable that the photoelectron spectrum of NaI^-,[241] displays a similar Franck-Condon envelope, associated with extensive vibrational excitation of the neutral NaI stretching mode. In the photoelectron spectrum, the NaI^- photodetachment band displays a FWHM of ~ 0.3 eV, which is similar to the λ_{max}~4.63 eV absorption band of I^-·NaI.

Figures 6.2b and 6.2c display the corresponding photodepletion spectra of the I^-·KI and I^-·CsI clusters. These spectra are similar to that of I^-·NaI with strong absorption peaks below the calculated VDEs, followed by gradually increasing absorption profiles. The range scanned for the I^-·KI cluster covers the region of the DBES associated with the upper spin-orbit state ($^2P_{½}$) of the photodetached iodine, and a distinctive peak in the photodepletion cross section (λ_{max}~5.2 eV) is visible ~0.94 eV above the dominant λ_{max}~4.3 eV centred band. Discernible shoulders are again visible on the low-energy side of the λ_{max}~4.3 eV I^-·KI band, which may again be associated with excitation of vibrational modes of the detached cluster. It is notable that the main absorption feature of I^-·KI (λ_{max}~4.3 eV) is somewhat narrower than that of the corresponding I^-·NaI feature (λ_{max}~4.63 eV). This mirrors the trend observed in the photoelectron spectra of NaI^- and KI^-, where KI^- displays a narrower FWHM ~ 0.2 eV band compared to NaI^- (FWHM~0.3 eV).[32] Further interpretation of the differences in the Figure 6.2 spectra will likely require the measurement of photoelectron spectra as future work.

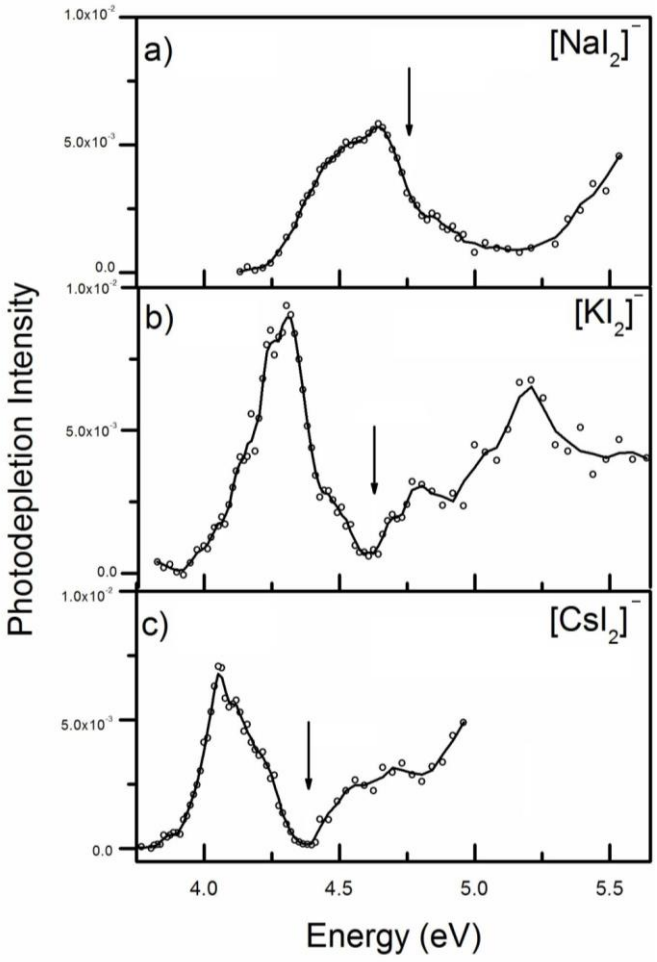

Figure 6.2; a) Photodepletion (absorption (arb. Units)) spectra of a) $[NaI_2]^-$, b) $[KI_2]^-$, and c) $[CsI_2]^-$. The solid lines are 3 point smooths through the data points. The calculated VDEs are indicated by the vertical arrows (see text for details).

6.3.2 Analysis of photofragments

To gain further insight into the nature of the excited state being accessed in the region of the VDE of the I^-·MI clusters, the anionic photofragments produced at the peak of the absorption spectra were analysed. Figure 6.1b displays the photofragment mass spectrum obtained from

excitation of I^-·NaI at 4.7 eV, the peak of the below VDE absorption feature. $[NaI]^-$ is observed as the dominant photofragment along with I^- as a secondary fragment. The action spectra for production of both photofragments are shown in Figures 6.3b and 6.3c, along with the absorption spectrum (Figure 6.3a). The action spectra clearly illustrate that both photofragments are produced only through the 4.7 eV centred band. It seems that I^- is produced through fragmentation of the primary NaI^- photofragment, since both fragments are produced with identical profiles, with the I^- fragment consistently appearing at lower intensity than NaI^- across this band.

The overall profile of the near-threshold absorption spectrum of the I^-·NaI cluster is highly reminiscent of spectra obtained for complexes such as I^-·CH_3CN.[191, 206] Such clusters display distinctive, intense dipole-bound excited states that are peaked just below the vertical detachment energies. These excited states are observed to decay with production of dipole-bound photofragment ions, e.g. CH_3CN^- from the I^-·CH_3CN cluster, when the dipole moment of the polar molecule is above ~2 D. By comparison, we anticipate that the $[NaI]^-$ photofragment initially produced from I^-·NaI in this study similarly corresponds to a dipole-bound anion, given that the dipole moment of NaI is ~10 D.[235] It should be noted that Mabbs and co-workers have recently identified the related AgF^- anion as a dipole-bound anion.[242]

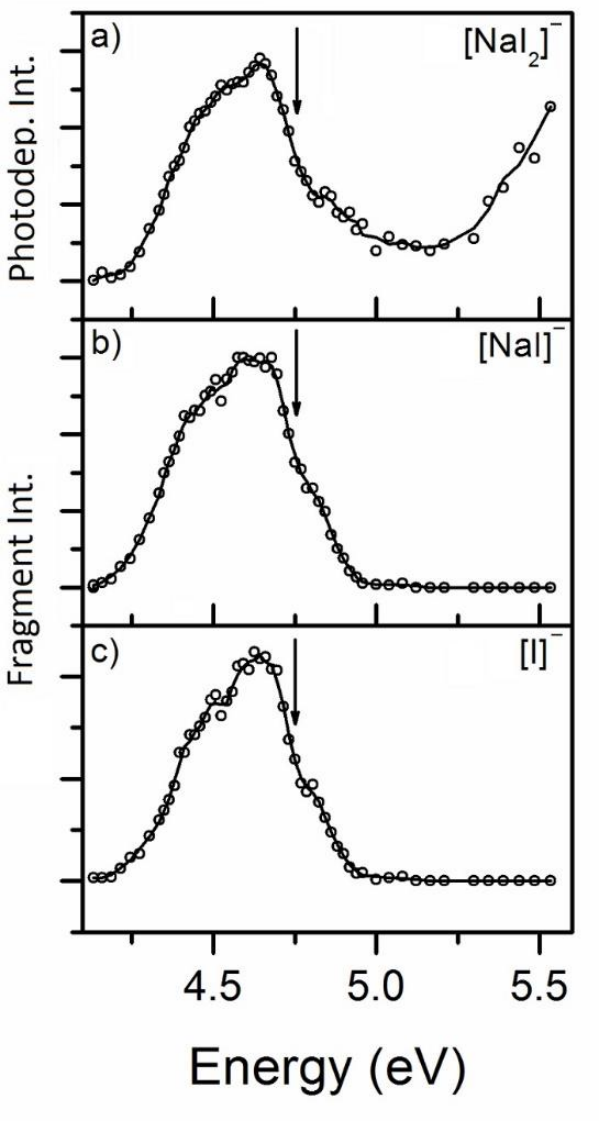

Figure 6.3; a) Photodepletion (absorption (arb. Units)) spectrum of $[NaI_2]^-$ displayed with the corresponding photofragment action spectra of the (b) $[NaI]^-$ and (c) I^- photofragments. The solid lines represent 3 point smooths through the data points. The arrows indicate the calculated VDEs.

The observation of I^- as a secondary photofragment from $I^-{\cdot}NaI$ is indicative of decay of the initially formed $[NaI]^-$ dipole-bound photofragment via a dissociative valence anion state. Such behaviour has been previously observed for the $I^-{\cdot}CH_3I$ and $I^-{\cdot}CH_3NO_2$ clusters.[243, 244] Photodetachment spectroscopy and computational studies of $[MX]^-$ alkali halide anions have

indicated that the ground-state electronic structures correspond to a neutral metal atom that is polarization-bound to the halide anion,[241, 245, 246] while their first excited states are predicted to be dipole-bound.[246, 247] It seems probable that the initial dipole-bound $[NaI]^-$ anion relaxes via a vibrational Feschbach resonance to produce the final valence anion, i.e. $Na{\cdot}I^-$. This final polarization-bound atomic cluster will be highly susceptible to fragmentation into Na and I^-, particularly for the ambient temperature ions (~300 K) produced by the electrospray source used in this experiment.

The photofragment action spectra of the $I^-{\cdot}KI$ and $I^-{\cdot}CsI$ clusters are similar to that of $I^-{\cdot}NaI$, with both clusters decaying with production of the respective $[MI]^-$ ion as the dominant photofragment along with the less-intense I^- ion through the strong below-threshold band. Figure 6.4 presents the $[MI]^-$ photofragment spectra obtained from each of the $I^-{\cdot}MI$ clusters for comparison. As noted for the photoabsorption spectra, partially resolved vibrational envelopes are evident on each of the spectra, but the spectral resolution (laser step size) employed in this preliminary work limits further analysis of these features at this point. It is likely that the ambient ion internal temperatures of the electrosprayed ions also contribute to the partial spectral resolution observed here. Further interpretation of the differences in the Figure 6.4 spectra would certainly be aided by the direct measurement of the cluster photoelectron spectra.

The $[KI]^-$ photofragment spectrum displayed in Figure 6.4b illustrates that no $[KI]^-$ is produced across the region of the DBES associated with the upper spin-orbit iodine state (λ_{max}~5.2 eV), despite the fact that an enhanced absorption cross section is present in the

photodepletion spectrum over this region (Figure 6.2b). (We note that no [I^-] photofragment is produced across this region, either.) It is probable that the lack of photofragments results from rapid spin-orbit relaxation of the upper iodine $^2P_{1/2}$ state accompanied by electron detachment occurring on a timescale that is faster than decay to ionic photofragments. Such dynamics have been observed in a recent study of iodide ion-molecule complexes, where the photodetachment dynamics in the vicinity of the $^2P_{1/2}$ state threshold are strongly correlated with the molecular dipole.[248]

Close inspection of the photofragment spectra displayed in Figure 6.4 reveal the presence of distinct but low intensity bands in the high-energy tail (most clearly visible for the I^-·CsI spectrum at ~4.45 eV). The "vertical dipole moments" of the alkali halides studied in this work are on the order of 10 D,[235] well above the expected critical value for the presence of a second dipole-bound excited state,[249, 250] suggesting that the low-intensity higher-energy bands may be associated with a second excited state. Bloomfield and co-workers have observed such excited states in the photoelectron spectra of alkali-halide cluster anions, i.e. $(KI)_2^-$, $(NaI)_2^-$ and $(NaCl)_2^-$.[251] The second dipole-excited state was observed to lie ~0.1 eV higher than the first dipole-bound excited state, broadly in line with the peak separation observed here.

6.4 Conclusions

In summary, these first laser photodissociation spectra of the $I^-\cdot MI$ salt microclusters have revealed the presence of strong absorption bands close to the expected VDEs, which have been attributed to dipole-bound excited states. It is proposed that these excited states decay with initial formation of an $[MI]^-$ transient dipole-bound anion, subsequently relaxing to an $[MI]^-$ valence-anion ground-state.

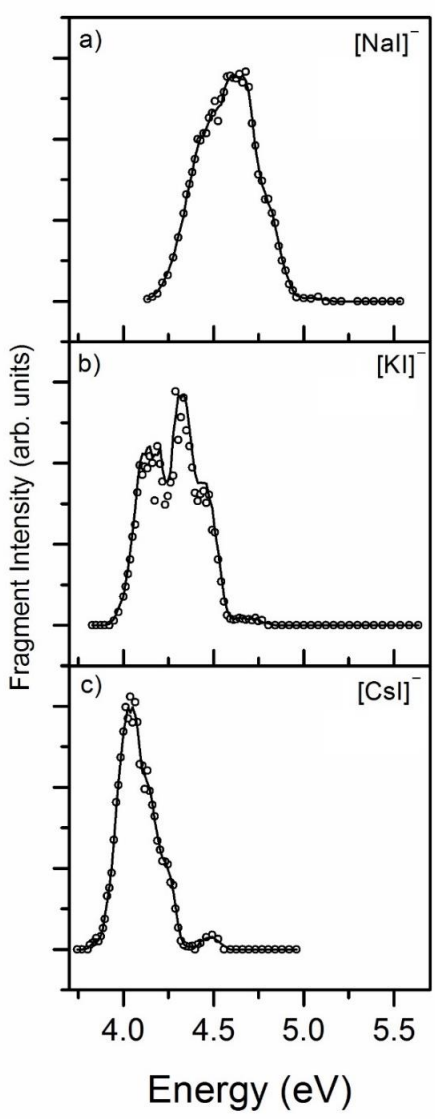

Figure 6.4; a) Photofragmentation action spectra of a) $[NaI]^-$ from $I^-\cdot NaI$, b) $[KI]^-$ from $I^-\cdot KI$, and c) $[CsI]^-$ from $I^-\cdot CsI$. The solid lines represent 3 point smooths through the data points.

Time-resolved experiments would be warranted in the future to test this hypothesis. The large dipole moment of the MI moiety appears to lead to substantial localization of the detachment continuum oscillator strength below the VDEs,[206] with the above threshold detachment cross section falling very close to zero in the region immediately above the VDE for the $I^{-}{\cdot}KI$ and $I^{-}{\cdot}CsI$ clusters (Figs. 6.2b and 6.2c). The experiments presented here have demonstrated that DBES can be identified in the relatively high-collision environment of a quadrupole ion-trap instrument, in particular for systems with large dipole moments associated with the presence of charge separation. This indicates considerable potential for future experiments exploring biomolecular structure and charge separation using the methodology and instrumentation employed herein, via the identification of DBES associated with high-dipole neutral cores.[230]

Chapter 7

Conclusions and Future Work

7.1 What has been learned, and what comes next?

In Chapter 3, the ability of halide anions to stabilise an energetically unfavourable tautomer of Arginine was explored. Results showed that Br^- could stabilise the zwitterionic form of arginine relative to the canonical form, however for Cl^- the canonical form remained lowest in energy. It would be beneficial to use IR to study these complexes more thoroughly, to check if experiment matches up to theory. An excellent tool to use when gathering IR data would be cryogenic messenger-tagging of the complexes.[158] This would allow for IR data on cold ions to be gathered easily.

In Chapter 4, a study was undertaken to evaluate the suitability of the M06[176-178] suite of functionals to calculate energies of canonical and zwitterionic forms of arginine, complexed with Chloride and Bromide ions. Non-covalent interactions had been found to be very important for the tautomeric energy ordering for these clusters.[184] Overall, the functionals

did very well, predicting the lowest energy conformers well when compared to more computationally expensive methods such as MP2. For further study, it would be desirable to explore some of the newer Minnesota functionals designed by the group of Truhlar, such as the newer M08[252] and M11[253, 254]

In Chapter 5, the gas-phase behaviour of charged, ionic liquid clusters was explored, using ESI as a method for producing these ions. It was found that ESI, coupled with our modified mass spectrometer used in Chapters 2 and 3, was an easy way of monitoring the excited state photophysics arising from UV photoabsorbtion of charged ionic liquid clusters. In Chapter 5, the cationic fragment of the ionic liquid contained the chromophore in both compounds studied. It would be interesting to see if the spectra change when the chromophore is present on the anionic unit, and if a chromophore is present on both units, whether this has any unexpected effects on the fragmentation pathways of these systems. Another beneficial study would be to use a laser with a large wavelength spread, as this would allow for scanning over the entire band, rather than just the peak and local energies.

Finally, it would be interesting to look at higher *n* clusters for the archetype $[C_nA_{n+/-1}]^{n-/+1}$ as these larger clusters were found to be present on initial scans of the electrosprayed solutions. These may require solvation to stabilise them however, and in this case, recent solvation studies such as those done by Voss *et al.* would prove useful.[255]

In Chapter 6, dipole bound excited states of alkali-halide anionic clusters generated using ESI were studied, inspired by the type of charged complex formed by the gas-phase ionic liquids in Chapter 5. It was found that using our modified mass spectrometer gave a facile method for generating these weakly-bound species, even in the relatively high-collision environment of the QIT. A potential pathway to dissociation was also suggested, with the relaxation of a transient dipole-bound anion to a valence-anion ground state.

There are many possible future studies possible for this experimental system. Firstly, some computational chemistry using Time-Dependant Density Functional Theory (TD-DFT) would be a boon as it would allow us to simulate a photoabsorbtion spectrum for the dipole-bound anion to probe the nature of the interaction. As with Chapter 4, it would be interesting to see how well the M06 suite (or more recent suites) performed with this system. Secondly, it would be useful to probe the same system under different conditions. For instance, solvated ionic clusters, to see how electronic transitions change with solvation.[256] It would also be interesting to attempt to create the system in a nanotube[257] or inside a crown ether[258] to see how this affects the formation of the dipole-bound excited state, would it be more stable within a molecular scaffold of some type?

It would also be useful to analyse the positive-mode data, i.e $[M_nI_{n-1}]^+$ M = Na, K, Cs. This has actually already been started within the group, and data for the positive clusters is complete and awaiting analysis. Early analysis suggests that there may be multiple structures for the $n = 2$ cluster, which would require computational studies to clarify.

Finally, from Chapter 6, we could also look at using our mass spectrometer to trap a dipole-bound excited state of zwitterionic arginine, as it would be expected to have a large dipole moment, in excess of the ~10 D required for a dipole-bound excited state to form. As well as exploring a new and exciting electronic system, this would be a great way of tying together some of the most recent work that we have been doing within the group.

Chapter 8

References

1. Duncan. MA, Int. J. Mass Spec., 200, 545 (2000)
2. Hobza. P, Řezáč. J, Chem. Rev., 116, 4911 (2016)
3. Lisy. JM, J. Chem. Phys., 125, 132302 (2006)
4. Johnson. MA, Robertson. WH, Annu. Rev. Phys. Chem., 54, 173 (2003)
5. Walker. NR, Walters. RS, Duncan. MA, New J. Chem., 29, 1495 (2005)

5b. Vaida. V, Kjaergaard. HG, Feierabend. KJ, Int. Rev. Phys. Chem., 22, 203 (2003)

6. Jouvet. C, Dedonder-Lardeaux. C, Grégoire. G, Martrenchard. S, Solgadi. D, Chem. Rev., 100, 4023 (2000)
7. Neumark. DM, Asmis. KR, Acc. Chem. Res., 45, 43 (2011)
8. Herzberg. G, Spectra of Diatomic Molecules, Molecular Spectra and Molecular Structure Vol. I, Van Nostrand Reinhold, New York, 1950; (b) Electronic Spectra and Electronic Structure of Polyatomic Molecules, Molecular Spectra and Molecular Structure, Vol. III, Van Nostrand Reinhold, New York, 1966; (c) The Spectra and Structure of Simple Free Radicals, Cornell University Press, Ithaca, 1971.
9. (a) Ervin. KM, Lineberger. WC, Adv. Gas Phase Ion Chem., 1, 121 (1992); (b) Wenthold. PG, Lineberger. WC, Acc. Chem. Res., 32, 597 (1999)
10. Kroto. HW, Heath. JR, O'Brien. SC, Curl. RF, Smalley. RE, Nature, 318, 162 (1985)
11. Gerlich. D, J. Chem. Soc., Faraday Trans., 89, 2199 (1993)
12. Hopkins. WS, Mol. Phys., 113, 21, 3151 (2015)

13. Meot-ner. M, Chem. Rev., 105, 1, 213 (2005)
14. Aakeroy. CB, Beatty. AM, Aust. J. Chem., 54, 409 (2001)
15. Wang. AHJ, Quigley. GJ, Kolpak. FJ, Crawford. JL, van Boom. JH, van der Marel. G, Rich. A, Nature, 282, 680 (1979)
16. Hutchens. TW, Nelson. RW, Allen. MH, Li. CM, Yip. TT, Biol. Mass Spec., 21, 151 (1992)
17. Taqui Khan. MM, Martell. AE, J. Am. Chem. Soc., 88, 668 (1966)
18. Bian. H, Wen. X, Li. J, Chen. H, Han. S, Sun. X, Song. J, Zhuang. W, Zheng. J, PNAS, 108, 12, 4737 (2011)
19. Faul. CFJ, Antonietti. M, Adv. Mat., 15, 9, 673 (2003)
20. Shin. SK, Beauchamp. JL, J. Am. Chem. Soc., 112, 2057 (1990)
21. Shin. SK, Beauchamp. JL, J. Am. Chem. Soc., 112, 2066 (1990)
22. Kirkwood. DA, Stace. AJ, J. Am. Chem. Soc., 120, 12316 (1999)
23. Kelly. CP, Cramer. CJ, Truhlar. DG, J. Chem. Theory. Comput., 1, 1133 (2005)
24. Wesolowski. TA, Warshel. A, J. Phys. Chem., 97, 30, 8050 (1993)
25. Dehmelt. HG, Jeffers. KB, Phys. Rev. 125, 1318 (1962)
26. Oka. T, Phys. Rev. Lett., 45, 531 (1980)
27. (a) Coe. JV, Owrutsky. JC, Keim. ER, Agman. NV, Hovde. DC, Saykally. RJ, J. Chem. Phys., 90, 3893 (1989) ; (b) Coe. J.V, Saykally. RJ, in Ion and Cluster Ion Spectroscopy and Structure, J.P. Maier (Ed.), Elsevier, Amsterdam, 1989, p. 131.
28. (a) Okumura. M, Yeh. LI, Lee. YT, J. Chem. Phys. 83, 3705 (1985) ; (b) Okumura. M, Yeh. LI, Meyers. JD, Lee. YT, ibid. 85, 2328 (1986)
29. Wohlgennant. M, Graupner. W, Leising. G, Vardeny. ZV, Phys. Rev. Lett., 82, 3344 (1999)
30. Massey. HSW, Electron Collisions with Molecules and Photoionization, Oxford University Press, Oxford, 1969.

31. Chemical Reactions in Electrical Discharges, Blausen. BD, (Ed.), Advances in Chemistry Series No. 80, American Chemical Society, Washington, DC, 1969.
32. Reactive Intermediates in the Gas Phase, Setser. DW, (Ed.), Academic, New York, 1979.
33. Johnson MA, Lineberger WC. 1988. Techniques for the Study of Gas-Phase Ion Molecule Reactions. New York: Wiley
34. Arnold. ST, Hendricks. JH, Bowen. KH, J. Chem. Phys. 102, 39 (1995)
35. Lenzer. T, Yourshaw. I, Furlanetto. MR, Pivonka. NL, Neumark. DM, J. Chem. Phys. 15, 3578 (2001)
36. Becker. I, Cheshnovsky. O, J. Chem. Phys. 110, 6288 (1999)
37. Stampfli. P, Phys. Rep., 255, 1 (1995)
38. Scheidemann. A, Schilling. B, Toennies. JP, J. Phys. Chem. 97, 2128 (1993)
39. Ellis. AM, Yang. S, Phys. Rev. A, 76, 032714 (2007)
40. An der Lan. L, Bartl. P, Leidlmair. C, Schobel. H, Jochum. R, Denifl. S, Maerk. TD, Ellis. AM, Scheier. P, J. Chem. Phys., 135, 044309 (2011)
41. Schulz. CP, Hohndorf. J, Brockhaus. P, Noack. F, Hertel. IV, Chem. Phys. Lett., 239, 18 (1995)
42. Takasu. R, Hashimoto. K, Fuke. K, Chem. Phys. Lett., 258, 94 (1996)
43. Zwier. TS, Annu. Rev. Phys. Chem., 47, 205 (1996)
44. Lehr. L, Zanni. MT, Frischkorn. C, Weinkauf. R, Neumark. DM, Science, 284, 635 (1999)
45. Weinheimer. CJ, Lisy. JM, Phys. Chem., 100, 15305 (1996)
46. Yamabe. S, Hirao. K, Chem. Phys. Lett., 84, 598 (1981)

46b. Tandy. J, Feng. C, Boatwright. A, Sarma. G, Sadoon. AM, Shirley. A, Rodrigues. ND, Cunningham. EM, Yang. SF, Ellis. AM, J. Chem. Phys., 114, 121103 (2016)

47. Langer. S, Pemberton. RS, Finlayson-Pitts. BJ, J. Phys. Chem. A, 101, 1277 (1997)
48. Oum. KW, Lakin. MJ, DeHaan. DO, Brauer. T, Finlayson-Pitts. BJ, Science, 279, 74 (1998)

49. Battan. LJ, Cloud Physics and Cloud Seeding; Doubleday: Garden City, NY, 1962.
50. Matsumura. H, Mafuné. F, Kondow. T, J. Phys. Chem. B, 103, 838 (1999)
51. Kohno. J, Mafuné. F, Kondow. T, J. Phys. Chem. A, 103, 1518 (1999)
52. Gebhardt. GR, Schröder. H, Kompa. L, Nature, 400, 544 (1999)
53. Grégoire. G, Mons. M, Jouvet. C, Dedonder-Lardeux, C. Eur. Phys. J., D, 1, 5 (1998)
54. Grégoire. G, Mons. M, Dimicoli. I, Dedonder-Lardeux. C, Jouvet. C, Martrenchard. S, Solgadi. D, J. Chem. Phys., 110, 1521 (1999)
55. Siegbahn. H, Siegbahn. K, J. Electron Spectrosc., 2, 319 (1973)
56. Mafuné F, Takeda. Y, Nagata. T, Kondow. T, Chem. Phys. Lett., 199, 615 (1992)
57. Vostrikov. AA, Zadorozhny. AM, Dubov. DY, Witt. G, Kasakova. IV, Bragin. OA, Kasakov. VG, Kikhtenko. VN, Tyutin. AA, Z. Phys. D, 40, 542 (1997)
58. Andersson. PU, Petersson. JBC, Z. Phys. D, 41, 57 (1997)
59. Grégoire. G, Dedonder-Lardeux. C, Dimicoli. I, Jouvet. C, Martrenchard. S, Solgadi. D, J. Chem. Phys., 112, 8794 (2000)
60. Barnett. RN, Landman. U, Scharf. D, Jortner J, Acc. Chem. Res. 22, 350 (1989)
61. Ochsenfeld. C, Ahlrichs. R, J. Chem. Phys. 97, 3487 (1992)
62. Bader. RFW, Platts. JA, J. Chem. Phys. 107, 8545 (1997)
63. Alexandrova. AN, Boldyrev. AI, Fu. YJ, Yang. X, Wang. XB, Wang. LS, J. Chem. Phys. 121, 5709 (2004)
64. Scheller. MK, Cederbaum. LS, J. Chem. Phys., 99, 441 (1993)
65. Gutsev. GL, Bartlett. RJ, Boldyrev. AI, Simons. J, J. Chem. Phys., 107, 3867 (1997)
66. Hotop. H, Lineberger. WC, J. Phys. Chem. Ref. Data, 14, 731 (1985)
67. Gutsev. GL, Boldyrev. AI, Chem. Phys. Lett. 56, 277 (1981)
68. Srivastava. AK, Misra. N, Electrochem. Comm., 68, 99 (2016)
69. Sikorska. C, PCCP, 18, 28, 18739 (2016)
70. Chen. ZY, Mao. RQ, Liu. Y, Curr. Drug Metab., 13, 1035–1045 (2012)

71. Dellinger. A, Zhou. ZG, Connor. J, Madhankumar. AB, Pamujula. S, Sayes. CM, Kepley. CL, Nanomedicine, 8, 1191–1208 (2013)
72. Jin. T, Zhang. BB, Song. J, Jiang. L, Qui. YS, Zhuang. W, J. Phys. Chem. A, 118, 9157 (2014)
73. Wleklinski. M, Sarkar. D, Hollerbach. A, Pradeep. T, Cooks. RG, PCCP, 17, 18364 (2015)
74. Khairallah. GN, O'Hair. RAJ, Angew. Chem., Int. Ed., 44, 728–731 (2005)
75. Luo. Z, Gamboa. GU, Smith. JC, Reber. AC, Reveles. JU, Khanna. SN, Castleman. AW, J. Am. Chem. Soc., 134, 18973–18978 (2012)
76. Luo. Z, Berkdemir. C, Smith. JC, Castleman Jr AW, Chem. Phys. Lett., 582, 24–30 (2013)
77. Greenwood. NN, Earnshaw. A, Chemistry of the Elements, 2nd ed.; Butterworth einemann: Oxford, Great Britain, 1997, p 1250
78. Murphy. WM, Schock. EL, Environmental Aqueous Geo-chemistry of Actinides. In Uranium: Mineralogy, Geochemistry, and the Environment; Burns. PC, Finch. R., Eds.; Mineralogical Society of America: Washington, D.C., 1999; p 221–254
79. Clavaguera-Sarrio. C, Brenner. V, Hoyau. S, Marsden. CJ,
80. Millie. P, Dognon. JP, Modeling of Uranyl-Cation-Water Clusters. J. Phys. Chem. B 107, 3051 (2003)
81. Chien. W, Anbalagan. V, Zandler. M, Van Stipdonk. M, Hanna. D, Gresham. G, Groenewold. G, J. Am. Soc. Mass. Spectrom., 15, 777 (2004)
82. Jagoda-Cwiklik. B, Jungwirth. P, Rulíšek. L, Milko. P, Roithová. J, Lemaire. J, Maitre. P, Ortega. JM, Schröder. D, ChemPhysChem, 8, 1629 (2007)
83. Pace. CN, Trevino. S, Prabhakaran. E, Scholtz. JM, Philos. Trans. R. Soc. London, Ser. B, 359, 1225 (2004)
84. Locke. MJ, McInver. RT, Jr. J. Am. Chem. Soc., 105, 4226 (1983)
85. Wilenska. D, Skurski. P, Anusiewicz. I, Mol. Phys., 114, 1494 (2016)
86. Kim. JY, Ahn. DS, Park. SW, Lee. S, RSC Adv., 4, 16352 (2014)
87. Milner. EM, Nix. MGD, Dessent. CEH, J. Phys. Chem. A, 116, 801 (2012)

88. Xu. SJ, Zheng. WJ, Radisic. D, Bowen. KH, J. Chem. Phys., 122, 091103 (2005)
89. Price. AD, Jockusch. RA, Williams. ER, J. Am. Chem. Soc., 119, 11988 (1997)
90. Welton. T, Chem. Rev., 99, 2071 (1999)
91. Wassercheid. P, Keim. W, Angew. Chem. Int. Ed., 39, 3772 (2000)
92. Hagfelt. A, Boschloo. G, Sun. L, Kloo. L, Petterson. H, Chem. Rev., 110, 6595 (2010)
93. Plechkova. NV, Seddon. KR, Chem. Soc. Rev., 37, 123 (2008)
94. Hallett. JP, Welton. T, Chem. Rev., 111, 3508 (2011)
95. D'Alessandro. DM, Smit. B, Long. JR, Angew. Chem. Int. Ed., 49, 6058 (2010)
96. Zhang. Y, Gao. H, Joo. YH, Shreeve. JM, Angew. Chem. Int. Ed., 50, 9554 (2011)
97. Rebelo. LPN, Lopes. JNC, Esperança. JMSS, Filipe. E, J. Phys. Chem. B, 109, 6040 (2005)
98. Earle. MJ, Esperança. JMSS, Gilea. MA, Lopes. JNC, Rebelo. LPN, Magee. JW, Seddon. KR, Widegren. JA, Nature, 439, 831 (2006)
99. Deyko. A, Lovelock. KRJ, Licence. P, Jones. RG, Phys. Chem. Chem. Phys., 13, 16841 (2011)
100. Kirchner. B, Malberg. F, Firaha. DS, Holloczki. O, J. Phys.-Condesnsed Matt., 27, 463002 (2015)
101. Zhao. DB, Aus. J. Chem., 57, 509 (2004)
102. Jackson. GP, Duckworth. DC, Chem. Commun., 522 (2004)
103. Bruker Daltronics, Esquire 6000 manual
104. Simons. JP, Mol. Phys., 107, 2435 (2009)
105. Bruker Daltronics, amaZon manual
106. Fenn. JB, Mann. M, Meng. CK, Wong. SF, Whitehouse. CM, Mass Spec. Reviews., 9, 37 (1990)
107. Fenn. JB, Ang. Chem. Int. Ed., 42, 3871 (2003)
108. Taylor. G, Proceedings of the Royal Society of London. Series A. Mathematical and Physical Sciences, 280, 383 (1964)

109. Smith. JN, Flagan. RC, Beauchamp. JL, J. Phys. Chem. A, 106, 9957 (2002)

110. Dole. M, Mack. LL, Hines. RL, Mobley. RC, Ferguson. LD, Alice. MB, J. Chem. Phys., 49, 2240 (1968)

111. Mack. LL, Kralik. P, Rheude. A, Dole. M, J. Chem. Phys. 52, 4977 (1970)

112. Iribarne. JV, Thomson. BA, J. Chem. Phys., 64, 2287 (1976)

113. Nguyen. S, Fenn. JB, Proceedings of the National Academy of Sciences, 104, 1111 (2007)

114. Banerjee. S, Mazumdar. S, Int. J. Anal. Chem., 2012, 282574 (2012)

115. March. RE, J. Mass. Spec., 32, 351 (1997)

116. Paul. W, Ang. Chem. Int. Ed. In English, 29, 739 (1990)

117. Mathieu. É, J. de Mathématiques Pures et Applicquées, Editon edn., 137 (1868)

118. Louris. JN, Cooks. RG, Syka. JEP, Kelley. PE, Stafford. GC, Todd. JFJ, Anal. Chem., 59, 1677 (1987)

119. Dessent. CEH, Bailey. CG, Johnson. MA, J. Chem. Phys., 102, 6335 (1995)

120. Born. M, Oppenheimer. R, Annalen der Physik, 389, 457 (1927)

121. Becke. AD, J. Chem. Phys., 98, 5648 (1993)

122. Hohenberg. P, Kohn. W, Phys. Rev., 136, B864-B871 (1964)

123. Allinger. NL, Yuh. YH, Lii. JH, J. Am. Chem. Soc., 111, 8551 (1989)

124. Box. VGS, Molecular Modelling annual, 3, 124 (1997)

125. Cramer. CJ, Essentials of Computational Chemistry, John Wiley and Sons (2002)

126. Forbes. MW, Bush. MF, Polfer. NC, Oomens. J, Dunbar. RC, Williams. ER, Jockusch. RA, J. Phys. Chem. A, 111, 11759 (2007)

127. Mertens. LA, Marzluff. EM, J. Phys. Chem. A, 115, 9180 (2011)

128. Jockusch. RA, Lemoff. AS, Williams. ER, J. Am. Chem. Soc., 123, 12255 (2001)

129. Bush. MF, Oomens. J, Saykally. RJ, Williams. ER, J. Am. Chem. Soc., 130, 6463 (2008)

130. Rodgers. MT, Armentrout. PB, Acc. Chem. Res., 37, 989 (2004)

131. Hofstetter. TE, Howder. C, Berden. G, Oomens. J, Armentrout. P, J. Phys. Chem. B, 115, 12648 (2011)

132. Armentrout. PB, Yang. B, Rodgers. MT, J. Phys. Chem. B, 117, 3771 (2013)

133. Burt. MB, Decker. SGA, Atkins. CG, Rowsell. M, Peremans. A, Fridgen. TD, J. Phys. Chem. B, 115, 11506 (2011)

134. Wu. R, McMahon. TB, Angew. Chem., 119, 3742 (2007)

135. Kapota. C, Lemaire. J, Maitre. P, Ohanessian. G, J. Am. Chem. Soc., 126, 1836 (2004)

136. Hoffmann. EK, Biochem. Biophys. Acta, 864, 1 (1986)

137. Raghavan. A, Sheik. T, Graham. BH, Craigen. WJ, Biomembranes, 1818, 1477 (2012)

138. Kass. SR, J. Am. Chem. Soc., 127, 13098 (2005)

139. Yang. G, Zu. Y, Liu. C, Fu. Y, Zhou. L, J. Phys. Chem. B, 112, 7104 (2008)

140. Tian. SX, Li. HB, Yang. J, ChemPhysChem, 10, 1435 (2009)

141. O'Brien. JT, Prell. JS, Beden. G, Oomens. J, Williams. ER, Int. J. Mass Spectrom., 297, 116 (2010)

142. Skurski. P, Gutowski. M, Barrios. R, Simons. J, Chem. Phys. Lett., 337, 143 (2001)

143. Rak. J, Skurski. P, Simons. J, Gutowski. M, J. Am. Chem. Soc., 123, 11695 (2001)

144. Deppmeier. BJ, Driessen. AJ, Hehre. TS, Hehre. WJ, Johnson. JA, Klonzinger. PE, Leonard. JM, Ohlinger. WS, Pham. IN, Pietro. WJ, Yu. J, PC Spartan Pro, Wavefunction, Inc.; Irvine, CA, 2000.

145. Kaminsky. J, Jensen. F, J. Chem. Theory Comput., 3, 1774 (2007)

146. Burke. RM, Dessent. CEH, J. Phys. Chem. A, 113, 2683 (2009)

147. Burke. RM, Pearce. JK, Boxford. WE, Bruckmann. A, Dessent. CEH, J. Phys. Chem. A, 109, 9775 (2005)

148. Frisch. MJ, *et al*. Gaussian 09, Revision C.01, Gaussian, Inc., Pittsburgh, PA, (2010)

149. Boys. SF, Bernardi. F, Mol. Phys., 19, 553 (1970)

150. Mardirossian. N, Lambrecht. DS, McCaslin. L, Xantheas. SS, Head-Gordon. M, J. Chem. Theor. Comput., 9, 1368 (2013)

151. Schmidt. J, Kass. SR, J. Phys. Chem. A., 117, 4863 (2013)

152. Rak. J, Skurski. P, Gutowski. M, J. Chem. Phys., 114, 10673 (2001)

153. Diken. EG, Headrick. JM, Johnson. MA, J. Chem. Phys., 122, 224317 (2005)

154. DaSilva. FF, Denifl. S, Mark. TD, Ellis. AM, Scheier. P, J. Chem. Phys., 132, 214306 (2010)

155. Kim. J, Lee. HM, Suh. SB, Majumdar. D, Kim. KS, J. Chem. Phys., 113, 5259 (2000)

156. Hobza. P, Müller-Dethlefs. K, Non-Covalent Interactions, RSC Publishing, 2009.

157. Prell. JS, Chang. TM, Biles. JA, Berden. G, Oomens. J, Williams. ER, J. Phys. Chem. A, 115, 2745 (2011)

158. Leavitt. CM, Wolk. AB, Fournier. JA, Kamrath. MZ, Garand. E, Van Stipdonk. MJ, Johnson. MA, J. Phys. Chem. Lett., 3, 1099 (2012)

159. Wolk. AB, Leavitt. CM, Garand. E, Johnson. MA, Acc. Chem. Res., 47, 202 (2014)

160. Luxford. TFM, Milner. EM, Yoshikawa. N, Bullivant. C, Dessent. CEH, Chem. Phys. Lett., 577, 1 (2013)

161. Robertson. EG, Simons. JP, PCCP, 3, 1 (2001)

162. Wyttenbach. T, Bowers. MT, Top. Curr. Chem., 225, 207 (2003)

163. Barran. PE, *et al.*, Int. J. Mass. Spectrom., 240, 273 (2005)

164. Schinle. F, Crider. PE, Vonderach. M, Weis. P, Hampe. O, Kappes. MM, PCCP, 15, 6640 (2013)

165. Marcum. JC, Kaufman. SH, Weber. JM, Int. J. Mass Spectrom., 303, 129 (2011)

166. Nielsen. LM, Hoffmann. SV, Nielsen. SB, Chem. Comm., 48, 10425 (2012)

167. Alonso. JL, Pena. I, Sanz. ME, Vaquero. V, Mata. S, Cabezas. C, Lopez. JC, Chem. Comm., 49, 3443 (2013)

168. Bazso. G, Najbauer. EE, Magyarfalvi. G, Tarczay. G, J. Phys. Chem. A, 117, 1952 (2013)

169. Schwing. K, Fricke. H, Bartl. K, Polkowska. J, Schrader. T, Gerhards. M, ChemPhysChem., 13, 1576 (2012)

170. Vaden. TD, de Boer. TSJA, MacLeod. NA, Marzluff. EM, Simons. JP, Snoek. LC, PCCP, 9, 2549 (2007)

171. Stearns. JA, Mercier. S, Seaiby. C, Guidi. M, Boyarkin. OV, Rizzo. TR, J. Am. Chem. Soc., 129, 11814 (2007)

172. Nir. E, Hunig. I, Kleinermanns. K, de Vries. MS, PCCP, 5, 4780 (2003)

173. Porath. D, Bezryadin. A, de Vries. S, Dekker. C, Nature, 403, 635 (2000)

174. Ullrich. S, Tarczay. G, Tong. X, Dessent. CEH, Müller-Dethlefs. K, Angew. Chem., Int. Ed., 41, 166 (2002)

175. Keutsch. FN, Saykally. RJ, Proc. Natl. Acad. Sci., 98, 10533 (2001)

176. Zhao. Y, Truhlar. DG, Theor. Chem. Acc., 120, 215 (2008)

177. Zhao. Y, Truhlar. DG, J. Phys. Chem. A, 110, 13126 (2006)

178. Zhao. Y, Truhlar. DG, J. Chem. Phys., 125, 194101 (2006)

179. Jurecka. P, Svozil. D, Hobza. P, Sponer. J, PCCP, 12, 3522 (2010)

180. Smith. SA, Hand. KE, Love. ML, Hill. G, Magers. DH, J. Comput. Chem., 34, 558 (2013)

181. Liu. Y, Zhao. J, Li. F, Chen. Z, J. Comput. Chem., 34, 121 (2013)

182. Jones. GJ, Robertazzi. A, Platts. JA, J. Phys. Chem. B., 117, 3315 (2013)

183. Walker. M, Sen. A, Harvey. AJA, Dessent. CEH, Chem. Phys. Lett., 588, 43 (2013)

184. Goerigk. L, Grimme. S, J. Chem. Theory Comput., 7, 291 (2011)

185. Sharkas. K, Toulouse. J, Savin. A, J. Chem. Phys., 134, 064113 (2011) and references therein

186. Grimme. S, J. Comput. Chem., 27, 1787 (2006)

187. Becke. AD, J. Chem. Phys., 107, 8554 (1997)

188. v. Mourik. T, Gdanitz. RJA, J. Chem. Phys., 116, 9620 (2002)

189. Nei. YW, Hallowita. N, Steill. JD, Oomens. J, Rodgers. MT, J. Phys. Chem. A, 117, 1319 (2013)

190. Dessent. CEH, Bailey. CG, Johnson. MA, J. Chem. Phys., 103, 2006 (1995)

191. Khodabandeh. MH, Reisi. H, Davari. MD, Zare. K, Zahedi. H, Ohanessian. G, ChemPhysChem, 14, 1733 (2013)

192. Ionic Liquids (Topics in Current Chemistry), Kirchner. B, Springer, (2013)

193. The Structure of Ionic Liquids (Soft and Biological Matter), Caminiti. R, Gontrani. L, Springer, (2013)

194. Dong. K, Zhao. L, Wang. Q, Song. Y, Zhang. S, PCCP, 15, 6034 (2013)

195. Leal. JP, Esperança. JMSS, Minas da Piedade. ME, Lopes. JNC, Rebelo. LPN, Seddon. KR, J. Phys. Chem. A, 111, 6176 (2007)

196. Cremer. T, Kolbeck. C, Lovelock. KRJ, Paape. N, Wölfel. R, Schulz. PS, Wasserscheid. P, Weber. H, Thar. J, Kirchner. B, Maier. F, Steinrück. H-P, Chem. Eur. J., 16, 9018 (2010)

197. Katsyuba. SA, Zvereva. EE, Vidiš. A, Dyson. PJ, J. Phys. Chem. A, 111, 352 (2006)

198. Hunt. PA, Ashworth. CR, Matthews. RP, Chem. Soc. Rev., 44, 1257 (2015)

199. Johnson. CJ, Fournier. JA, Wolke. CT, Johnson. MA, J. Chem. Phys., 139, 224305 (2013)

200. Wang. C, Luo. H, Li. H, Dai. S, PCCP, 12, 7246 (2010)

201. Ogura. T, Akai. N, Kawai. A, Shibuya. K, Chem. Phys. Lett., 555, 110 (2013)

202. Cooper. R, Zolot. AM, Boatz. JA, Sporleder. DP, Stearns. JA, J. Phys. Chem. A, 117, 12419 (2013)

203. Sen. A, Luxford. TFM, Yoshikawa. N, Dessent. CEH, PCCP, 16, 15490 (2014)

204. Sen. A, Dessent. CEH, J. Phys. Chem. Lett., 5, 3281 (2014)

205. Dessent. CEH, Kim. J, Johnson. MA, Acc. Chem. Res., 31, 527 (1998)

206. Alfassi. ZB, Huie. RE, Milman. BL, Neta. P, Anal. Bioanal. Chem., 377, 159 (2003)

207. Gozzo. FC, Santos. LS, Augusti. R, Consorti. CS, Dupont. J, Eberlin. MN, Chem. Eur. J., 10, 6187 (2004)

208. Nakurte. I, Mekss. P, Klavins. K, Zicmanis. A, Vavilina. G, Dubrovina. S, Eur. J. Mass Spectr., 15, 471 (2009)

209. Fernandes. AM, Rocha. MAA, Freire. MG, Marrucho. IM, Coutinho. JAP, Santos. LMNBF, J. Phys. Chem. B, 115, 4033 (2011)

210. Bolovinos. A, Tsekeris. P, Philis. J, Pantos. E, Andritsopoulos. G, J. Mol. Spectrosc.,103 240 (1984)

211. Devine. AL, Cronin. B, Nix. MGD, Ashfold. MNR, J. Chem. Phys., 125, 184302 (2006)

212. Barbatti. M, Lischka. H, Salzmann. S, Marian. CM, J. Chem. Phys., 130, 034305 (2009)

213. Koh. CJ, Leone. SR, Mol. Phys., 110, 1705 (2012)

214. Niedermeyer. H, Ashworth. C, Brandt. A, Welton. T, Hunt. PA, PCCP, 15, 11566 (2013)

215. Paul. A, Samanta. A, J. Chem. Sci, 118, 335 (2006)

216. Paul. A, Mandal. PK, Samanta. A, Chem. Phys. Lett. 402, 375 (2005)

217. Nockemann. P, Binnemans. K, Driesen. K, Chem. Phys. Lett., 415, 131 (2005)

218. Mak. CC, Peslherbe. GH, Mol. Sim., 41, 156 (2015)

219. Mak. CC, Timerghazin. QK, Peslherbe. GH, J. Phys. Chem. A, 117, 7595 (2013)

220. Liu. HT, Ning. CG, Huang. DL, Wang. LS, Ang. Chem. Int. Ed., 53, 2464 (2014)

221. (a) Yandell. MA, King. SB, Neumark. DM, J. Chem. Phys. 140, 184317 (2014): (b) King. SB, Yandell. MA, Stephansen. AB, Neumark. DM, J. Chem. Phys., 141, 224310 (2014): (c) Yandell. MA, King. SB, Neumark. DM, J. Am. Chem. Soc., 135, 2128 (2013)

222. (a) Adams. CL, Weber. JM, J. Chem. Phys., 134, 244301 (2011): (b) Adams. CL, Schneider. H, Ervin. KM, Weber. JM, J. Chem. Phys., 130, 074307 (2009)

223. Van Duzor. M, Mbaiwa. F, Lasinski. J, Holtgrewe. N, Mabbs. R, J. Chem. Phys., 134, 214301 (2011)

224. Mbaiwa. F, Van Duzor. M, Wei. J, Mabbs. R, J. Phys. Chem. A., 114, 1539 (2010)

225. Jagau. TC, Dao. DB, Holtgrewe. NS, Krylov. AI, Mabbs. R, J. Phys. Chem. Lett., 6, 2786 (2015)

226. Smith. BH, Buonaugurio. A, Chen. J, Collins. E, Bowen. KH, Compton. RN, Sommerfield. T, J. Chem. Phys., 138, 234304 (2013)

227. Fortenberry. RC, Crawford. TD, Lee. TJ, Astrophys. J., 762, 121 (2013)

228. Jackson. RL, Zimmerman. AH, Brauman. JI, J. Chem. Phys., 71, 2088 (1979)

229. Mbaiwa. F, Holtgrewe. N, Dao. DB, Lasinski. J, Mabbs. R, J. Phys. Chem. A, 118, 7249 (2014)

230. Huang. DL, Liu. HT, Ning. CG, Wang. LS, J. Phys. Chem. Lett., 6, 2153 (2015)

231. Huang. DL, Liu. HT, Ning. CG, Wang. LS, J. Chem. Phys., 142, 124309 (2015)

232. Weichman. L, Kim. JB, Neumark. DM, J. Phys. Chem. A, 119, 6140 (2015)

233. Walker. M, Harvey. AJA, Sen. A, Dessent. CEH, J. Phys. Chem. A, 117, 12590 (2013)

234. Chang. TM, Berden. G, Oomens. J, Williams. ER, Int. J. Mass Spec., 377, 440 (2015)

235. CRC Handbook of Chemistry and Physics, 95th Edition (2014)

236. Suich. DE, Caplins. DW, Shearer. AJ, Harris. CB, J. Phys. Chem. Lett., 5, 3073 (2014)

237. Daxner. M, Denifl. S, Scheier. P, Ellis. AM, Ang. Chem. Int. Ed., 53, 13528 (2014)

238. Bichoutskaia. E, Pyper. NC, J. Chem. Phys., 137, 184104 (2012)

239. Rienstra-Kiracofe. JC, Tshcumper. GS, Schaefer. HF, Nandi. S, Ellison. GB, Chem. Rev., 102, 231 (2002)

240. Arnold. CC, Neumark. DM, Cyr. DM, Johnson. MA, J. Phys. Chem., 99, 1633 (1995)

241. Miller. TM, Leopold. DG, Murray. KK, Lineberger. WC, J. Chem. Phys., 85, 2368 (1986)

242. Dao. DB, Mabbs. R, J. Chem. Phys., 141, 154304 (2014)

243. Dessent. CEH, Bailey. CG, Johnson. MA, J. Chem. Phys., 105, 10416 (1996)

244. Dessent. CEH, Kim. J, Johnson. MA, Farad. Discuss., 115, 395 (2000)

245. Jordan. KD, Luken. W, J. Chem. Phys., 64, 2760 (1976)

246. Hazi. AU, J. Chem. Phys., 75, 4586 (1981)

247. Adamowicz. L, McCullough. E Jr., Chem. Phys. Lett., 107, 72 (1984)

248. Mbaiwa. F, Dao. D, Holtgrave. N, Lasinski. J, Mabbs. R, J. Chem. Phys., 136, 114303 (2012)

249. Crawford. OH, Mol. Phys., 20, 585 (1971)

250. Garrett. WR, J. Chem. Phys., 73, 5721 (1980)

251. Fatemi. FK, Dally. AJ, Bloomfield. LA, Phys. Rev. Lett., 84, 51 (2000)

252. Zhao. Y, Truhlar. DG, J. Chem. Theo. Comp., 4, 1849 (2008)

253. Peverati. R, Truhlar. DG, J. Chem. Phys. Lett., 3, 117 (2012)

254. Peverati. R, Truhlar. DG, J. Chem. Phys. Lett., 2, 2810 (2011)

255. Voss. JM, Marsh. BM, Zhou. J, Garand. E, PCCP, 18, 18905 (2016)

256. Chiou. MF, Sheu. WS, J. Phys. Chem. A, 116, 7694 (2012)

257. Baughman. RH, Zakhidov. AA, Heer. WA, Science, 297, 787 (2002)

258. Gokel. GW, Leevy. WM, Weber. ME, Chem. Rev., 104, 2723 (2004)